DESIGNING INHIBITORS VIA MOLECULAR MODELLING METHODS FOR MONOAMINE OXIDASE ISOZYMES A AND B

FİLİZ VARNALI

KADİR HAS UNIVERSITY
2012

DESIGNING INHIBITORS VIA MOLECULAR MODELLING METHODS FOR MONOAMINE OXIDASE ISOZYMES A AND B

FİLİZ VARNALI
M.S. in Computational Biology and Bioinformatics, Kadir Has University, 2012

Submitted to the Graduate School of Science and Engineering in partial fulfilment of the requirements for the degree of Master of Science in Computational Biology and Bioinformatics

KADİR HAS UNIVERSITY
2012

DESIGNING INHIBITORS VIA MOLECULAR MODELING METHODS FOR MONOAMINE OXIDASE ISOZYMES A AND B

Abstract

In drug development studies, a large number of new drug candidates (leads) have to be synthesized and optimized by changing several moieties of the leads in order to increase efficacies and decrease toxicities. Each synthesis of these new drug candidates include multi-steps procedures. Overall, discovering a new drug is a very time-consuming and very costly works. The development of molecular modelling programs and their applications in pharmaceutical research have been formalized as a field of study known computer assisted drug design (CADD) or computer assisted molecular design (CAMD).

In this study, using the above techniques, Monoamine Oxidase isozymes, which play an essential role in the oxidative deamination of the biogenic amines, were studied. Compounds that inhibit these isozymes were shown to have therapeutic value in a variety of conditions including several psychiatric and neurological as well as neurodegenerative diseases.

First, a series of new pyrazoline derivatives were screened using molecular modelling and docking methods and promising lead compounds were selected, and proposed for synthesis as novel selective MAO-A or –B inhibitors.
Both experimentally and computationally promising compounds were selected using Discovery Studio's De Novo Design program in order to enhance their binding affinity. Pharmachophoric properties of the active site of the enzymes were also mapped.

The results obtained computationally in this thesis stimulate the further studies and provide invaluable data for the design of more selective and potential MAO-A and MAO-B inhibitors.

Keywords: Monoamine Oksidase (MAO), molecular modelling, drug design, pyrazoline derivatives, Accelerys, AutoDock, GOLD, CAESAR

MONOAMIN OKSIDAZ A VE B İZOZİMLERİNE MOLEKÜLER MODELLEME YÖNTEMLERİ İLE İNHİBİTÖR TASARLANMASI

Özet

İlaç geliştirilme çalışmaları, geleneksel olarak basamaklı sentez prosedürlerine dayanmaktadır ve aktivite profillerinin optimizasyonu için çok sayıda bileşiğin sentezini gerektirmektedir. Bu sebepten dolayı yapılan araştırmalar artık moleküllerin aktivite profillerinin çıkarılmasına dayalı bilgisayar tabanlı moleküler modelleme teknikleri kullanılarak yapılmaya başlanmıştır. Bu moleküler modelleme tekniklerine bilgisayar yardımlı ilaç tasarımı (Computer Assisted Drug Design (CADD)) veya bilgisayar yardımlı moleküler tasarım (Computer Assisted Molecular Design (CAMD)) adı verilmektedir.

Bu çalışmada bu yöntemlerden yararlanılarak biyojenik aminlerin oksidatif deaminasyonunda önemli rol oynayan monoamin oksidaz (MAO); MAO-A ve MAO-B olarak isimlendirilen farklı iki izoformdaki enzimle çalışılmıştır. Bu izoformları inhibe eden bileşiklerin duygusal bozukluklar ve nörodejeneratif hastalıklar gibi birçok hastalıkta tedavi edici değeri olduğu bilinmektedir.

Çalışmada esas olarak bir dizi yeni pirazolin türevi üretilmis ve moleküler modelleme yöntemleri ile taranarak ve potansiyel inhibitör adayları tespit edilmiştir.

Auto Dock, GOLD ve Accelrys Discovery Studio CAESAR programları modelleme, tarama ve görüntüleme işlerinde kullanılmıştır. Daha sonra seçilen bu bileşiklerin MAO-A ve MAO–B izoformları ile etkileşimi incelenmiştir. Elde edilen veriler MAO enzimleri ile daha sonra yapılabilecek seçimli inhibitör geliştirme çalışmaları için önemli ve yol gösterici sonuçlara ulaşılmasını sağlamıştır.

Anahtar Kelimeler: Monoamin Oksidaz (MAO), moleküler modelleme, ilaç tasarımı, pirazolin türevleri, Accelrys, AutoDock, GOLD, CAESAR

Acknowledgements

This dissertation would not have been possible without the guidance and the help of several individuals who in one way or another contributed and extended their valuable assistance in the preparation and completion of this study.

First and foremost, I would like to express my sincere gratitude to my advisor Prof. Kemal Yelekçi for the continuous support of my master's study and research, for his patience, motivation, enthusiasm, and immense knowledge. His guidance helped me throughout my research. I could not have imagined having a better advisor and mentor for my masters study.

Besides my advisor, I would like to thank the rest of my thesis committee: Dr. M. Vezir Kahraman, Dr. E. Demet Akten Akdoğan, and Dr. Tuba Arzu Özal, for their encouragement, and insightful comments. All the people in our faculty, especially for their guidance and help during my study.

Ms. Evrim Besray Ünal for helping me learn the GOLD software procedures, Mr. Ahmet Emre Aladağ for his continuous efforts helping me solve the software related problems.

Mr. Ruşit Ümit for his untiring effort in editing my thesis and his guidance and support.

Last but not the least, my beloved mother Fatma and sister Deniz for their patient love and endless support.

This thesis is dedicated to Prof. Nihat Aktaç

Who has been my guide and inspiration…

Table of Contents

Abstract..... ii
Özet..... iv
Acknowledgements..... vi
Dedication..... vii
Table of Contents..... viii
List of Tables..... xi
List of Figures..... xii
List of Equations..... xv
List of Abbrevations..... xvi
1 PROPERTIES OF MONOAMINE OXIDASE ENZYMES
1.1 Introduction……..... 1
1.2 General Properties of MAO Isoenzymes..... 2
1.3 Crystallographic and Structural Properties of MAO Isoenzymes 5
1.4 Biosynthesis and Biodegradation of Neurotransmitters..... 11
1.5 Amine Catalysis Reaction of MAO Isoenzymes..... 14
1.5.1 Single Electron Transfer Mechanism (SET)..... 15
1.5.2 Polar Addition-Elimination Pathway..... 15
1.5.3 Hydrogen atom transfer (HAT)..... 17
2 CLASSIFICATIONS OF MONAMINE OXIDASE INHIBITORS
2.1 Introduction..... 18
2.2 Irreversible (Non-Selective) MAO Inhibitors..... 19
2.3 Reversible and selective MAO inhibitors..... 21

3 METHODS AND PROCEDURES USED IN MOLECULAR MODELLING

3.1 Introduction..... 25
3.2 Preparation of Enzymes and Ligands..... 27
3.3 Auto Dock and Molecular Docking Studies performed by AUTODOCK..... 28
3.4 GOLD and Molecular Docking Studies performed by GOLD..... 33
3.5 CAESAR and Molecular Docking Studies performed by CAESAR..... 35

4 LIGANDS DESIGNED BY DENOVO MOLECULAR MODELING METHODS

4.1 Introduction..... 36
4.2 Properties of the Scaffolds and Side Groups of the Generated Ligands..... 37
4.3 Ligands Chemical Structure of Selected According AUTODOCK, GOLD and CAESAR Results 39

5 RESULTS and DISSCUSION

5.1 Introduction..... 45
5.2 Docking Results of MAO-A and MAO-B Isoenzymes..... 46
5.3 Correlation Between Docking Results 49
5.4 Detailed Analysis of the Fundamental Results of Docking Studies..... 51
5.4.1 Ligands Selected for MAO-A Enzyme..... 51
5.4.1.1 Evaluation of 4bcr/4bcs Ligands for MAO-A Enzyme..... 51
5.4.1.2 Evaluation of 4dar/4das Ligands for MAO-A Enzyme..... 56
5.4.1.3 Evaluation of 5bar/5bas Ligands for MAO-A Enzyme..... 60
5.4.2 Ligands Selected for MAO-B Enzyme..... 65
5.4.2.1 Evaluation of 1der/1des Ligands for MAO-B Enzyme..... 65

5.4.2.2 Evaluation of 3bar/3bas Ligands for MAO-B Enzyme..... 70
5.4.2.3 Evaluation of 3car/3cas Ligands for MAO-B Enzyme..... 75
5.5 Conclusion..... 79
Curriculum Vitae..... 80
REFERANCES..... 81

List of Tables

Table-1.1	Important structural properties for MAO isoenzymes……	7
Table 2.1	Some important medicines used for MAOIs and their properties	23
Table-3.1	Important parameters used for Auto Dock studies……..	32
Table-3.2	Important parameters used for CAESAR studies……	35
Table-4.1	Naming of the ligands…….……..…….....	37
Table-4.2	Chemical structure of selected ligands according to AutoDock, GOLD and CAESAR results…….……..……..	39
Table-5.1	Docking scores of the 50 ligands obtained by Autodock, GOLD and CAESAR for MAO-A and MAO-B isoenzymes…….……...	46

List of Figures

Figure-1.1	The 3-D image obtained by positioning monomer units of MAO-A and MAO-B enzymes on top of each other.....	3
Figure-1.2	Sequence similarity between MAO-A and MAO-B.....	3
Figure-1.3	FAD's molecular structure.....	4
Figure-1.4	LIGPLOT illustration binding FAD to MAO-B.....	5
Figure-1.5	MAO-A structure is shown in illustration.....	8
Figure-1.6	MAO-B structure is shown in illustration.....	9
Figure-1.7	Binding of MAO-A the mitochondrial membrane.....	10
Figure-1.8	Binding of MAO-B to the mitochondrial membrane.....	10
Figure-1.9	Chemical structures of some amines which are related with MAO isoenzymes.....	12
Figure-1.10	Biosynthesis of neurotransmitters that are synthesized from tyrosine and tryptophan.....	13
Figure 1.11	Biodegredation of Catecholamines via COMT and MAO enzymes	14
Figure-1.12	Amine catabolism reaction.....	14
Figure 1.13	Chemical reaction catalyzed by MAO isoenzymes.....	15
Figure-1.14	Proposed radical mechanism for MAO catalysis.....	15
Figure-1.15	Proposed polar addition-elimination mechanism.....	16
Figure-1.16	Proposed hydrogen atom transfer mechanism.....	17
Figure 2.1	Chemical structure of hydrazine derivatives.....	19
Figure-2.2	Chemical structure of cyclopropylamine derivatives.....	20
Figure-2.3	Chemical structure of propylamine derivatives.....	20

Figure-2.4 Chemical structure of fluoroallilamin derivatives..... 21
Figure-2.5 Chemical structure of hydrazolone..... 22
Figure 3.1 Darwinian and Lamarckian local search algorithms..... 29
Figure 3.2 Energy evaluation of binding in Autodock 30
Figure-5.1 Correlation between docking methods for MAO-A graphic..... 49
Figure-5.2 Correlation between docking methods for MAO-B graphic..... 50
Figure-5.3 Position of 4bcr ligand in MAO-A enzyme and 2-D representation of its interactions..... 52
Figure-5.4 Position of 4bcr ligand in MAO-A enzyme and 3-D representation of its interactions..... 53
Figure-5.5 Position of 4bcs ligand in MAO-A enzyme and 2-D representation of its interactions..... 54
Figure-5.6 Position of 4bcs ligand in MAO-A enzyme and 3-D representation of its interactions..... 55
Figure-5.7 Position of 4dar ligand in MAO-A enzyme and 2-D representation of its interactions..... 57
Figure-5.8 Position of 4dar ligand in MAO-A enzyme and 3-D representation of its interactions..... 57
Figure-5.9 Position of 4dar ligand in MAO-A enzyme and 3-D representation of its interactions..... 59
Figure-5.10 Position of 4das ligand in MAO-A enzyme and 3-D representation of its interactions..... 59
Figure-5.11 Position of 5bar ligand in MAO-A enzyme and 2-D representation of its interactions..... 61
Figure-5.12 Position of 5bar ligand in MAO-A enzyme and 3-D representation of its interactions..... 62

Figure-5.13 Position of 5bas ligand in MAO-A enzyme and 2-D representation of its interactions..... 63

Figure-5.14 Position of 5bas ligand in MAO-A enzyme and 3-D representation of its interactions..... 64

Figure-5.15 Position of 1der ligand in MAO-B enzyme and 2-D representation of its interactions..... 66

Figure-5.16 Position of 1der ligand in MAO-B enzyme and 3-D representation of its interactions..... 67

Figure-5.17 Position of 1des ligand in MAO-B enzyme and 2-D representation of its interactions..... 68

Figure-5.18 Position of 1des ligand in MAO-B enzyme and 3-D representation of its interactions..... 69

Figure-5.19 Position of 3bar ligand in MAO-B enzyme and 2-D representation of its interactions..... 71

Figure-5.20 Position of 3bar ligand in MAO-B enzyme and 2-D representation of its interactions..... 72

Figure-5.21 Position of 3bas ligand in MAO-B enzyme and 2-D representation of its interactions..... 73

Figure-5.22 Position of 3bas ligand in MAO-B enzyme and 3-D representation of its interactions..... 74

Figure-5.23 Position of 3car ligand in MAO-B enzyme and 2-D representation of its interactions..... 75

Figure-5.24 Position of 3car ligand in MAO-B enzyme and 3-D representation of its interactions..... 76

Figure-5.25 Position of 3cas ligand in MAO-B enzyme and 2-D representation of its interactions..... 77

Figure-5.26 Position of 3cas ligand in MAO-B enzyme and 3-D representation of its interactions..... 78

List of Equations

Equation-3.1	Autodock force field equation.....	30
Equation-3.2	AutoDock ΔG and scoring function equation.....	31
Equation-3.3	GOLD score parameters……..	33
Equation-3.4	Chem-Score parameters…….	34
Equation-3.5	The complete equation for binding free energy calculated by Chem-Score…….	34

List of Abbreviations

MAO	Monoamine Oxidase
MAO-A	Monoamine Oxidase A
MAO-B	Monoamine Oxidase B
MAOIs	Monoamine oxidase inhibitors
EC	Enzyme Commission Number
FAD	Flavin Adenine Dinucleotid
$FADH_2$	Reduced flavin
$FADH^{\cdot}$	Flavin semiquinone
5-HT	Serotonin
PEA	2-phenylethylamine
MPTP	1-methyl-4-phenyl-1, 2, 3, 6-tetrahydropyridine
L-DOPA	3,4-4-dihydroxy phenylalanine
PNMT	Fenylethanolamine-N-methyltransferase
COMT	Catechol-O-methyl-tansferase
SET	Single electron transfer mechanism
HAT	Hydrogen atom transfer mechanism
PDB	Protein Data Bank
2-D	Two-dimensional
3-D	Three-dimensional
NMR	Nuclear Magnetic Resonance
SA	Simulated Annealing
GA	Genetic Algorithm
MGL Tools	Molecular Graphics Laboratory Tools
ADT	Auto Dock Tools

Accelrys DS tool Accelrys Discovery Studio Tool

Chapter 1: Properties of Monoamine Oxidase Enzymes

1.1 Introduction

Monoamine Oxidase (MAO) isoenzymes are related with neurodegenerative diseases and emotional disorders (like Parkinson, Alzheimer diseases and major depression) which affect the nervous system. Today, millions of people are affected with these diseases. Increasing world population and aging ratio exhibits the importance of development of powerful methods and new drug to treat these diseases [1, 2, 3].

Therefore, this study is focused on determining the required inhibitors for treatment of MAO isoenzymes related diseases. The objective of this study is the search new, selective and reversible, MAO isoenzyme using inhibitors to in-silico drug design methods. Computational model studies will increase the changes of finding the required drugs before synthesizing the hundreds of model compounds. This will both fasten the time needed to develop a target compound and will decrease the cost drastically [1, 2, 3].

First general structural properties of MAO isoenzymes and their crystallographic structure, second importance of related neurotransmitters, and finally amine catalysis reactions and importance of those reactions for MAO isoenzymes are described.

1.2 General Properties of MAO Isoenzymes

Monoamine Oxidase enzymes (*EC 1.4.3.4.*) contain FAD (flavin adenine dinucleotid), catalyze oxidative deamination reaction of biological amines in CNS (central nervous system) and peripheral tissues. These isoenzymes are Monoamine Oxidase-A and Monoamine Oxidase-B (MAO-A and MAO-B). MAO-A and MAO-B can be found as integral proteins in the outer mitochondrial membrane in neuronal and some other tissues. When we consider total MAO activity, MAO-A shows an intense activity in placenta, intestine, liver, adrenal medulla and MAO-B in platelets, brain, adrenal medulla and liver [4-7].

MAO-A consist of 527 and MAO-B consist of 520 amino acids respectively. MAO isoenzymes have 70% similarity based on amino acid sequences (Figure-1.1, 1.2). The active sites of both of these isoenzymes include cysteine, which is bonded covalently with coenzyme FAD (Ser-Gly-Gly-Cys-koenzyme-Tyr). Cys406 of MAO-A and Cys497 of MAO-B are making covalent bonds with 8-α-methyl group of FAD via thioether linkage [1,8]. FAD' s molecular structure can be seen in Figure-1.3.

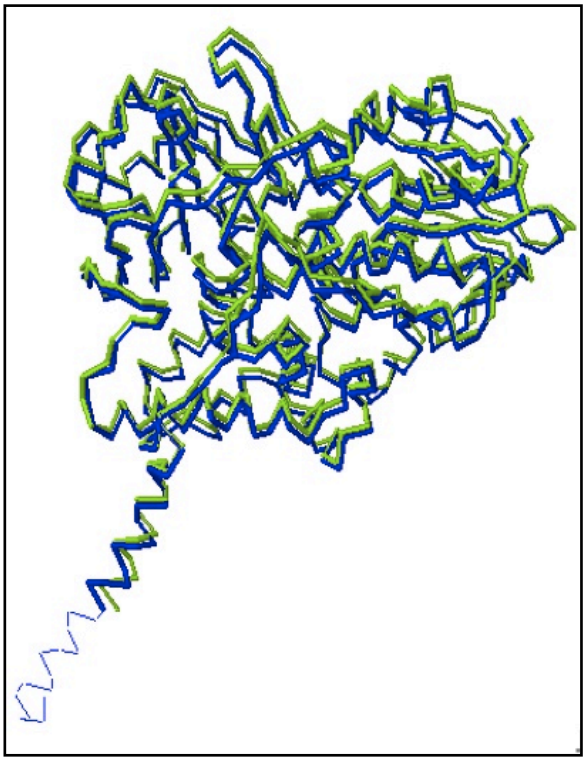

Figure-1.1: The 3-D image obtained by positioning monomer units of MAO-A and MAO-B enzymes on top of each other. MAO-A, represented in green and, MAO-B in blue [9].

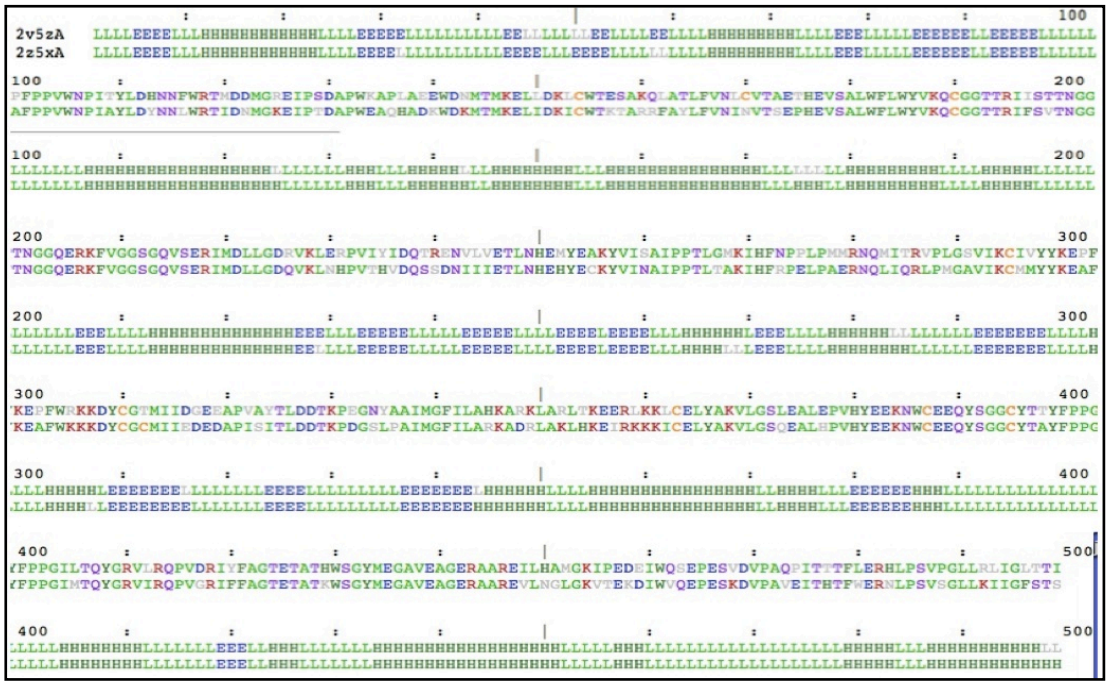

Figure-1.2: Sequence similarity between MAO-A and MAO-B [9].

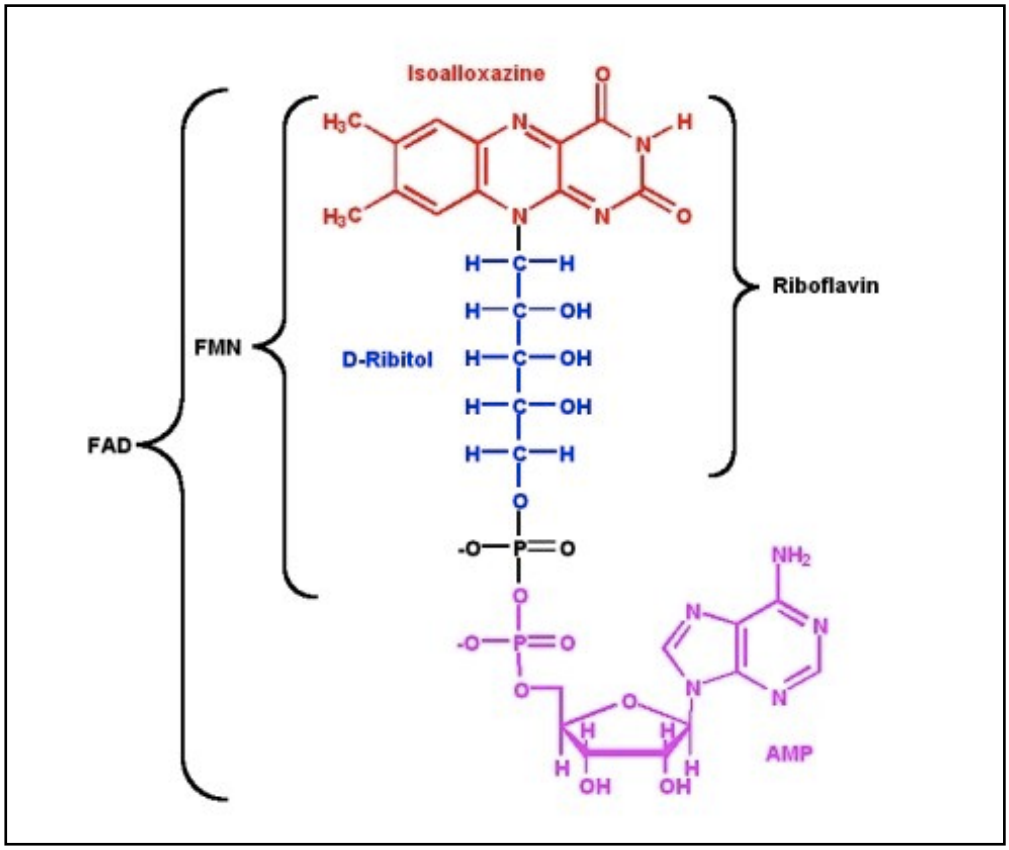

Figure-1.3: FAD's molecular structure[10]

Covalent and non-covalent interactions between isoalloxazine ring of FAD and Lys305 on MAO-A and Lys296 on MAO-B are fundamental for enzyme stabilization. These residues link to N5 atom of FAD with hydrogen bond. Interaction pattern of FAD with related amino acids is illustrated in Figure-1.4 for MAO-B [1, 8].

These amino acids are in MAO-A Ile19, Gly20, Gly22, Ile23, Ser24, Leu42, Glu43, Ala44, Arg45, Gly50, Arg51, Gly67, Ala68, Tyr69, Val244, Ile273, Leu277, Trp397, Tyr402, Cys406, Tyr407, Gly434, Thr435, Gly443, Tyr444 and Met445. On the other hands Gly11, Gly13, Ile14, Ser15, Leu33, Glu34, Ala35, Arg36, Gly41, Arg42, Gly58, Ser59, Tyr60, Val235, Ala263, Ile264, Trp388, Tyr393, Cys397, Tyr398, Gly425, Thr426, Gly434, Tyr435, Met436 residues are in MAO-B which are interacting with FAD [1, 8, 11].

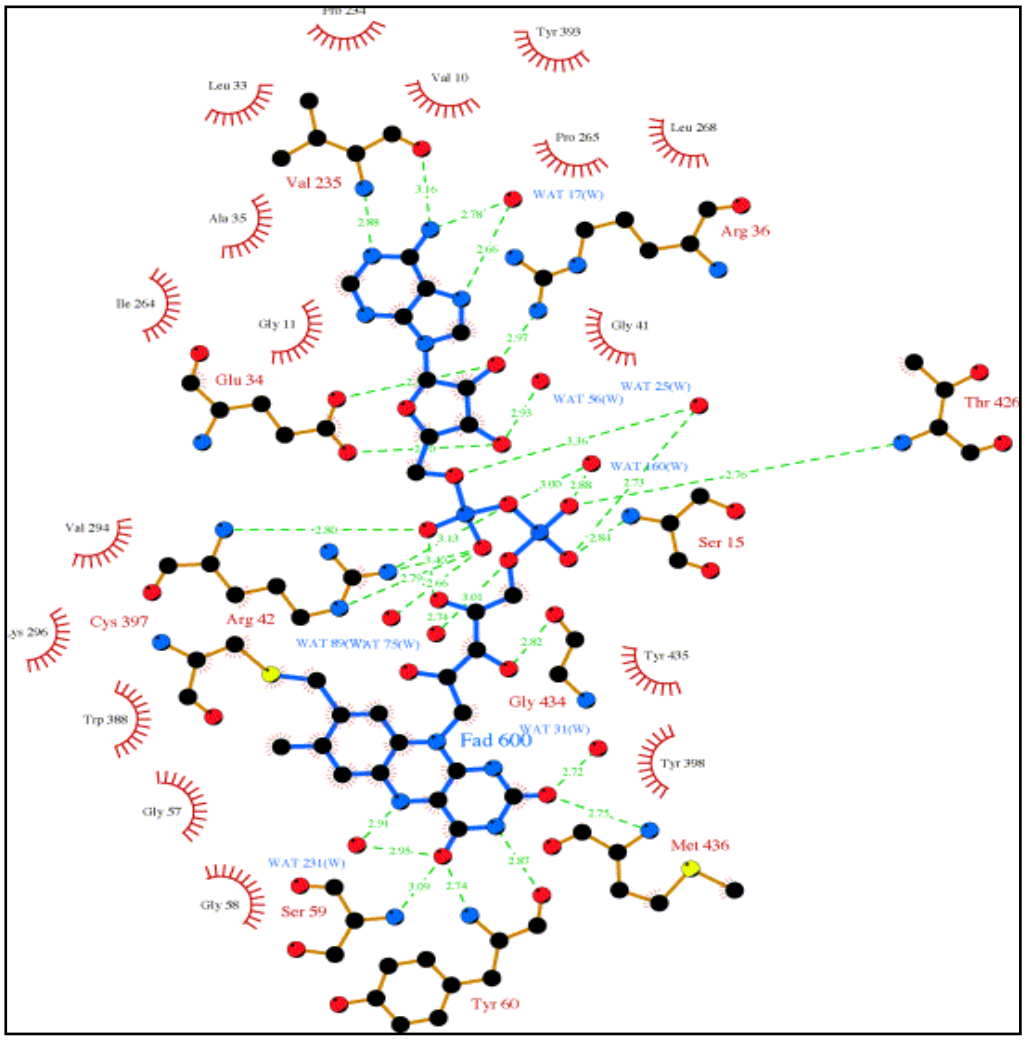

Figure-1.4: LIGPLOT illustration binding FAD to MAO-B. (Dashed lines-hydrogen bonds, carbons-black, nitrogens-blue, oxygens-red, sulphurs-yellow, water molecules- cyan spheres) [12].

1.3 Crystallographic and Structural Properties of MAO Isoenzymes

Previous crystallographic studies and computational molecular simulations show us some important information about these molecules. According to these studies MAO-A crystallizes as monomers but MAO-B crystallizes as dimmer. MAO-A includes only one cavity, which is named as *substrate binding cavity*, but MAO-B has an additional cavity named as *entrance cavity* [1, 4, 11 and 13].

MAO-B entrance cavity volume is about 290Å^3. MAO-B has a cavity-shaping loop, which is formed by amino acid residues between 99-112. This loop structure redirects substrate into entrance cavity. Entrance cavity is hydrophobic and surrounded by Phe103, Pro104, Trp119, Leu164, Leu167, Phe168, Leu171, Ile199, Ile316 and Tyr326. Ile199 acts like a gate for entrance of substrate. Therefore, large substrates can be positioned using these two cavities. On the other hand MAO-A isoenzyme does not have an entrance cavity therefore substrate can directly enter into the single cavity (substrate binding cavity) [1, 4, 11 and 13].

On both isoenzymes, substrate reaches to the hydrophobic substrate-binding cavity. Volume of this cavity in MAO-A is ~390Å^3 and in MAO-B is ~550Å^3. Substrate cavity is covered with Ile180, Asn181, Phe208, Ile335 residues in MAO-A and Leu171, Cys172, Ile199, Tyr326 residues in MAO-B.

FAD is surrounded by a cage consisting of two aromatic amino acids that are fundamental for oxidation reaction. These aromatic amino acids are Tyr407, Tyr444 in MAO-A and Tyr398 and Tyr435 in MAO-B. The residues around the aromatic cage are fundamental for ligand selectivity for MAO-A, amino acid residues between 161 and 375, and for MAO-B, amino acid residues between 152 and 366 are playing important roles [1, 4, 11 and 13].

Important structural properties for MAO isoenzymes are summarized are below in Table 1.1:

Table-1.1: Important structural properties for MAO isoenzymes

Enzyme property	**MAO-A**	**MAO-B**
Crystallographic structure	Monomer	Dimmer
Cavity number	1	2
Entrance cavity volume	No entrance cavity	290Å^3
Substrate cavity volume	550Å^3	390Å^3 Total cavity size is in open conformation 700Å^3
Aromatic cage residues	Tyr407 and Tyr444	Tyr398 and Tyr435
Gate between cavities	No	Ile199
Hydrophobic properties	Quite hydrophobic than MAO-B	Hydrophobic
Flexibility for lig. Entrance	More flexible than MAO-B	Ligands can be placed in the two cavities via gate residue (Ile199)

In Figure-1.5 and Figure-1.6 cavity locations, domains and active sites are illustrated for MAO isoenzymes.

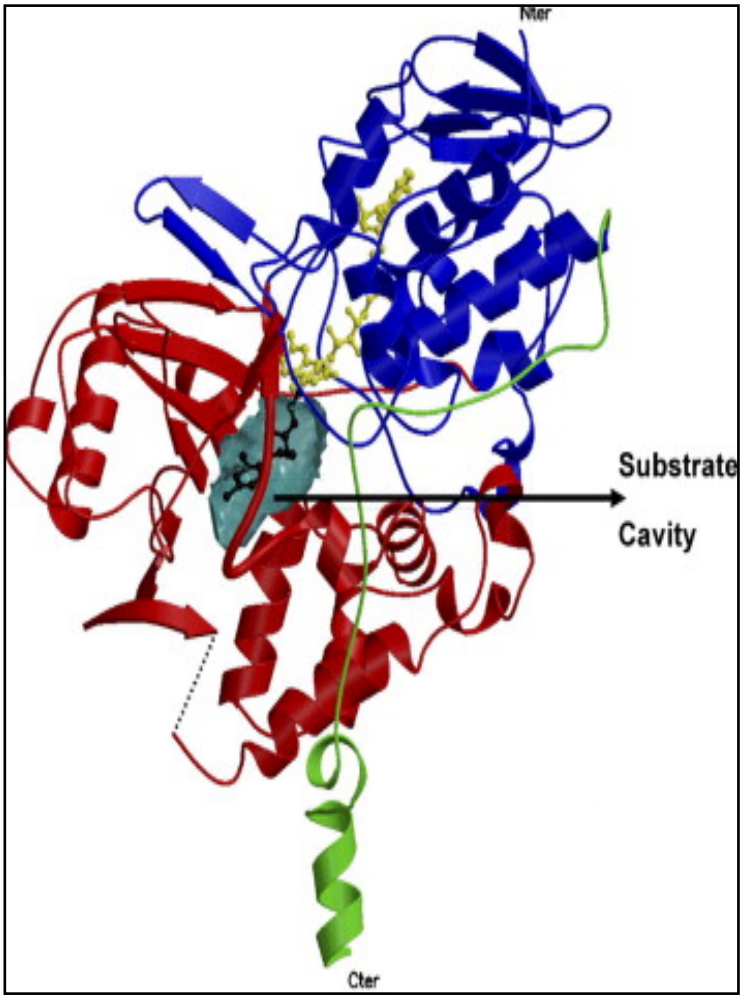

Figure-1.5: MAO-A structure is shown in illustration. The FAD-binding domain illustrated with blue, the substrate-binding domain red, and the C-terminal membrane region green.

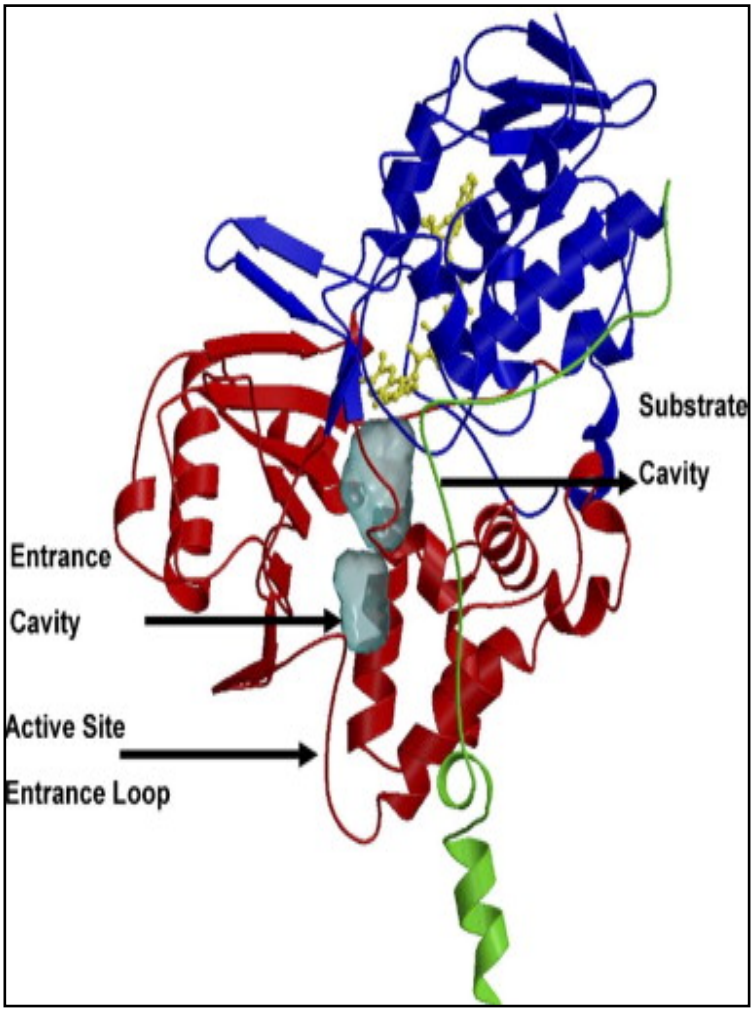

Figure-1.6: MAO-B structure is shown in illustration. The FAD-binding domain illustrated with blue, the substrate-binding domain red, and the C-terminal membrane region green.

The section, named as *C-terminal tail*, of MAO enzymes ensures binding to the mitochondrial membrane. This C-terminal tail is composed of a hydrophobic α-helix on every monomer's globular section for MAO isoenzymes (between residues 461-520) [13,14,15,16]. The function of this part is believed to be directing the ligands to the designated area of the enzyme and illustrated in Figure-1.7 and 1.8.

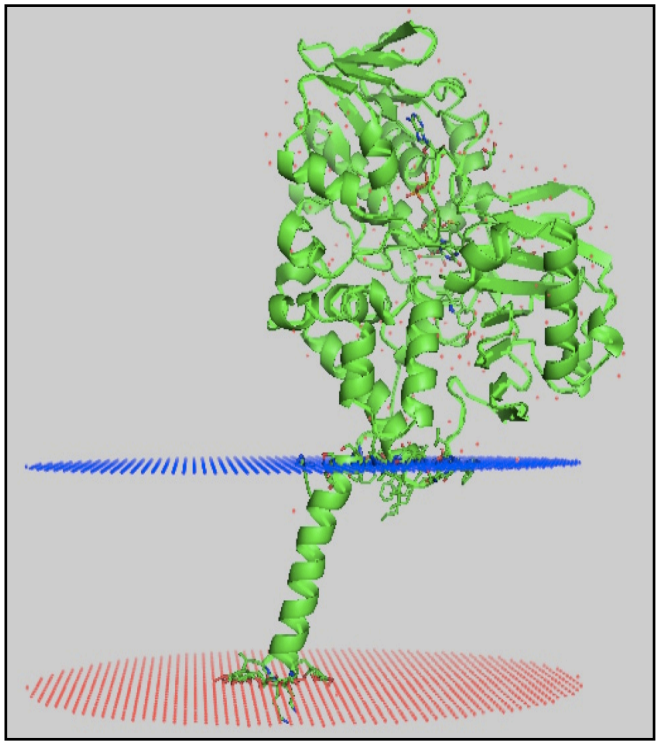

Figure-1.7: Binding of MAO-A the mitochondrial membrane and locations of amino acids at the membrane binding regions, according to crystallographic data [17].

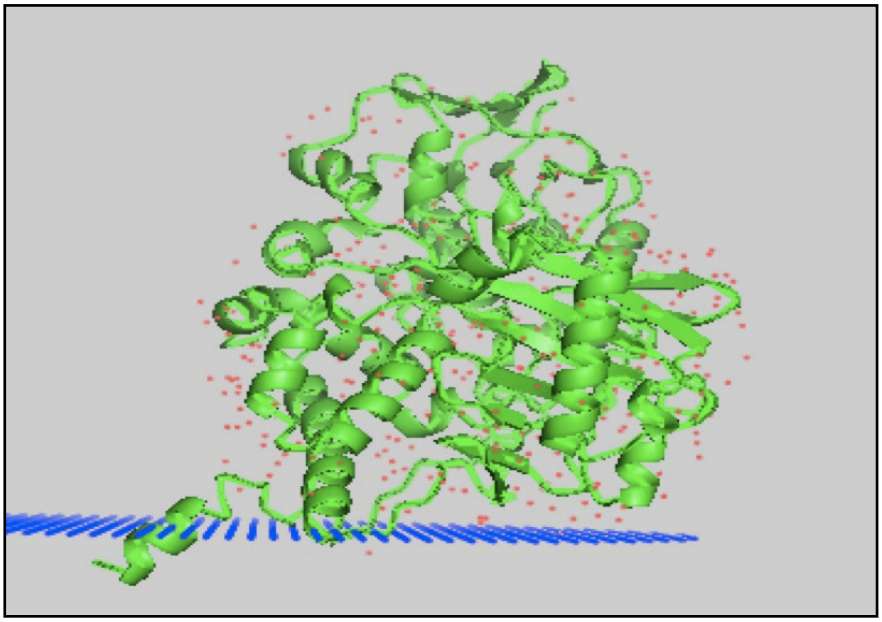

Figure-1.8: Binding of MAO-B to the mitochondrial membrane and locations of amino acids at the membrane binding regions, according to crystallographic data [17]

1.4 Biosynthesis and Biodegradation of Neurotransmitters

MAO catalyzes the oxidative deamination of neurotransmitters and some other biologic amines. Some of these neurotransmitters and amines are dopamine, epinephrine (adrenaline), norephinephrine (noradrenalin, NA), serotonin (5-HT), tyramine, tryptamine, PEA (2-phenylethylamine) and MPTP (1-methyl-4-phenyl-1, 2,3,6-tetrahydropyridine). Furthermore MAO also serves as a cytoprotective role by degrading exogenous amines, which exert their toxicity by affecting cardiovascular and endocrine homeostasis.

Norephinephrine and serotonin are inhibited by MAO-A and phenylethylamine and benzylamine are inhibited by MAO-B. Both of the two enzymes inhibit dopamine, and tyramine, but dopamine by MAO-A, and tyramine by MAO-B are inhibited much more effectively (Figure-1.9).

MAO-A inhibition (e.g. with *clorgiline*) regulates depressive and anxiolytic influences caused by increasing of 5-HT and NA levels at the brain. MAO-B inhibition (e.g. with *l*-deprenyl) helps the treatment of neurodegenerative diseases caused by increasing of PEA, benzylamine, and MPTP levels.

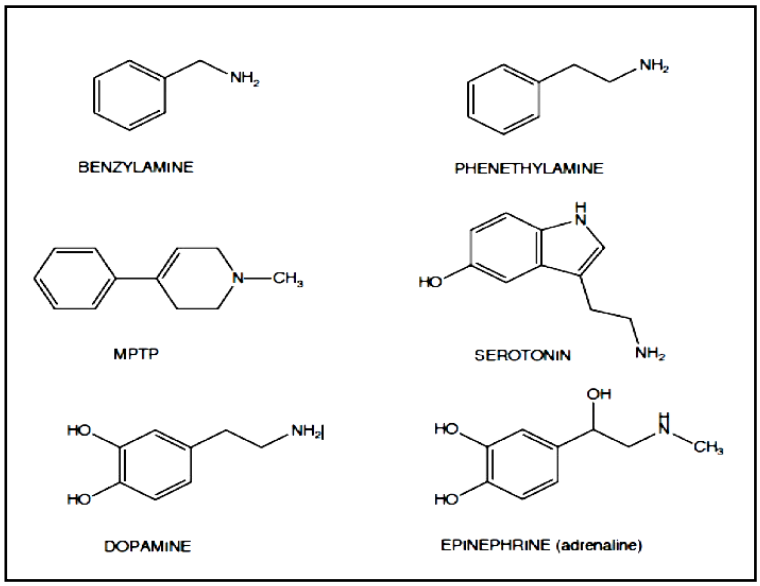

Figure-1.9: Chemical structures of some amines which are related with MAO isoenzymes.

Biosynthesis and metabolization steps of these catecholamine's can be summarized like this:

L-DOPA (3,4-4 dihydroxy phenylalanine) is synthesized from tyrosine by tyrosine hydroxylase enzyme. L-DOPA is decarboxylased into dopamine by dopa decarboxylase enzyme. After crossing blood-brain barrier, L-DOPA is converted to dopamine. Dopamine is stored in chromaffin cells and vesicles. Dopamine in the dopamine vesicles is hydroxylased into norephinephrine by hydroxylase enzyme. Norephinephrine, which is released into cytoplasm from vesicles, is methylated by *fenylethanolamine-N-methyltransferase* (PNMT) enzyme and turned into epinephrine (Figure-1.10).

For serotonin biosynthesis, 5-hydroxy tryptophan is produced from tryptophan amino acid by *tryptophan hydroxylase* enzyme. After that 5-hydroxy tryptamine (serotonin) is produced by using L-amino acid decarboxylase enzyme (Figure-1.10).

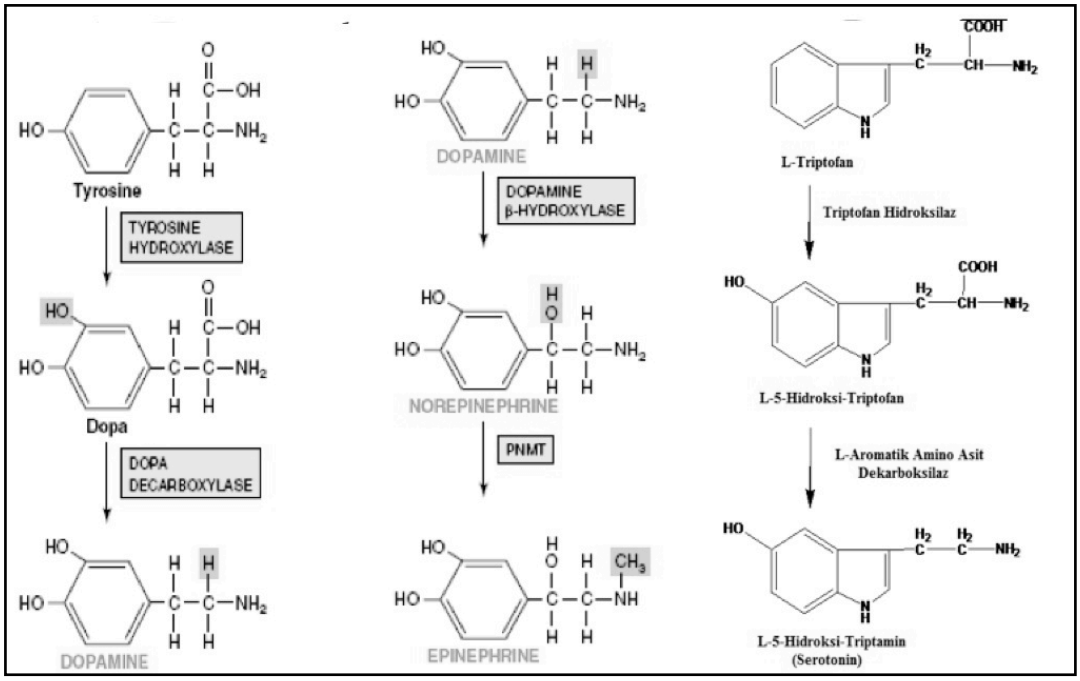

Figure-1.10: Biosynthesis of neurotransmitters that are synthesized from tyrosine and tryptophan.

Catecholamines are released into synaptic cleft, and then they bind into effectors cell receptors and perform their specific activity. After that catecholamines biodegrade in intercellular or extracellular environment by MAO isoenzymes, and catechol-O-methyl-tansferase (COMT) reuptake from synaptic cleft by specific enzyme transporters. (Figure-1.11)

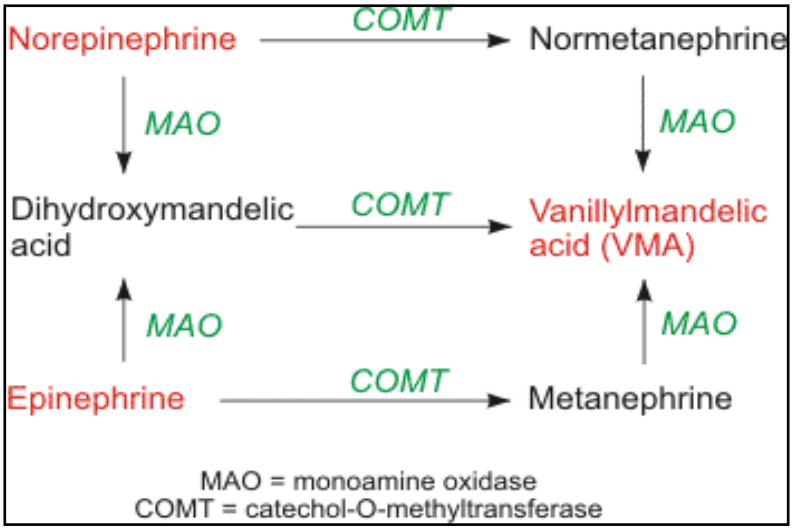

Figure 1.11: Biodegredation of catecholamines via COMT and MAO enzymes

1.5 Amine Catalysis Reaction of MAO Isoenzymes

The chemical reaction catalyzed by MAO requires FAD as a redox cofactor and it is performed on monoamine substrates in their neutral, deprotonated forms (Edmondson et al., 1993, Miller and Edmondson, 1999) and consists of the conversion of monoamines into corresponding aldehydes [6, 7, 11, 18, 19].

Research has shown that the catalytic action of MAO starts with cleavage of the C_{α}-H bond of the deprotonated form of monoamine substrates. Specifically, FAD accepts two hydrogen atoms and is reduced to $FADH_2$, while the amine is converted into the corresponding imine (Figure-1.12, 1.13):

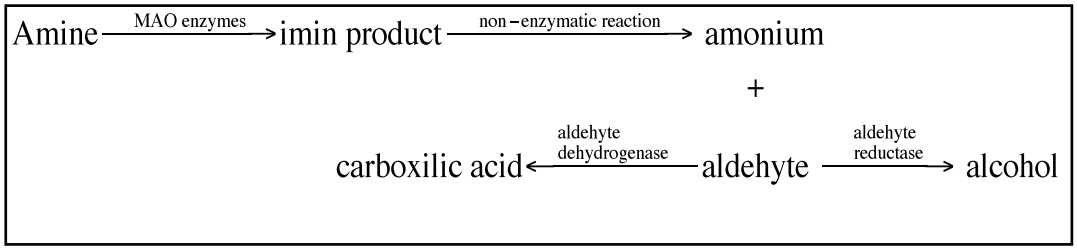

Figure-1.12: Amine catabolism reaction

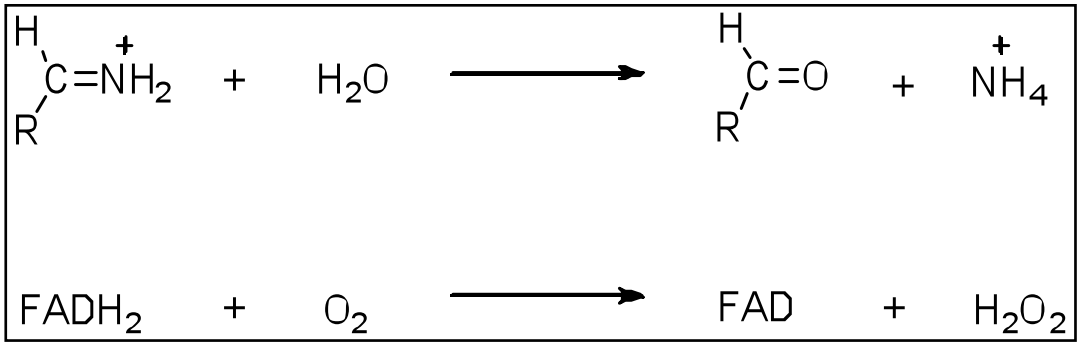

Figure 1.13: Chemical reaction catalyzed by MAO isoenzymes

In most cases, the second step of MAO reaction consists of the re-oxidation of $FADH_2$, with the conversion of oxygen into hydrogen peroxide. Finally, the imine is hydrolyzed into the corresponding aldehyde and ammonia.

Today the mechanism of MAO oxidation reaction of amines has not been identified thoroughly, but three proposed mechanisms are important. These are summarized below:

1.5.1 Single Electron Transfer Mechanism (SET)

The SET pathway proposed by Silverman and colleagues (Figure 1.14). The SET pathway is believed to proceed via one-electron transfer from the amine lone pair to the oxidized flavin adenine dinucleotide, which gives the amine radical cation (**2,** Figure 1.14) and the flavin semiquinone ($FADH^{\cdot}$). Loss of a proton gives the α -amino radical (**3,** Figure 1.14), which can transfer the second electron to the

flavin semiquinone to give the reduced flavin ($FADH_2$) and the iminium product (**4,** Figure 1.14) [6, 7, 11, 18, 19].

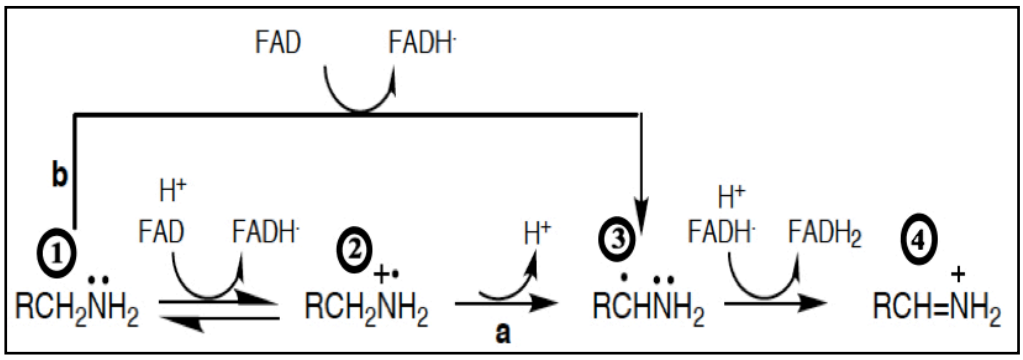

Figure-1.14: Proposed Radical Mechanism for MAO Catalysis

1.5.2 Polar Addition-Elimination Pathway

The flavin analog *3-methyl-5-ethyl-lumiflavinium perchlorate* (Figure-1.15) was used by *Mariano*. He worked on a chemical model to study three major MAO inactivators; cyclopropylamines, α-silylamines and hydrazine's. From the results of these studies, Mariano proposed that the MAO catalysis could proceed via an addition-elimination mechanism (Figure-1.16). The amine (**1)** (Figure-1.16) acts as a nucleophile to attack the activated flavin to form an amine-flavin adduct (**2)** (Figure 1.16). In a concerted step that follows, the amine-flavin adduct cleaves to release the imine (**3)** (Figure 1.16) and the reduced flavin. Further hydrolysis of the imine leads to the aldehyde (**4**) (Figure 1.16) and ammonia [6, 7, 11, 18, 19].

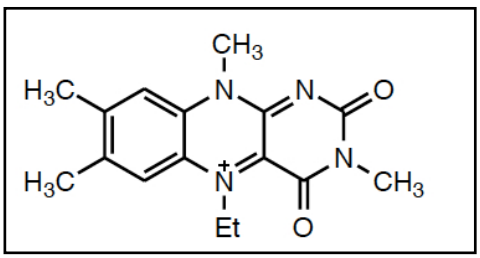

Figure-1.15: Chemical structure of flavin analog 3-methyl-5-ethyllumiflavinium perchlorate

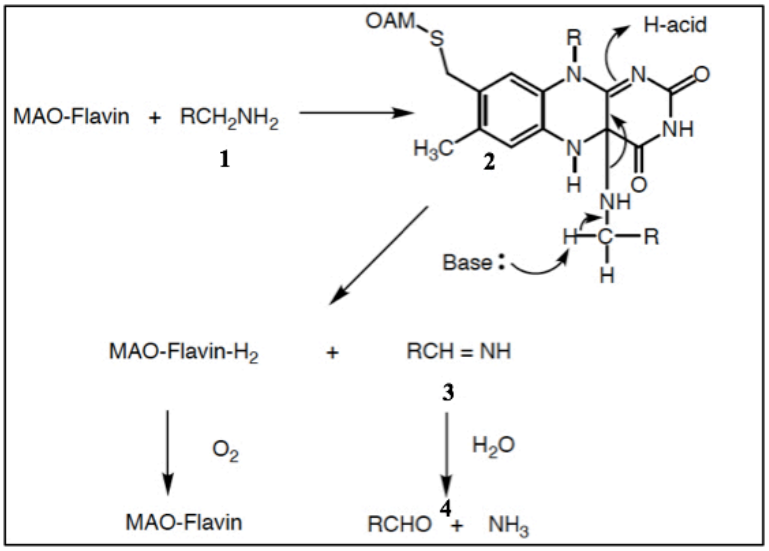

Figure-1.16: Proposed Polar Addition-Elimination Mechanism

1.5.3 Hydrogen Atom Transfer (HAT)

In 1967, *Hull* performed studies on primary amine oxidations by ClO_2 and demonstrated that in addition to the SET pathway, there was also an operative HAT pathway that generated a carbon centred radical by hydrogen atom abstraction from the α-carbon of amines like (**1)** (Figure-1.14, 1.17). Later *Edmondson et al.,* based on work with substituted benzylamines have proposed an alternative pathway for MAO catalysis, which involves hydrogen atom abstraction. The HAT pathway (Figure-1.17) generates the α- carbon radical (**3)** (Figure-1.14, 1.17**)** directly and therefore bypasses the aminium radical cation (**2)** (Figure-1.14**)**. Loss of an electron from (**3**) (Figure-1.14, 1.17) yields (**4)** (Figure-1.14**)**.

$$\overbrace{RCH_2\ddot{N}H_2}^{1} \xrightarrow{FAD \mapsto FADH.} \overbrace{R\dot{C}H_2\ddot{N}H_2}^{3}$$

Figure-1.17: Proposed hydrogen atom transfer mechanism

According to present day information, most of natural substrates are metabolized by both of the MAO isoenzymes, since the cofactor part is similar in both of the MAO isoenzymes. Therefore, the structural differences responsible for substrate specificity are thought to be the other regions of the proteins [6, 7, 11, 18, 19, 20].

Chapter 2: Classifications of Monoamine Oxidase Inhibitors

2.1 Introduction

Monoamine Oxidase inhibitors (MAOIs) are classified as, reversible (competitive or slow tight-binding), and irreversible (affinity labelling agents or mechanism-based inactivators) MAOIs. First produced MAOIs were performing a mechanism-based inhibition by covalently binding to proteins to yield reactive

products. At the same time most of these compounds caused some hepatotoxic side effects by inactivating the P450.

One of the major side effects is called "*cheese effect*". Application of non-selective MAOI and consumption of tyramine contained foods causes the inactivation of both MAO isoenzymes resulting an increased blood tyramine level. Thus the increased tyramine level effects blood pressure and this causes fatal hypertensive crisis. These hypertensive and hepatotoxic side effects caused by the unknown selectivity of MAOIs has substantially limited the application of these drugs, until reversible and selective MAOIs came out. The increasing research on structural and functional information about MAO and their selective inactivation mechanism has created a substantial attention on reversible and selective MAOIs. Research based on new generation of MAO-A selective inhibitors tends to yield promising results for the treatment of depression and MAO-B inhibitors seem to be promising for the treatment of Parkinson and Alzheimer diseases.

According to selectivity and reversibility, MAOI can be classified like this:

2.2 Irreversible (Non-Selective) MAO Inhibitors

These compounds are divided into two as hydrazine derivatives and non-hydrazine derivatives. Iproniazid is the prototype of hydrazine derivatives. Iproniazid was firstly used as a tuberculostatic, but after the recognition of its euphoric effects in patients this drug started to be used as an antidepressant with the trade name "*Marsilid*". Then based on this structure, Phenelzine (Nardil), Isocarboksazid (Marplan) and Nialamide (Niamid) are developed as antidepressants. Later on, it was realized that these antidepressants showed very limited or no selectivity at all to MAO subtypes. These compounds are metabolized by *n-acetylation* and fast biosynthesis of the acetyl hydrazine's produced, creates the mechanism causing the fatal hepatotoxic effects.

The application of these drugs were drastically limited due to metabolization problems and side effects caused by non selective interactions with MAO isoenzyme and after the introduction of tricylic antidepressants, they lost all their popularity.

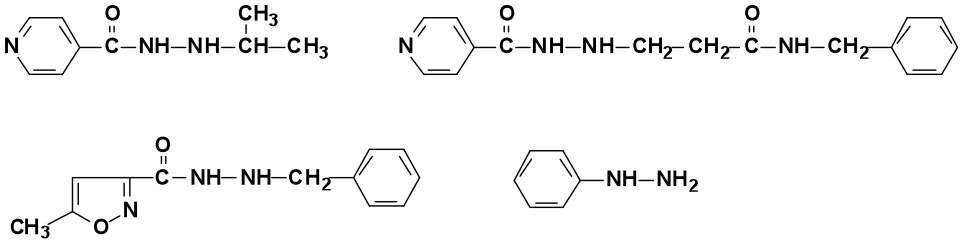

Figure-2.1: Chemical structure of hydrazine derivatives

In Figure-2.1 chemical structure of hydrazine derivatives are illustrated. Here are the major compounds used as a derivative of hydrazine: Benmoxine, Hydralazine, Iproclozide, Iproniazide, Isocaroxazid, Isoniazid, Mebanazine, Nialamide, Octamoxine, Phenelzine, Pheniprazine, Phenoxyproprazine, Pivalylbenzhydrazine, Procarbazine, Safrazine.

Chemical structures of compounds, which include non-hydrazine derivatives, can be seen in Figure-2.2, 2.3 and 2.4. Major molecules, which are used as drugs, are: Caraoxazone, Echinopsidine, Furazolidone, Linezolid and Trancylopromine.

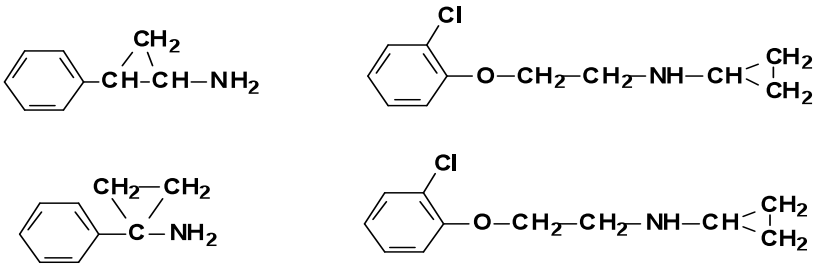

Figure-2.2: Chemical structure of cyclopropylamine derivatives

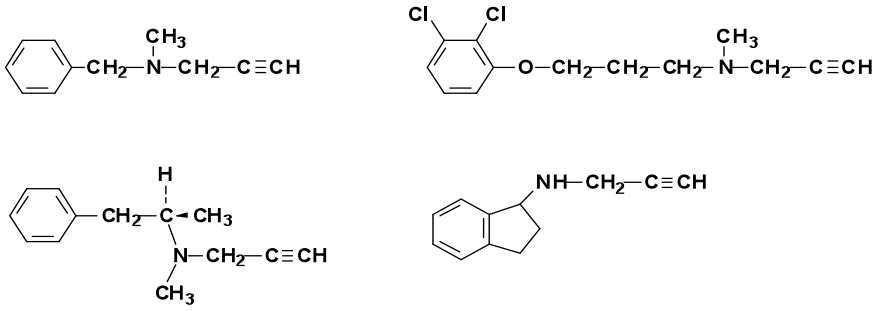

Figure-2.3: Chemical structure of propylamine derivatives

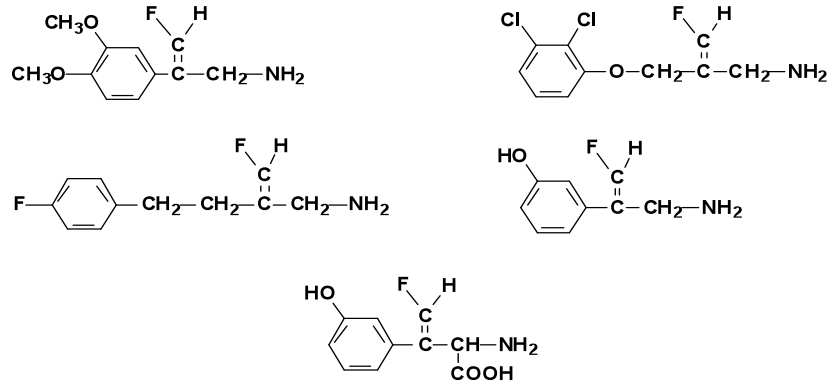

Figure-2.4: Chemical structure of Fluoroallilamin derivatives

2.3 Reversible and Selective MAO Inhibitors:

Different heterocyclic compounds with two or four nitrogen atoms in are the building blocks of reversible and selective MAOIs. Therefore oxadiazolons, tetrazoles and indenopiridazinons were realized to be powerful, reversible and selective MAO-B inhibitors.

Major common properties for substrate inhibition of these compounds can be listed as follows:

- They all contain a benzyloxy group.
- They contain a pentacyclic ring.
- Pentacyclic rings have better affinity to MAO-B than hexacyclic rings.

- The length of side chains of aryldiazo derivatives is not more than 2 carbons like substrates. 2-pyrazoline compounds that have hydrozone structure in the ring have been reported to show MAOI effects and specificity to MAO subtypes and antiparkinson and antidepressants effects.

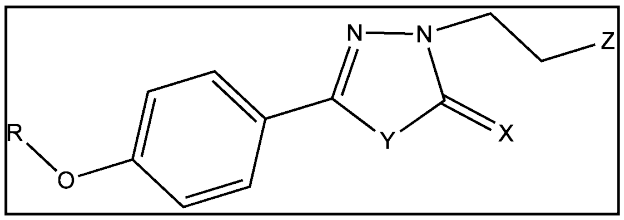

X: O, S Y: O, S, OCH_2 Z: CN, OH

Figure-2.5: Chemical structure of hydrazolone

Some selective MAO-A inhibitors used as medicine are: Brofaromine, Matralindole, Minaprine, Moclobemide, Pirlindole and Toloxatone. Also Lazabemide, Pargyline, Rasagiline, Selegiline can be considered as the major selective MAO-B inhibitors.

Apart from these, there are some compounds, which are currently researched. One of them is Metfendrazine, which is a nonselective MAO inhibitor and hydrazine derivative. Amiflamine, Bazinaprine, Befloxatone, Befol, Cimaxatone, Esuprone, Methylene Blue, Sercloramine, Tetrindole, Thesputiaint, Tyrima, D-Deprenyl, Ladostigil, Milacemide and Mofegiline are some of the promising compounds that inhibit MAO-B selectively [1, 20, 21].

In recent years for the inhibition of monoamine oxidase 8-benzyloxycaffeine, β-carboline, hydrazine, hydrazothiazole, chromone, indol, benzofuran, flavones, hexahydroindazole, 2-arylthiomorpholine, benzylidene-prop-2-ynyl-amines, naphthylisopropylamine, N-benzylamphetamine, (E)-styrylisatin and their derivatives are under investigation in recent years can be considered as important compounds [23-25].

Properties of some significant MAOIs explained are medicines used for and their properties explained below in Table-2.1.

Table-2.1: Some important medicines used for MAOIs and their properties

Name	**Chemical Structures**	**Used for**	**Inhibit MAO-A or MAO-B**	**Reversible/ irreversible**	**Selective/ non-selective**	**Important properties**
Nialamide (Niamid)	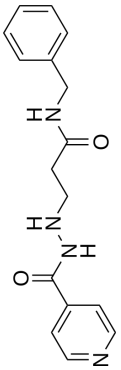	Antidepressant anxiolytic	A	Irreversible	Nonselective	Hydrazine derivative
Isocarboxazid (Enerzer, Marplan, Marplon)	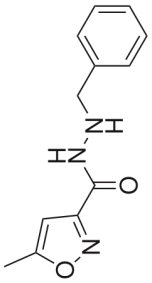	Antidepressant Anxiolytic	A	Irreversible	Nonselective	Hydrazine derivative and cheese effect

Phenelzine: (Nardil, Nardelzine)	Tranylcypromine (Parnate, Jatrosom)	Moclobemide (Aurorix, Manerix)	Selegiline (L-deprenyl, Eldepryl, Emsam, Zelapar)	Rasagiline (Azilect)
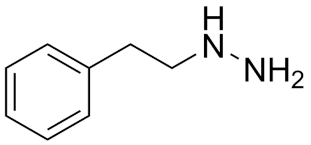	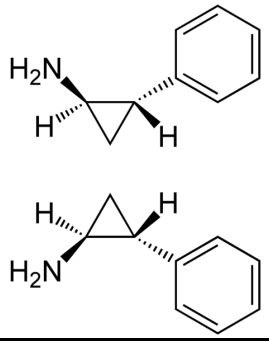	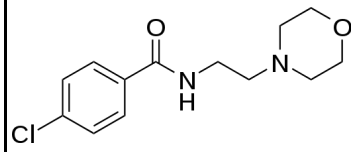	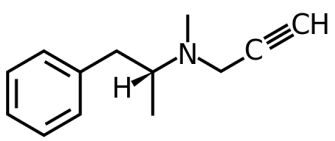	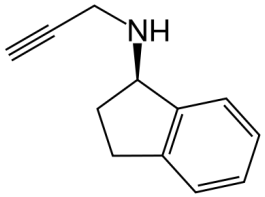
Antidepressant and anxiolytic.	Antidepressant and anxiolytic agent	Depression and social anxiety	Early-stage Parkinson's disease, depression and senile dementia.	Parkinson disease
A	A	A	B in large dose also inhibit A MAO-A	B
Irreversible	Irreversible	Reversible	Irreversible	Irreversible
Nonselective	Nonselective	Selective	Selective	Selective
Hydrazine derivative	Related with amphetamine	Cheese effect is not observed.	Phenylethylamine derivative related with amphetamine	

Name	Chemical Structures	Used for	Inhibit MAO-A or MAO-B	Reversible/ irreversible	Selective/ non-selective	Important properties

Continuation of Table-2.1

Chapter 3: Methods and Procedures Used in Molecular Modeling

3.1 Introduction

Drug molecules show their effect by inhibiting the enzymes. Molecules that have lower binding specificity to other enzymes and the substrates that inhibit the enzyme at a lower concentrate are considered to be strong inhibitors. These properties influence the side effects and toxicity of the drug.

The method I used in my study is called *Structure Based Drug Design* and it is one of the modern drug design methods. In this method firstly, using NMR, X-Ray, etc identifies the crystallographic structure of the enzyme. Today there are more than 70000 proteins in the Protein Data Bank (PDB) whose 3-D structure has been determined by crystallography of NMR techniques, and they are the fundamental source for computer aided drug design studies.

Then many ligands are docked to the enzyme in silico. In my study ligands, that were not previously synthesized, were designed. This is called "*de-novo design*". Then these ligands were docked with MAO enzymes.

Docking is a term used for computational drug design that attempts to find best matching between a receptor and a ligand. Docking studies consist of three main steps. Those are; the representation of the system, the conformational space search, and the ranking of potential solutions. To find best docking results, an efficient search procedure and a good scoring function, and ideally, the best matching algorithms and scoring schemes should be combined [36-38].

Interaction or binding affinity between two molecules (ligand and the enzyme) is predicted by the scoring functions. First, a virtual system is composed. Then the ligand and the enzyme are placed in this system. Induced fit is achieved between the ligand and the enzyme by minimizing the free energy in the system. To get the optimum induced fit 2 criteria are used:

- Shape cohesion between the ligand and the enzyme
- Interaction Energy

When the ligand and enzyme are brought together, the ligand tries to position itself within the enzyme at the parts called active cavities. At this point the ligand is posed at different angles and its position is changed step by step. At every step (pose) the total energy of the system is estimated by using molecular mechanics force field, and the best score is given where the energy value is the lowest [36-40].

The search algorithm is a process where, all possible conformation and orientation of protein-ligand complex in the binding side, is searched. If ligand is flexible, then program will calculate the energy for each rotation made of each and every rotatable bond it can find. The system is divided into parts and relevant estimations are made for each part. Structural cohesion is observed for both the ligand and the enzyme. The basis of the search algorithm can be defined as follows:

1. Systematic or stochastic torsion search
2. Dynamic molecular simulations
3. Evolved genetic algorithms

In this chapter docking studies of de-novo designed ligands (compound that have not been chemically synthesized preciously), using software named AutoDock, CAESAR (Accelrys Discovery Studio) and GOLD are explained. The scoring functions and algorithms of these software's are explained in the procedure steps.

3.2 Preparation of Enzymes and Ligands

The crystal structures of MAO-A and MAO-B were extracted from the http://www.rcsb.org (Protein Data Bank). Their PDB codes are 2Z5X (MAO-A with inhibitor harmine, resolution 2,2Å) and 2V5Z(MAO-B with inhibitor safinamide, resolution 1,6Å) respectively.

The enzymes extracted from pdb.org were prepared for processing. *Protein Prepare Tool* of Accelrys was used. One monomer was selected for each enzyme and their ligands were deleted, missing parts were completed, and broken structures were aligned. Water molecules were added, physiological ph values were adjusted, ionic strength was set to 0.145 and dielectric constant was set to 10. Then the enzyme structure was minimized and the files were converted to relative formats and saved for the docking procedures [1, 36-40].

The ligands targeted for docking procedures were selected based on the previous studies. The identified main structure (scaffold) and the side chains (R groups) are explained in the next chapter. The 300 ligands structures that were selected, were illustrated by Accelrys software, re-organized, minimized, converted to necessary file formats and saved for the docking procedures [1, 36-40].

The docking procedures that were carried out using different docking software are explained in the following chapters:

3.3 AutoDock and Molecular Docking Studies Performed by AutoDock

AutoDock is an automated procedure for predicting the interaction of ligands with biomacromolecular targets. [41-44].

In the Lamarckian Genetic Algorithm used by AutoDock, the ligand is defined as a chromosome and genes. Ligand's Cartesian coordinates and variables specifying its orientation;and genes representing flexible torsional angles. After the genes are defined, for each individual, translation (x,y,z), orientation, and torsional angle genes are assigned randomly (within extents of grid maps). These gene values of these random individuals are then converted into a corresponding phenotype that allows the assessment of each individual's fitness (total interaction energy of the ligand).

After the selection of reproducing individuals, biological crossover and mutation events take place to create the next generation. In the crossover process, equivalent genes are swapped. A random mutation occurs on the basis of a *Cauchy* distribution is utilized to generate mutations on genes that are selected randomly.

In the LGA, each generation is followed by local search that based on the energy phenotype of each resulting chromosome. If obtained conformation has

lower energy than its predecessor, local search is repeated until encountering higher energy conformation. After this by reverse-transcription of the optimised phenotype back into the genome.

On the other hand, Darwinian local search is based on a blind phenotypic jump that can be either confirmed or ignored according to the phenotypic fitness. Thus, Lamarckian Genetic Algorithm is more efficient compared to Monte Carlo simulated annealing and traditional genetic algorithm (Figure-3.1) .

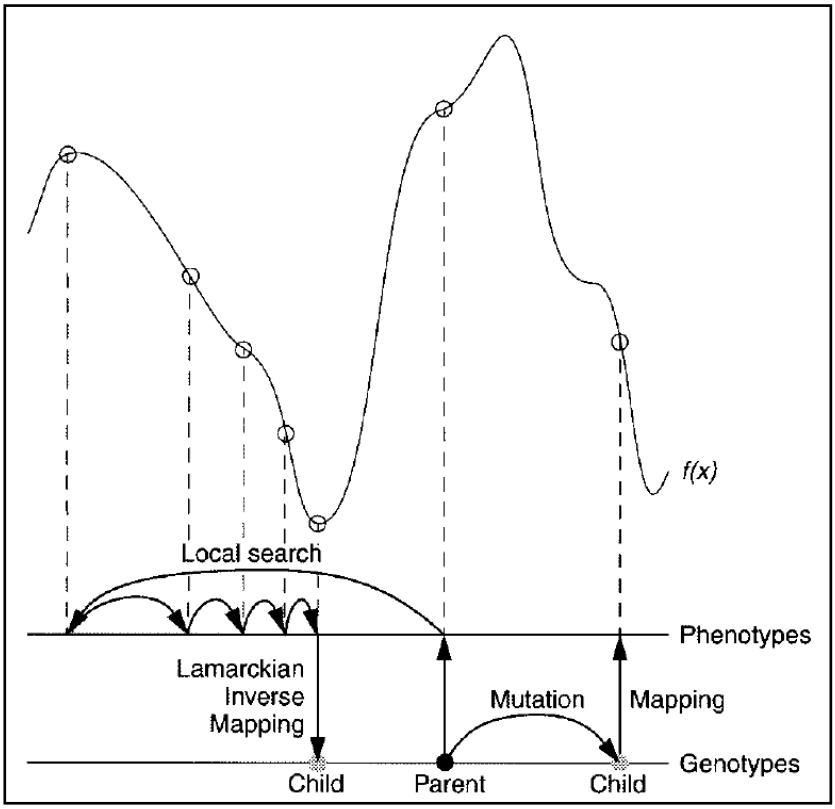

Figure-3.1: Darwinian (right) and Lamarckian(left) local search algorithms (*Morris et al., 1998)*

The force field in AutoDock evaluates binding in two steps which are shown in Figure-3.1. In the begining the ligand and protein start in an unbound conformation and the first step evaluates the intramolecular energetics of the transition state from unbound form to the bound form. In second step, when protein and ligand adopt in

the bound complex, the intermolecular energetics of combining ligand and protein, are evaluated (*Huey et al., 2007*).

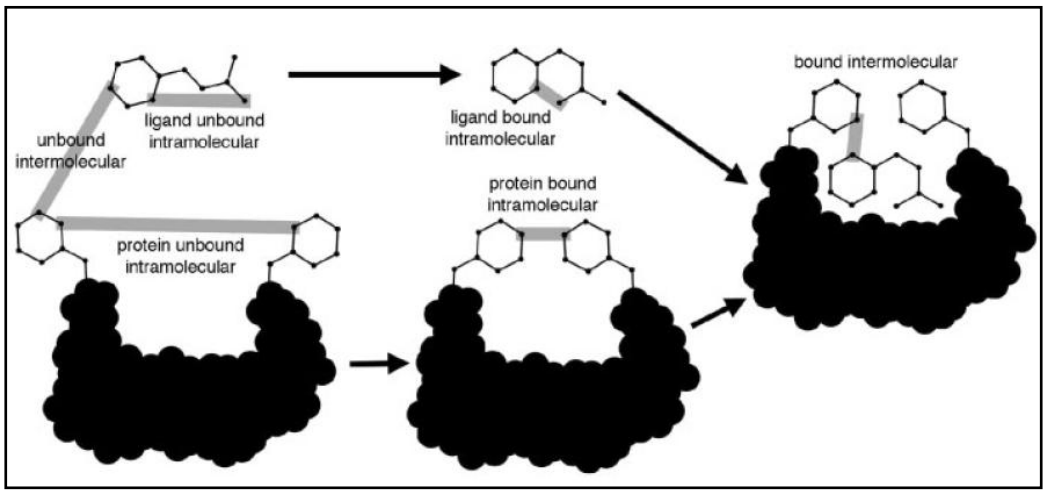

Figure-3.2: Energy evaluation of binding in AutoDock

The force field includes six pair-wise evaluations ($\Delta G^{i\text{-}i}$) and an estimate of the conformational entropy lost upon binding (ΔS_{conf})

$$\Delta G = (\Delta G^{L-L}_{bound} - \Delta G^{L-L}_{unbound}) + (\Delta G^{P-P}_{bound} - \Delta G^{P-P}_{unbound}) + (\Delta G^{P_L}_{bound} - \Delta G^{P-L}_{unbound} + \Delta S_{conf})$$

Equation-3.1: Autodock force field equation

In equation 3.2, L denotes ligand and P denotes for protein (receptor), respectively. First paranthesis are intramolecular energies of bound and unbound states for ligand, respectively. The second paranthesis include are intramolecular energies of bound and unbound states for protein, respectively. The terms in third paranthesis represents the change in intermolecular energy between the bound and unbound states. $\Delta G^{P-L}_{unbound}$ is zero, since it is assumed that two molecules are adequately distant from one another [41-45].

The pair-wise terms (free energies, ΔG) in Equation-3.3, is evaluated by a scoring function based on semiempirical free energy force field with the weighting constants (ΔG_i). These constants are experimentally determined by *Morris et al.in 1996 with* linear regression analysis from a set of protein-ligand complexes with

known binding constants. The Scoring function includes five terms to model dispersion/repulsion, hydrogen bonding, electrostatic interactions, internal ligand torsional constraints and desaolvation effects:

$$\Delta G = \Delta G_{\mathrm{vdW}} \sum_{i,j} \left(\frac{A_{ij}}{r_{ij}^{12}} - \frac{B_{ij}}{r_{ij}^{6}} \right) + \Delta G_{\mathrm{hbond}} \sum_{i,j} E(t) \left(\frac{C_{ij}}{r_{ij}^{12}} - \frac{D_{ij}}{r_{ij}^{10}} \right) + \Delta G_{\mathrm{elec}} \sum_{i,j} \frac{q_i q_j}{\varepsilon(r_{ij}) r_{ij}} + \Delta G_{\mathrm{tor}} N_{\mathrm{tor}} + \Delta G_{\mathrm{sol}} \sum (S_i V_j + S_j V_i) \mathrm{e}^{(-r_{ij}^2 / 2\sigma^2)}$$

Equation-3.2: AutoDock ΔG and scoring function equation

First term is Lennard-Jones 6/12 potential for dispersion/repulsion interactions. Distance between the atoms i and j is represented by r_{ij}. A and B are Amber force field's parameters. The second term is a directional hydrogen bond term based on a 10/12 potential. E(t) is a directional weight that depends on the angle (t) between the probe and the target atom .The third term represents the Coulomb potential for electrostatic interactions between charged particles. The parameters q_i, q_j are partial charges of the atoms, ε is the permittivity. Entropic penalty term is for the loss of torsional entropy upon binding (ΔG_{tor}), that is directly proportional to the number of rotatable bonds in the molecule (N_{tor}). The last term is a desolvation potential based on the volume (V_i and V_j) of the atoms surrounding a given atom. Parameter S (S_i and S_j) and σ are the weighting factors for volumes and distance, respectively [45].

In AutoDock, energy calculations are performed by creating grid maps before starting the docking of the ligand to the receptor. These maps are calculated by

Autogrid and created by placing the receptor protein inside a user defined three dimensional grid box. Probe atom is placed on each grid point, seperated by "*grid spacing*" and the maps are created for each type of atom involved in docking, then these maps are stored in seperate grid files that can later be sampled by the main AutoDock routine. Thus, recalculation of the distances involved in scoring function at each energy evaluation is avoided and this leads to a decrease in computational time [45].

Docking studies were performed using AutoDock 4.02 and MGLTools 1.5.4 based on protein and ligand files created by Accelrys. To achieve this firstly *. pdbqt files were generated from the *.pdb files. *.gpf files was generated as a template for ligands. Information of atoms in the summary.txt was edited in this *.gpf file for all ligands. Then the Auto Grid software is executed using *.pdbqt files and all the generated files (receptor *.pdbqt and *.gpf; ligand*.pdbqt and *.map) are stored in a directory. Then these files are reproduced by using a script for each ligand, and *.dpf files and docking directories were generated. Docking was performed with the necessary scripts and *.dlg files were generated. The main parameters used in this study are listed in Table 3.1:

Table-3.1: Important parameters used for AutoDock studies

Number of grid points in xyz	80 x 80 x 80
Grid spacing	0.375 Å
Centered atom	FAD N5 atom
Number of GA-LS runs	100
Number of individuals in population	150
Maximum number of energy evaluations	5000000
Maximum number of generations	27000
Rate of gene mutation	0.02
Rate of crossover	0.8
Cluster tolerance RMSD	2.0 Å

3.4 GOLD and Molecular Docking Studies Performed by GOLD

GOLD v.4.011 (*Genetic Optimization for Ligand Docking*) is an automated docking optimization tool that uses different genetic algorithms for docking flexible ligands into a protein-binding site (*Jones and al., 1995, 1997*). The scoring function that ranks the binding sides consists of terms of hydrogen bonding, pair wise dispersion potential that is able to describe a significant contribution to hydrophobic energy of binding and a molecular mechanics term of internal energy of the ligand [1, 39, 46, 47].

In my study, the fitness functions used in GOLD are Gold-Score (*Jones and al., 1995*) and Chem-Score (*Eldridge and al., 1997*). GOLD uses a genetic algorithm to search favorable ligand poses. A population of chromosomes is manipulated during genetic algorithm run, with each chromosome representing a trial docking. A chromosome contains all the information's needed to completely define a trial ligand pose and is associated with a fitness value, computed from the scoring function. The Gold-Score fitness function is the force field based and utilized to predict peptide binding positions, it consists of four components; Protein-ligand hydrogen bond energy, protein- ligand Vdw energy, ligand internal Vdw energy and ligand intramolecular hydrogen bond energy. The equation for Gold-Score fitness is shown in Equation-3.4 with ext (protein-ligand energy), int (ligand internal term) terms indicated. Score (int) includes both ligand Vdw energy and ligand torsional term.

$$GoldScore = Score_{hbond_ext} + Score_{vdW_ext} + Score_{hbond_int} + Score_{int}$$

Equation-3.3: GOLD score parameters

The Chem-Score fitness function is empirical and calculates the free energy of ligand binding. Chem-Score consists of contact terms as follows: lipophilic and

metal-ligand binding contributions, hydrogen bonding, internal torsion terms, covalent and constraint scores as shown in equation-3.5. The complete equation for binding free energy calculated by Chem-Score is shown in Equation-3.6.

$$ChemScore = \Delta G_{binding} + P_{clash} + c_{\text{int}} + (c_{\text{cov}} P_{\text{cov}} + P_{constra\,\text{int}})$$

Equation-3.4: Chem-Score parameters

$$\Delta G_{binding} = \Delta G_0 + \Delta G_{hbond} + \Delta G_{metal} + \Delta G_{lipo} + \Delta G_{prot}$$

Equation-3.5: The complete equation for binding free energy calculated by Chem-Score

Parameters in the equations above consist of binding free energy change, protein-ligand hydrogen bond contribution value and additional constraint contribution. Chem-Score hydrogen bond contribution is calculated over all donor-acceptor pairs of protein and ligand. Protein ligand lipophilic contribution is done by Chem-Score lipo term [1, 39, 46, 47].

In order to perform docking studies with GOLD software, the *.pdb files of the receptors and *.mol2 files of the ligands were used for docking. Firstly the receptors were configured by isolating the single monomer of each enzyme, adding hydrogen atoms, extracting water molecules and their ligands. Then a spherical binding region with a diameter of 15 Å was defined around N5 atom of the FAD. The ligands were defined as flexible. GA run was set to 100. GOLD score and Chem-Score were used for scoring function and the docking speed (the number of parameters that control the precise operation of the genetic algorithm) was set as “most accurate”. The other parameters were set as default [1, 39, 46, 47].

3.5 CAESAR and Molecular Docking Studies Performed by CAESAR

CAESAR (*Conformer Algorithm based on Energy Screening and Recursive Buildup*) is available for conformation generation in the Accelrys Discovery Studio product. Internally, the program represents a molecule as a tree, where the nodes are the smallest conformational units the molecule can be fragmented into and the edges are rotatable bonds linking the units. To expand this tree representation into 3-D space and to generate conformations, lists of conformational templates are assigned to the nodes. Energy calculations are performed by using the Catalyst force field and these parameters derived from the *CHARMm* [48, 49].

The previously generated *.dsv files that include the binding sites of the receptors and the *.sd files of the ligands were used for CAESAR. The parameters were set as default for each tool and runs of the software were performed. The main docking parameters are listed in Table 3.2.

Table-3.2: Important parameters used for CAESAR studies

Docking Parameters	CAESAR
Number of hot spots	100
Docking tolerance number	0.25
Docking preferences	Fast search
Conformation method	CAESAR

In the next chapter the ligands that were generated and the results of the molecular docking are described.

Chapter 4: Ligands Designed by Denovo Molecular Modelling Methods

4.1. Introduction

In the previous studies, the ligands that were designed for MAO isoenzymes have been investigated and their structural properties were analyzed in Chapter 2. Based on these properties, molecular structures called "*scaffold*" were formed. New ligands were created by adding subgroups to these scaffold structures. Since the chiral is the center, docking studies were performed for two optic isomers (R and S forms) of each compound.

These ligands, containing pyrazoline rings, were generated based on a total of 6 scaffolds. Docking procedures of these ligands were carried out by AutoDock, GOLD and CAESAR. Then the results were analyzed and a total of 50 ligands (25 pairs of R and S isoforms) that yield the best scores were selected. Then other docking procedures were carried out with these 50 ligands and the results were analyzed.

In this chapter firstly, structural information of these side groups and the added side groups are discussed. Secondly, the coding system used for this study is explained. And finally, chemical structures of the 50 ligands are listed in the Table-4.7.

4.2 Properties of the Scaffolds and Side Groups of the Generated Ligands

Table-4.1: Naming of the ligands [50].

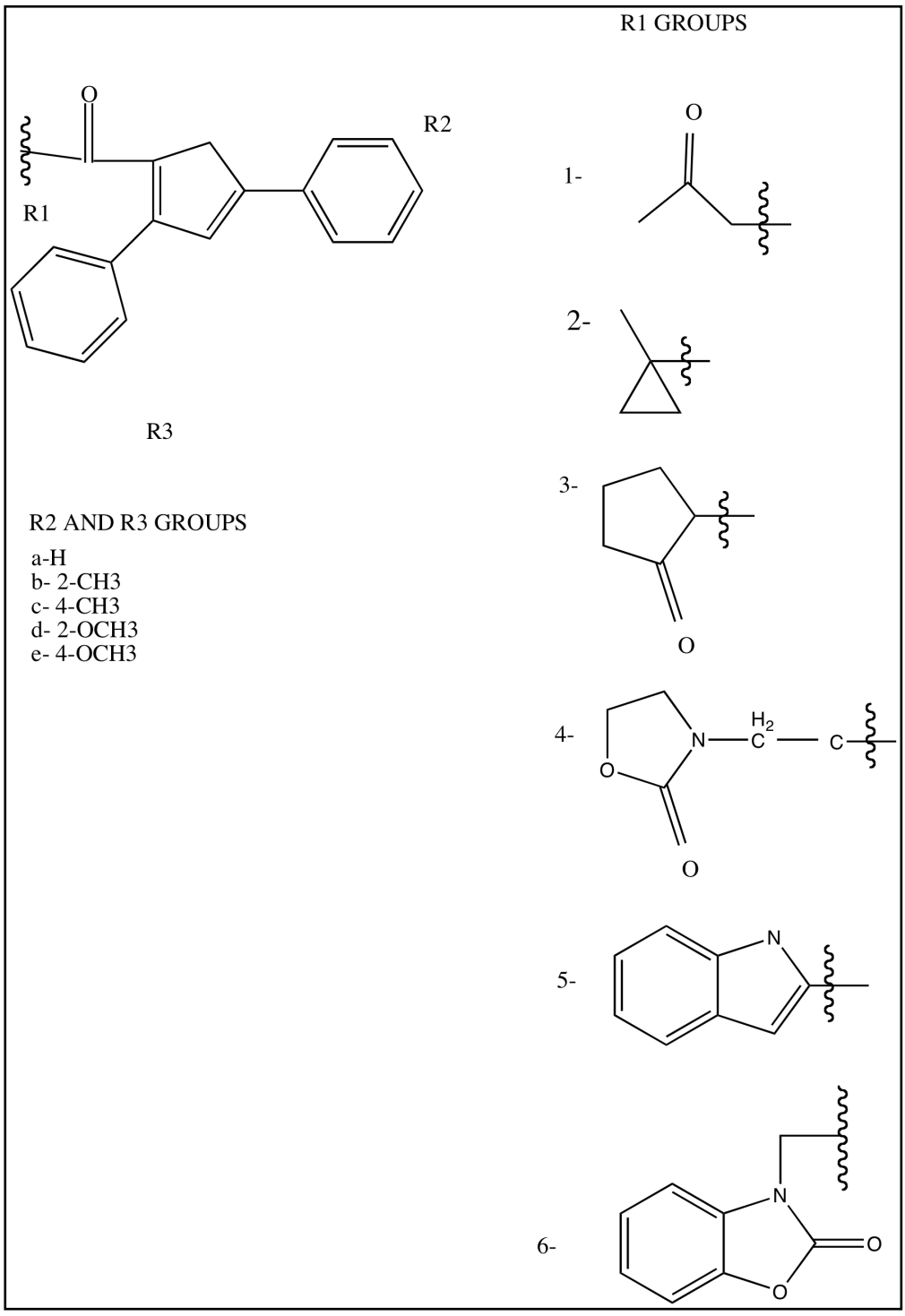

Main ligand structures were generated by adding R groups to a single scaffold for this group. While R1 represents these main ligand structures, R2 and R3

represent the repetition of the side groups that yielded the best scores on the previous studies.

Definitions of the codes that were assigned to ligands are as follows:

1. Parts that form the main scaffold structures were named as R1 and represented by the numbers 1, 2, 3, 4, 5, and 6.
2. Sections named as R2 and R3 are the side groups added to these scaffolds and are represented by the letters a, b, c, d, and e.
3. R and S isomers are represented with the letters “r” and “s” respectively.
4. A total of 300 ligands are generated.

The docking procedures of the ligands generated have been carried out using AutoDock, GOLD, CAESAR software as detailed in Chapter 3. The docking scores of these 2 programs were listed from the highest to the lowest. 25 pairs of ligands yielding the highest scores are selected for processing with the other docking software.

4.3 Ligands Chemical Structure of Selected According AUTODOCK, GOLD and CAESAR Results

Table-4.2: Chemical structure of selected ligands according to AutoDock, GOLD and CAESAR results

1	1aar	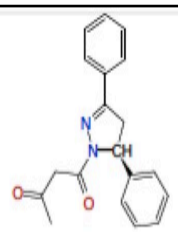	7	1bcr	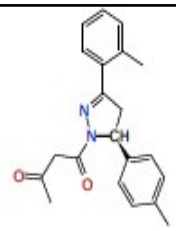
2	1aas	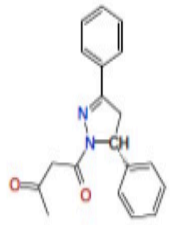	8	1bcs	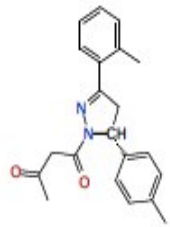
3	1acr	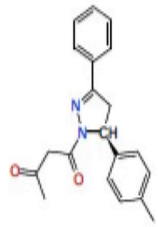	9	1car	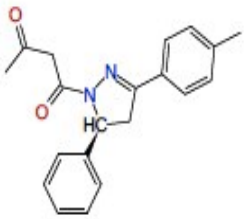
4	1acs	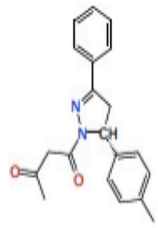	10	1cas	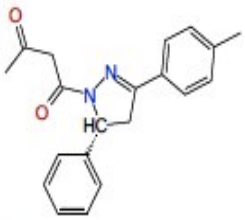
5	1aer	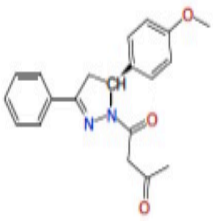	11	1ccr	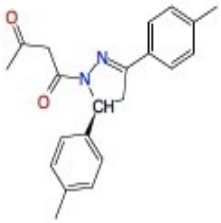
6	1aes	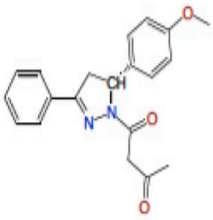	12	1ccs	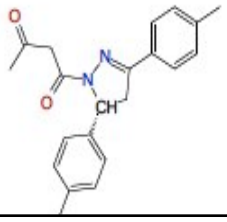

1	1aar	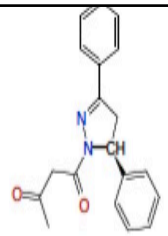
2	1aas	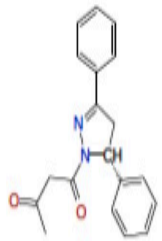
3	1acr	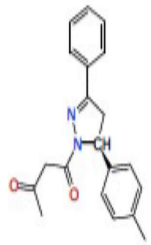
4	1acs	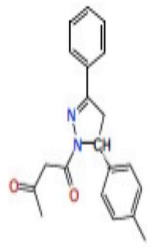
5	1aer	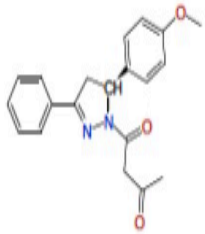
6	1aes	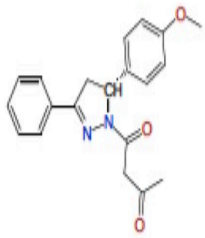
7	1bcr	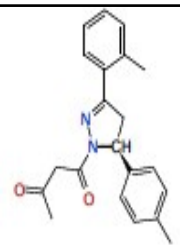
8	1bcs	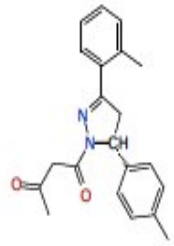
9	1car	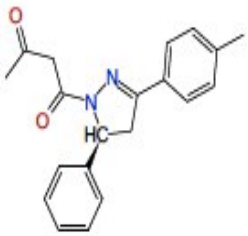
10	1cas	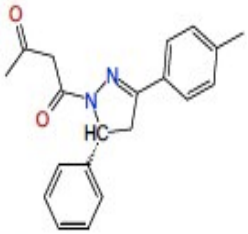
11	1ccr	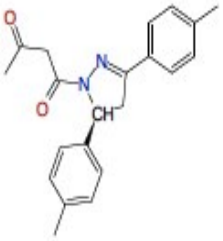
12	1ccs	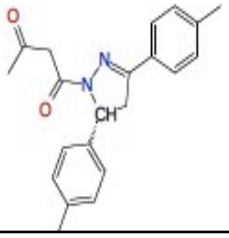

Continuation of Table-4.2

13	1dcr	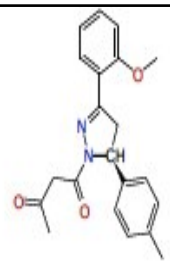	19	1ecr	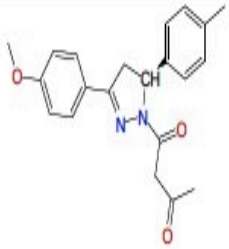
14	1dcs	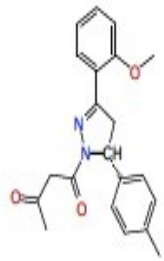	20	1ecs	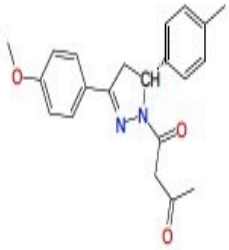
15	1der	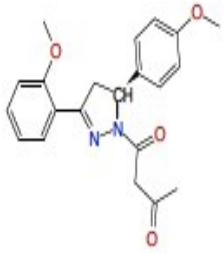	21	1eer	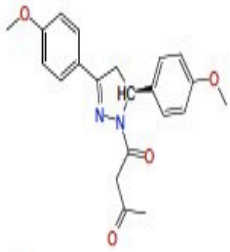
16	1des	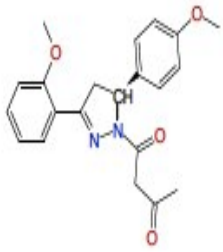	22	1ees	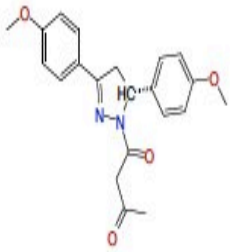
17	1ear	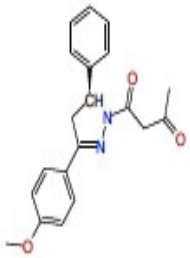	23	3aar	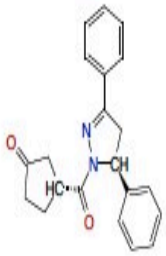
18	1eas	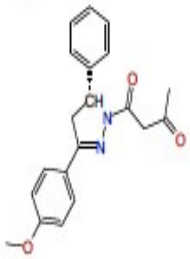	24	3aas	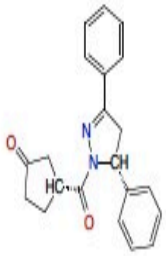

Continuation of Table-4.2

25	3bar	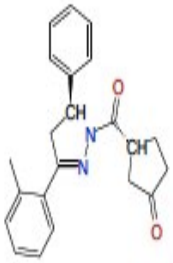	31	4aar	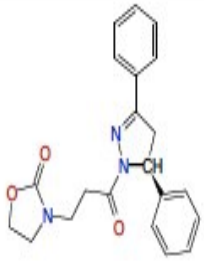
26	3bas	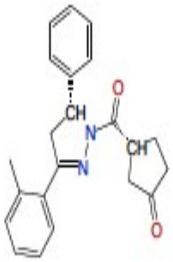	32	4aas	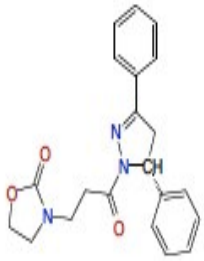
27	3car	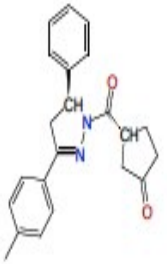	33	4abr	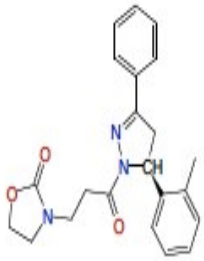
28	3cas	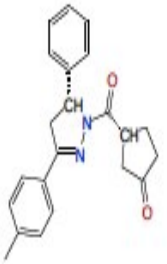	34	4abs	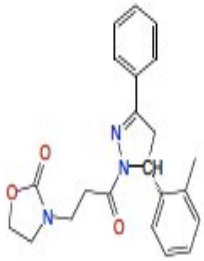
29	3ear	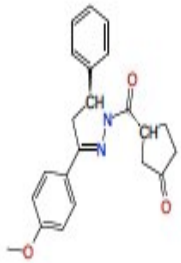	35	4acr	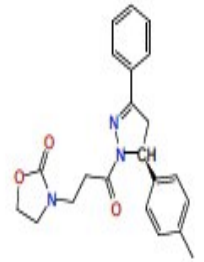
30	3eas	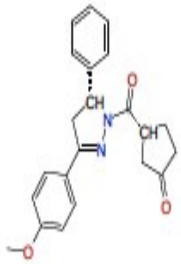	36	4acs	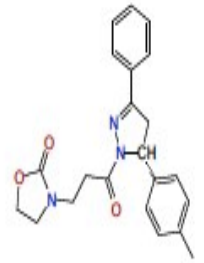

Continuation of Table-4.2

37	4bbr	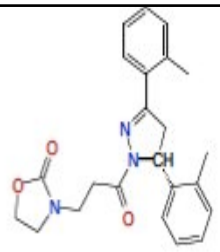
38	4bbs	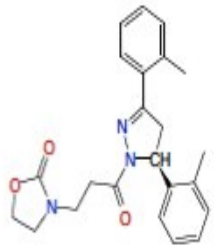
39	4bcr	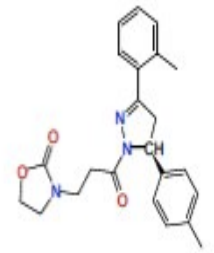
40	4bcs	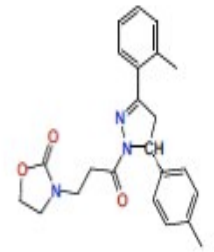
41	4dar	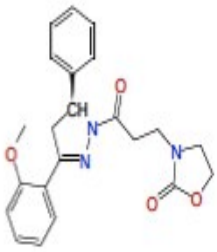
42	4das	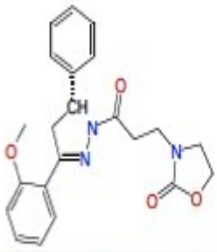

43	5aar	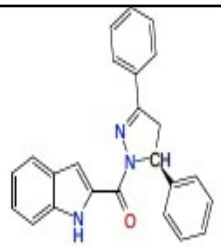
44	5aas	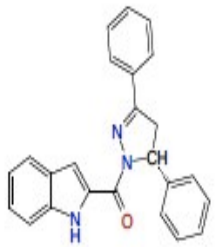
45	5bar	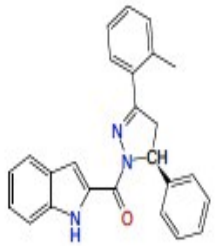
46	5bas	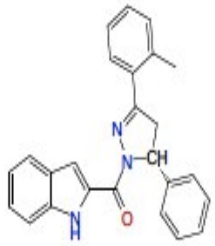
47	5car	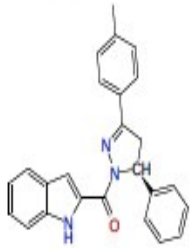
48	5cas	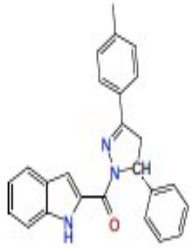

Continuation of Table-4.2

49	5dar	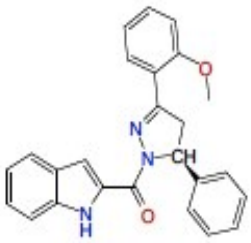
50	5das	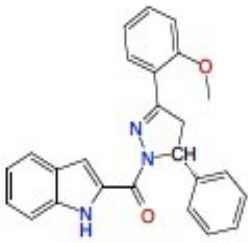

Continuation of Table-4.2

Chapter 5: Results and Discussion

5.1 Introduction

In this chapter 50 ligands that yielded the best scores were selected among the 300 ligands that were generated in this study and the results were analyzed.

Firstly, AutoDock, GOLD and CAESAR scores of all ligands that were generated for his study are listed. Secondly, the 25 pairs of ligands that yielded best scores are selected based on both 2 of the racemic forms (R and S forms). Thirdly, these scores and results were analyzed for both MAO enzymes and the highlights were listed.

Then 3 pairs of ligands (R and S forms) that have the highest potential to become drug candidates are selected for both MAO enzymes and the results were analyzed. Images of these ligands positioned at the sites in the enzymes were illustrated in both 2-D and 3-D format. Their interactions, selectivity and the results for both of the enzymes were analyzed and discussed.

5.2 Docking Results of MAO-A and MAO-B Isoenzymes

The results of the docking studies for the 50 ligands selected are listed on the Table 5.1 below. The criteria used for the selection of these ligands are as follows:

1. The ligand has to yield high scores for MAO-A or MAO-B enzyme in both of the racemic forms.
2. The ligand has to yield acceptable scores in all 3 of the docking methods.
3. If the ligand shows high affinity to only one of the enzymes, the unacceptable scores yielded for the other enzyme can be added to the table for re-evaluation.
4. Taking the above variables into account, the ligands yielding the highest scores among the 300 ligands can be eliminated if necessary.

The reason for this selection process is that, in the event of chemical synthesis both of the racemic forms of the ligand would be synthesized together and if one of the racemic forms yielded a lower score, the molecule containing both racemic forms would show a lower binding affinity and thus the molecule would fail as a drug candidate.

Table-5.1: Docking scores of the 50 ligands obtained by AutoDock, GOLD and CAESAR for MAO-A and MAO-B isoenzymes:

	MAO-A			**MAO-B**		
Ligand code	**AutoDock Ki**	**GOLD**	**CEASAR**	**AutoDock Ki**	**GOLD**	**CEASAR**
1aar	352,17 nM	69,28	104,39	227,08 nM	70,33	104,42
1aas	174,09 nM	73,84	98,11	2,65 uM	72,95	102,24
1acr	147,59 nM	74,21	108,54	160,31 nM	74,35	99,44
1acs	110,52 nM	72,11	99,37	2,64 uM	70,43	96,52
1aer	202,57 nM	75,99	93,14	386,45 nM	75,63	89,85
1aes	124,76 nM	78,5	118,38	5,43 uM	77,82	112,62
1bcr	80,67 nM	79,14	103,73	101,25 nM	79,15	95,62
1bcs	202,51 nM	76,79	123,08	1,54 uM	76,92	93,75
1car	377,10 nM	69,38	112,79	101,71 nM	67,61	109,15
1cas	161,41 nM	70,49	120,59	1,22 uM	70,63	108,99
1ccr	198,92 nM	70,96	105,01	70,71 nM	70,64	98,9
1ccs	163,46 nM	72,97	95,05	1,53 uM	70,12	98,4
1dcr	94,00 nM	77,07	88,03	219,13 nM	75,3	100,48
1dcs	109,60 nM	75,65	76,65	2,18 uM	75,09	98,69
1der	107,95 nM	81,46	86,24	214,96 nM	81,16	104,83

1des	135,20 nM	82,87	94,39	313,58 nM	81,78	104,65
1ear	141,26 nM	73,26	117,88	141,41 nM	73,21	96,85
1eas	165,55 nM	76,92	90,76	1,94 uM	76,88	117,07
1ecr	58,23 nM	76,68	109,66	149,25 nM	76,3	89,87
1ecs	169,92 nM	75,65	106,21	1,48 uM	76,56	95,88
1eer	92,14 nM	76,78	90,46	573,10 nM	76,37	103,92
1ees	307,55 nM	79,35	105,87	6,29 uM	79,05	95,32
3aar	162,43 nM	73,98	103,77	40,38 nM	73,9	102,95
3aas	22,09 nM	76,84	110,24	142,51 nM	76,7	110,21
3bar	118,56 nM	79,35	110,03	30,36 nM	79,14	113,85
3bas	94,69 nM	79,72	84,02	86,11 nM	78,47	85,68
3car	116,42 nM	73,48	105,01	17,53 nM	72,68	109,88
3cas	1,27 uM	72,29	84,66	70,07 nM	72,34	111,95
3ear	70,83 nM	74,86	117,65	33,11 nM	70,15	111,44
3eas	3,25 uM	76,7	83,37	122,55 nM	77,16	116,29
4aar	29,28 nM	78,86	117,84	590,69 nM	78,09	115,08
4aas	8,17 nM	83,54	116,85	1,22 uM	80,87	127,65
4abr	43,49 nM	69,85	116,98	1,29 uM	71,01	114,17
4abs	9,93 nM	82,29	123,08	24,46 uM	81,51	120,26
4acr	28,49 nM	82,69	87,13	571,79 nM	82,96	114,61
4acs	5,93 nM	84,32	112,93	2,13 uM	83,9	117,71
4bbr	11,59 nM	87,44	122,77	9,05 uM	86,88	102,97
4bbs	24,03 nM	74,84	123,34	558,86 nM	74	115,96
4bcr	19,15 nM	86,35	98,69	31,33 nM	85,56	105,28
4bcs	29,16 nM	86,82	107,47	1,28 uM	83,5	103,44
4dar	12,54 nM	81,82	99,7	104,20 nM	80,67	117,13
4das	7,81 nM	88	107,03	1,62 uM	81,24	76,25
5aar	54,25 nM	72,68	117,82	13,41 uM	72,26	116,2
5aas	94,23 nM	87,99	121,73	2,17 uM	87,3	105,8
5bar	27,13 nM	77,6	115,93	10,10 uM	77	106,11
5bas	41,87 nM	92,28	100,02	1,31 uM	91,75	81,45
5car	15,45 nM	69,38	95,13	28,77 mM	69,14	114,76
5cas	144,66 nM	81,46	108,17	211,63 uM	80,83	103,79
5dar	41,70 nM	76,77	118,57	18,77 uM	75,79	133,93
5das	54,58 nM	92,83	115,43	1,49 uM	90,5	114,54

Continuation of Table-5.1

Results based on the analysis of Table 5.1 are listed below:

- Taking the main scaffold structure into account, we observe that 6 scaffolds are generated based on this structure. I conducted my study by changing the side groups of these 6 scaffolds. While 1, 3, 4, 5 series ligands show a good potential as inhibitor candidates, 2 and 6 series seem to be inadequate.
- Ligands show a higher binding affinity to MAO-A enzyme, compared to MAO-B.
- K_i values obtained by AutoDock of the selected 50 ligands for MAO-A range between 5.93 nM and 3.25 uM. Values in micrometers (1 uM = 1000 nM) were observed for only 2 ligands. General average is approximately 104.5 nM, and this can be considered as a good score.
- GOLD scores of the selected 50 ligands for MAO-A are between 69.28 and 92.83. Average is approximately 78.1 and this can be considered as a good score.
- CAESAR scores of the selected 50 ligands for MAO-A are between 76.65 and 123.34. Average is approximately 105.5 and GOLD scores of the selected 50 ligands for MAO-B are between 67.61 and 91.75. Average is approximately 77.3 and this can be considered as a good score. In addition the values are in parallel with MAO-A values.
- CAESAR scores of the selected 50 ligands for MAO-B are between 76.25 and 133.93. Average is approximately 105.73 and this can be considered as a good score. In addition the values are in parallel with MAO-A values.
- Ki values obtained by AutoDock of the selected 50 ligands for MAO-B range between 17.53 nM and 211,63 uM. Values in micrometers (1 uM = 1000 nM) were observed for many more ligands compared to MAO-A. Even an extreme value of 28.77 mM was observed. General average is approximately 104.5 nM.
- If the 2 extreme values of 211.63 uM and 28.77 mM are omitted, the average is recalculated to be approximately 2.6 uM. Even though this score can be considered relatively unpromising, almost half of the ligands yielded nanomolar scores, and this confirm the possibility of obtaining ligands with good inhibition properties.

5.3 Correlation Between Docking Results

Correlation tables are shown below at the Figure-5.1 and 5.2. These correlation tables reflect the results of the three docking procedures relative to each other. The idea behind these correlation tables is to convert all the results into a single unit and discuss the relation and consistency of the procedures.

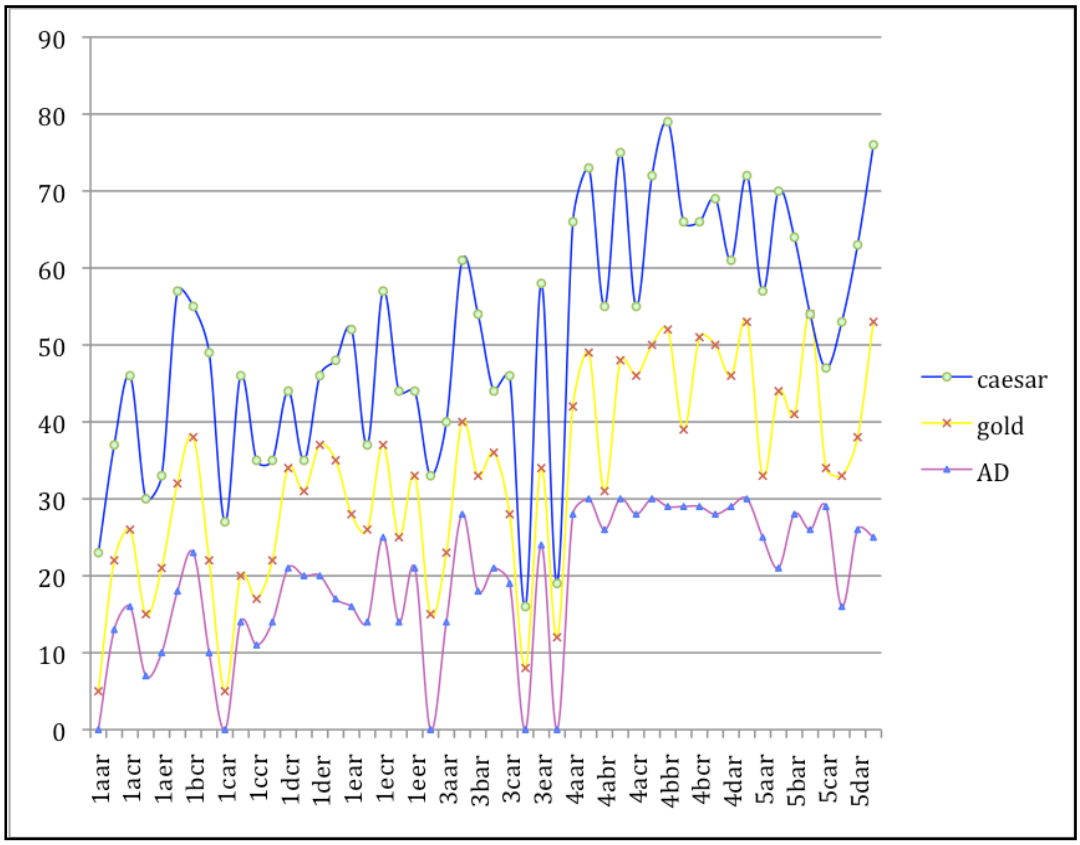

Figure-5.1: Correlation between docking methods for MAO-A graphic

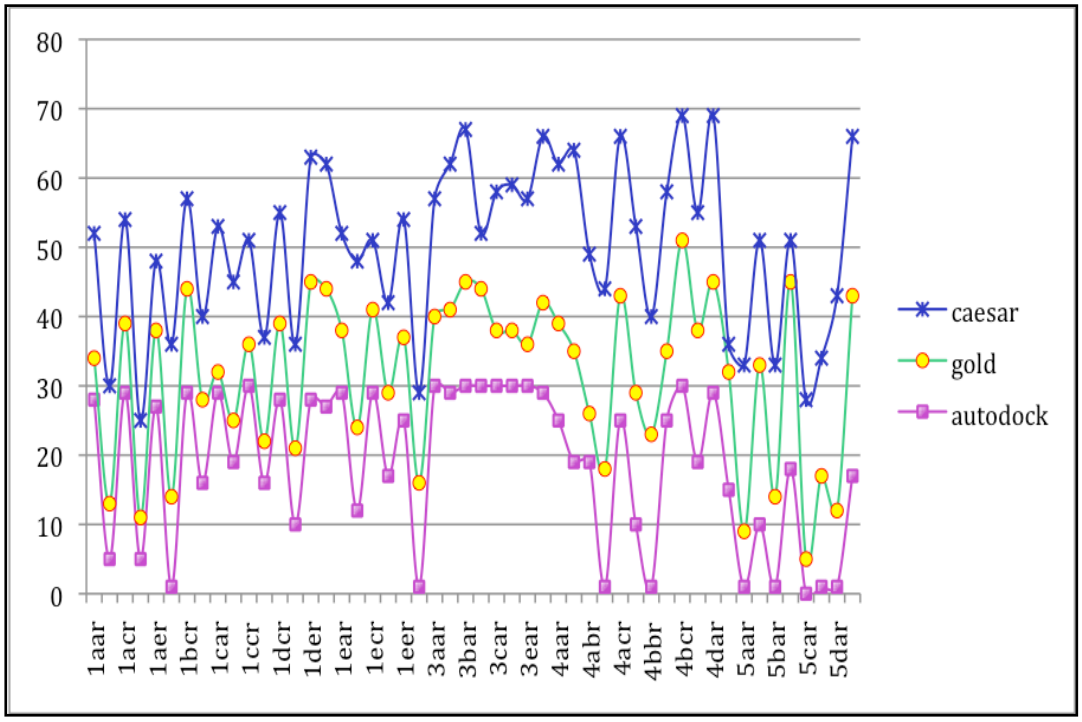

Figure-5.2: Correlation between docking methods for MAO-B graphic

A scoring system was developed in order to put these tables together. In this system, the docking scores yielding the best results were considered to be the highest score in the related interval. Since different docking software use different algorithms and scoring functions, it was not possible to obtain identical score values, but the relative consistency of the curves gives a general idea regarding the correlation of the docking programs. The results of this analysis are listed below:

- There is a high level of correlation between docking programs for MAO-A. Optimal results were observed at the scaffold series of 1, 4, and 5.
- Correlation between docking programs was observed to be better for MAO-B compared to MAO-A. Optimal results for CAESAR were observed at series 3 and 4, for GOLD at series 3, 4, 5, and for AutoDock at series 3 and 4.
- In general the results obtained by different docking software were observed to be in consistency with each other.

5.4 Detailed Analysis of the Fundamental Results of Docking Studies

In this section docking results of R and S isoforms of the 6 ligands that yielded the most promising results were discussed and analyzed in detail.

2-D and 3-D images of the ligands positioned at the binding sites of MAO enzymes were taken and their interactions were analysed according to these images.

5.4.1 Ligands Selected for MAO-A Enzyme

5.4.1.1 Evaluation of 4bcr/4bcs Ligands for MAO-A Enzyme

2-D and 3-D images of 4bcr inhibitor positioned at the active site cavity of MAO-A enzyme by molecular modelling method are illustrated on Figure-5.3 and 5.4

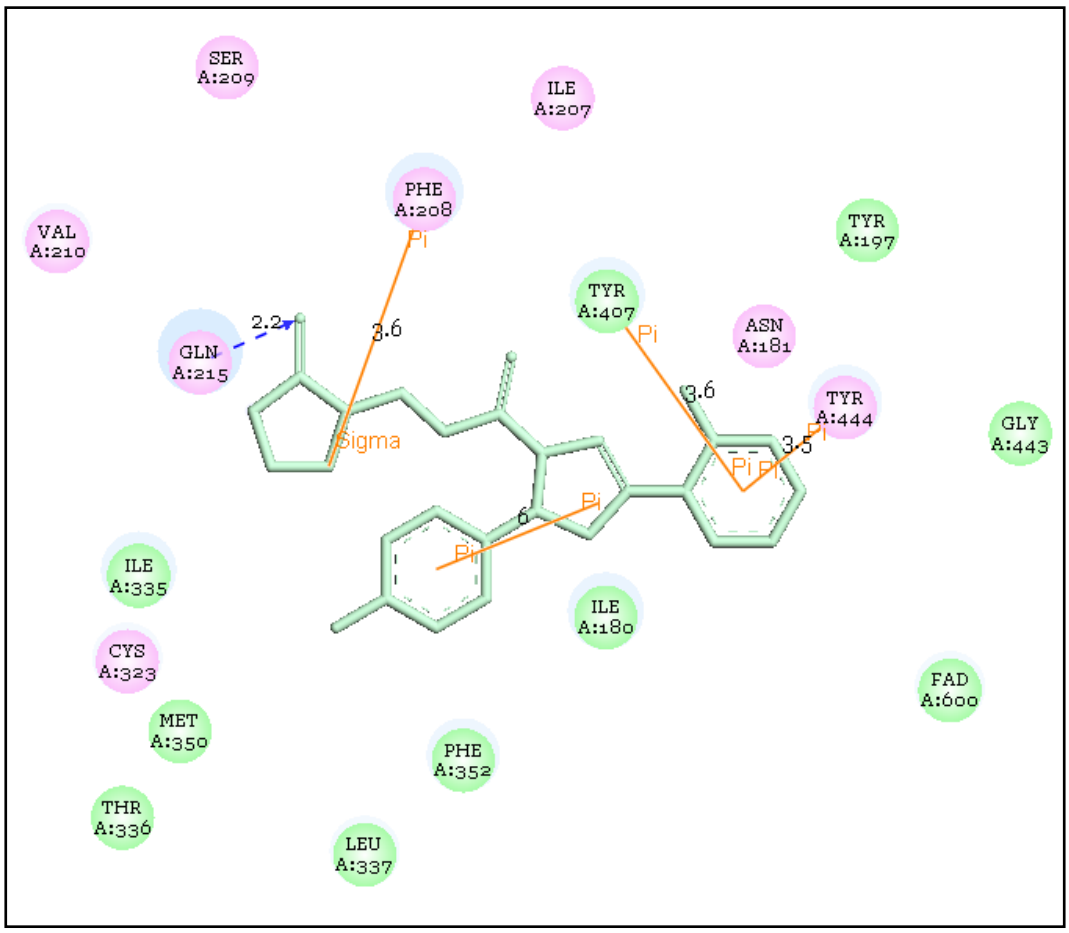

Figure-5.3: Position of 4bcr ligand in MAO-A enzyme and 2-D representation of its interactions

It was observed that pi-pi interaction took place between the phenyl ring of the ligand and the amino acid residues forming the aromatic cage at a distance of 3.5 and 3.6Å. In addition the ligand folded onto itself and formed a pi-pi interaction with furan ring at the center and the other phenyl ring at a distance of 6Å and this increased the stability of the ligand. Further more, a pi-sigma interaction was formed with Phe208 and the furan ring at 3.6Å, and a hydrogen bond was formed with Gln215.

VdW interactions were formed between the inhibitor and the surrounding Val210, Gln215, Cys323, Tyr444, Asn181, Ile207, Phe208, Ser209 amino acids. Polar interactions were formed between the inhibitor and both FAD coenzyme, and Ile335, Met350, Thr336, Leu337, Phe352, Tyr407, Tyr197, Gly443, Ile180 amino acids.

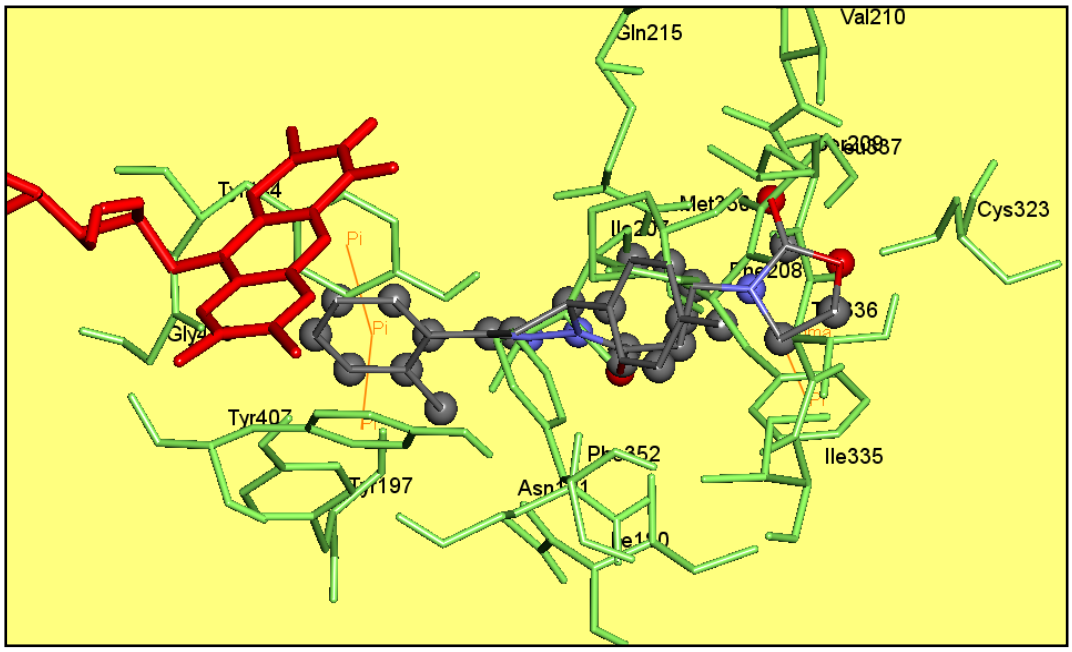

Figure-5.4: Position of 4bcr ligand in MAO-A enzyme and 3-D representation of its interactions

For Mao-A, AutoDock inhibition constant K_i= 19.15nM, GOLD score= 86.35 and CAESAR score= 98.69. For Mao-B, AutoDock inhibition constant K_i= 31.33nM, GOLD score= 85.56 and CAESAR score= 105.28.

Based on my analysis this inhibitor is considered to be a better MAO-A inhibitor candidate because of the interactions of the inhibitor with the coenzyme, the aromatic cage and many amino acids. In addition the phenyl and furan rings of the inhibitor bond with the MAO-A enzyme at a close range.

2-D and 3-D images of 4bcs inhibitor positioned at the active site cavity of MAO-A enzyme by molecular modelling method are illustrated on Figure-5.5 and 5.6.

According to this, pi-sigma interaction took place between the phenyl ring of the inhibitor and Asn181 amino acid at a distance of 3.9 Å.

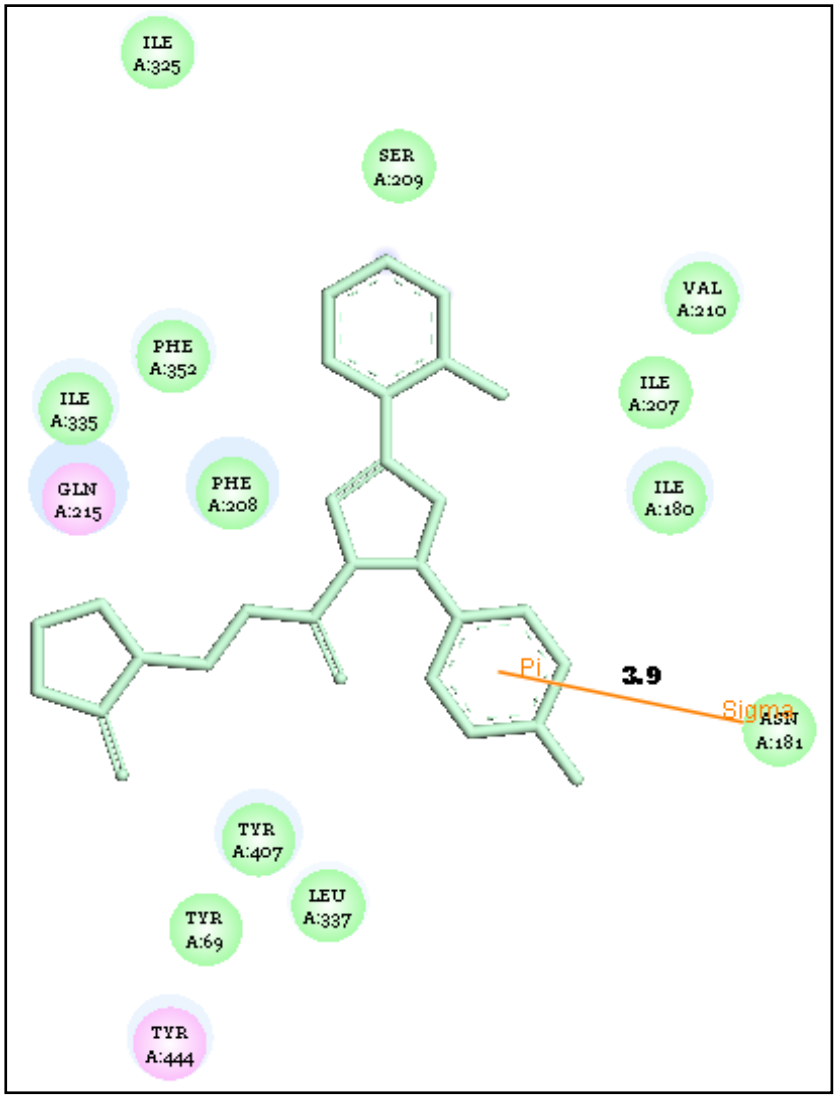

Figure-5.5: Position of 4bcs ligand in MAO-A enzyme and 2-D representation of its interactions

VdW interactions were formed between the inhibitor and the surrounding Ile335, Ser209, Val210, Ile207, Ile180, Asn181, Tyr407, Tyr69, Leu337, Phe208, Ile335, Phe352 amino acids. Polar interactions were formed between the inhibitor and Tyr 444, Gln215 amino acids.

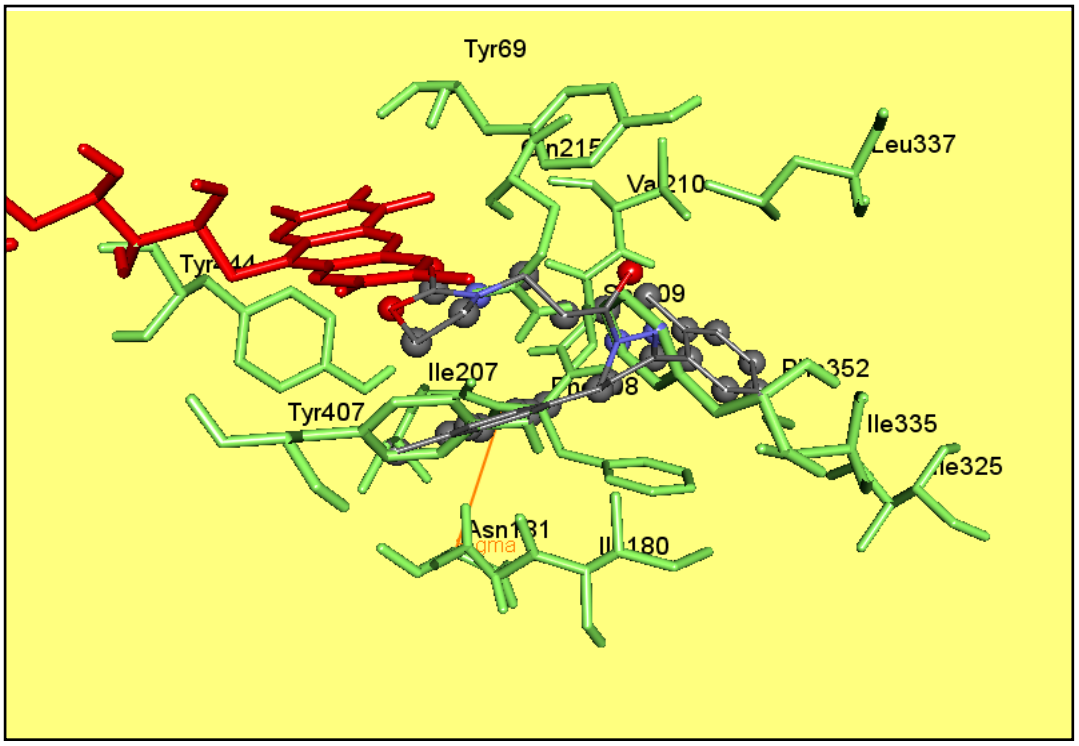

Figure-5.6: Position of 4bcs ligand in MAO-A enzyme and 3-D representation of its interactions

For Mao-A AutoDock inhibition constant K_i= 29.16nM, GOLD score= 86.82 and CAESAR score= 107.47. For Mao-B AutoDock inhibition constant K_i= 1.28uM, GOLD score= 83.50 and CAESAR score=103.44.

The high number of bonding and interactions of this inhibitor with MAO-A, and its positioning right in front of the aromatic cage, show that it is a potentially good MAO-A inhibitor candidate.

When the results of R and S isoforms of the inhibitor are analysed together, strong bonding to the aromatic cage and the great number of amino acid residues surrounding the inhibitor, make 4bcr/4bcs compounds effective inhibitor candidates for MAO-A. In addition when we compare the docking scores of the inhibitor for both MAO-A and MAO-B, we observe that the scores for MAO-A to be higher and this increases the possibility of the inhibitor to be MAO-A selective.

5.4.1.2 Evaluation of 4dar/4das Ligands for MAO-A Enzyme

2-D and 3-D images of 4dar inhibitor positioned at the active site cavity of MAO-A enzyme by molecular modelling methods are illustrated on Figure-5.7 and 5.8

According to this, a pi-pi interaction took place between the phenyl ring and Tyr444 located at the aromatic cage at a relatively short distance of 3.6Å. A pi-sigma interaction took place between the furan ring of the inhibitor and Phe208 at a distance of 3.5Å. In addition just like 4brc, a hydrogen bond was formed between the ligand and Gln215.

VdW interactions were formed between the inhibitor and the surrounding Leu337, Met350, Phe352, Ile335, Ile180, Gly443, Tyr197, Tyr407 amino acids. Polar interactions were formed between the inhibitor and both FAD coenzyme, and Tyr444, Gln215, Val210, Cys323, Asn181, Phe208, Ser209, Ile207 amino acids.

For Mao-A AutoDock inhibition constant K_i= 12.54nM, GOLD score= 81.82 and CAESAR score= 99.70. For Mao-B AutoDock inhibition constant K_i= 104.20nM, GOLD score= 80.67 and CAESAR score= 117.13.

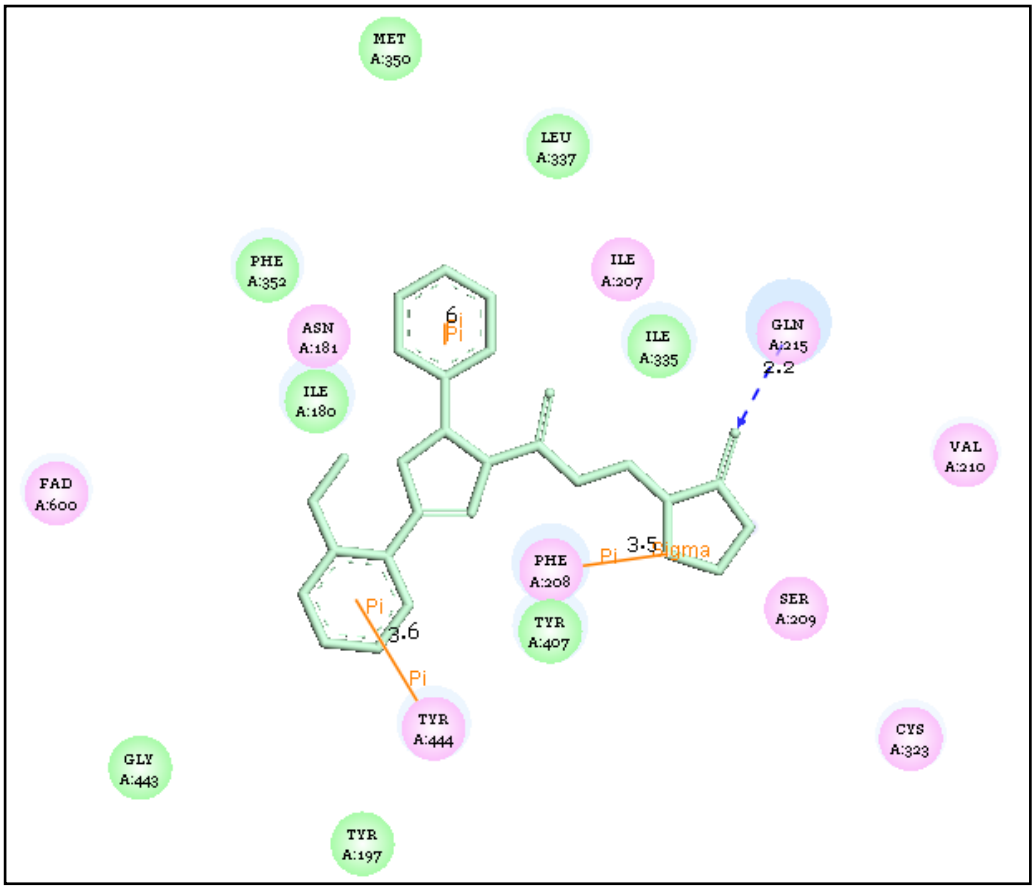

Figure-5.7: Position of 4dar ligand in MAO-A enzyme and 2-D representation of its interactions

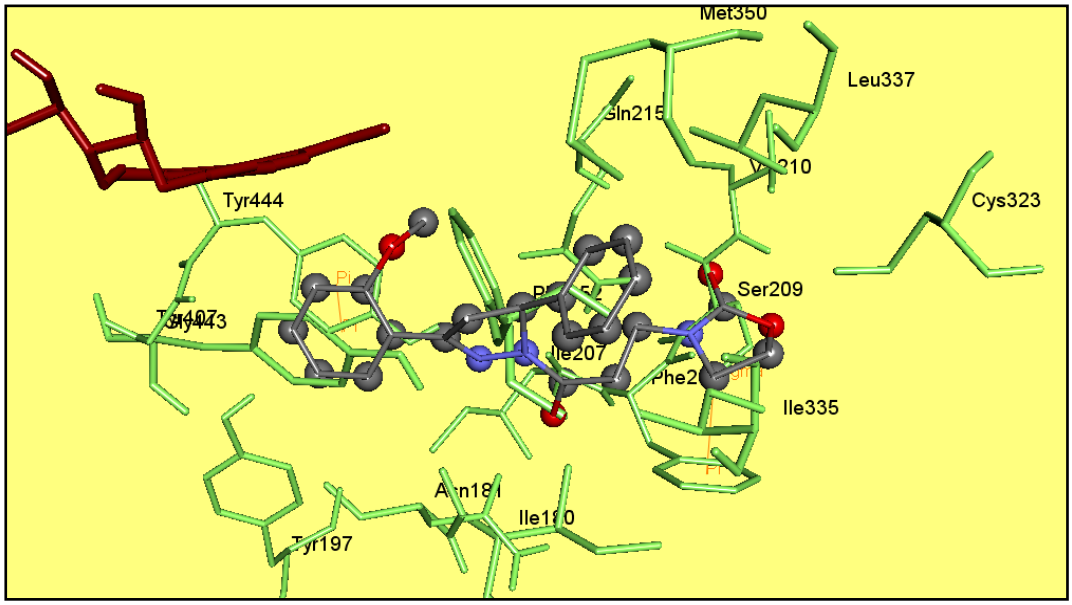

Figure-5.8: Position of 4dar ligand in MAO-A enzyme and 3-D representation of its interactions

The high number of bonding and interactions of this inhibitor with the residues in the aromatic cage, and its positioning right in front of the coenzyme, show that it is a potentially good MAO-A inhibitor candidate.

2-D and 3-D images of 4das inhibitor positioned at the active site cavity of MAO-A enzyme by molecular modelling method are illustrated on Figure-5.9 and 5.10.

Double pi-pi interactions took place between the phenyl ring of the inhibitor and Tyr444 and Tyr407 located in the aromatic cage. In addition pi-sigma interactions took place between Phe208 and furan ring of the inhibitor and Phe208 and another part of the inhibitor and these interactions improved the stability of the compound. Further more, a hydrogen bond was formed with Gln215 amino acid at 1.9Å.

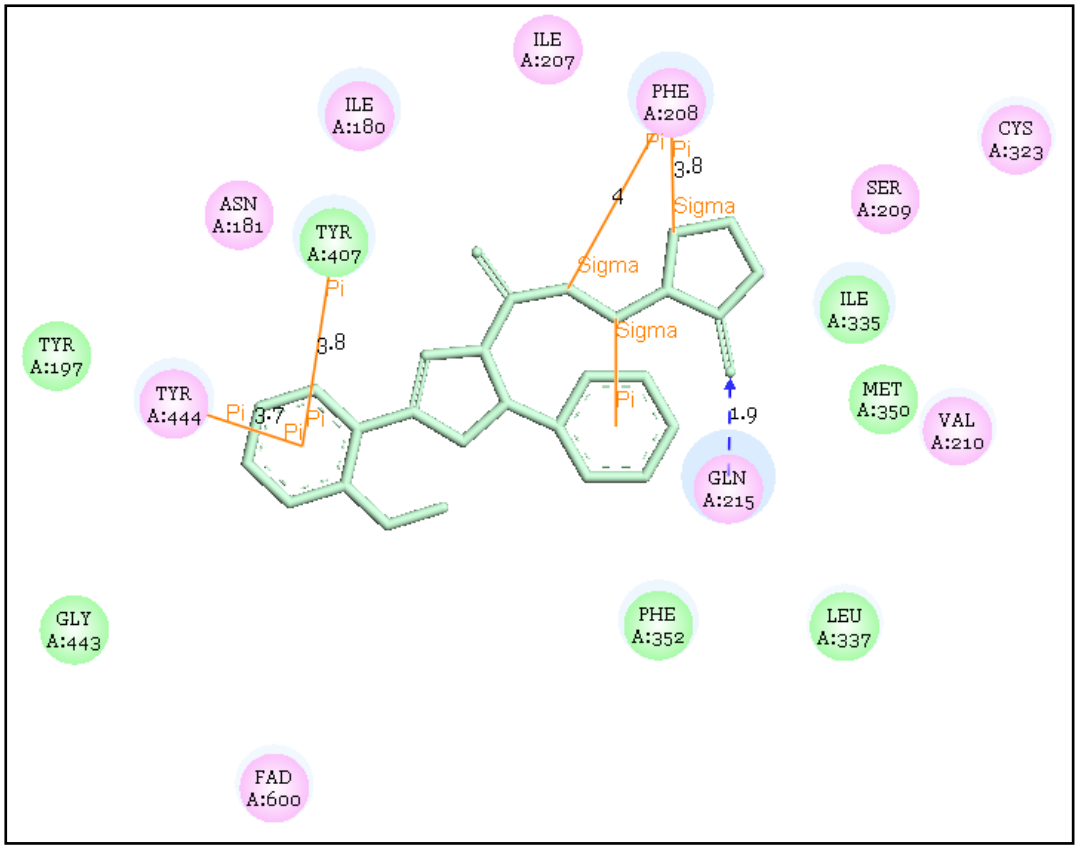

Figure-5.9: Position of 4dar ligand in MAO-A enzyme and 3-D representation of its interactions

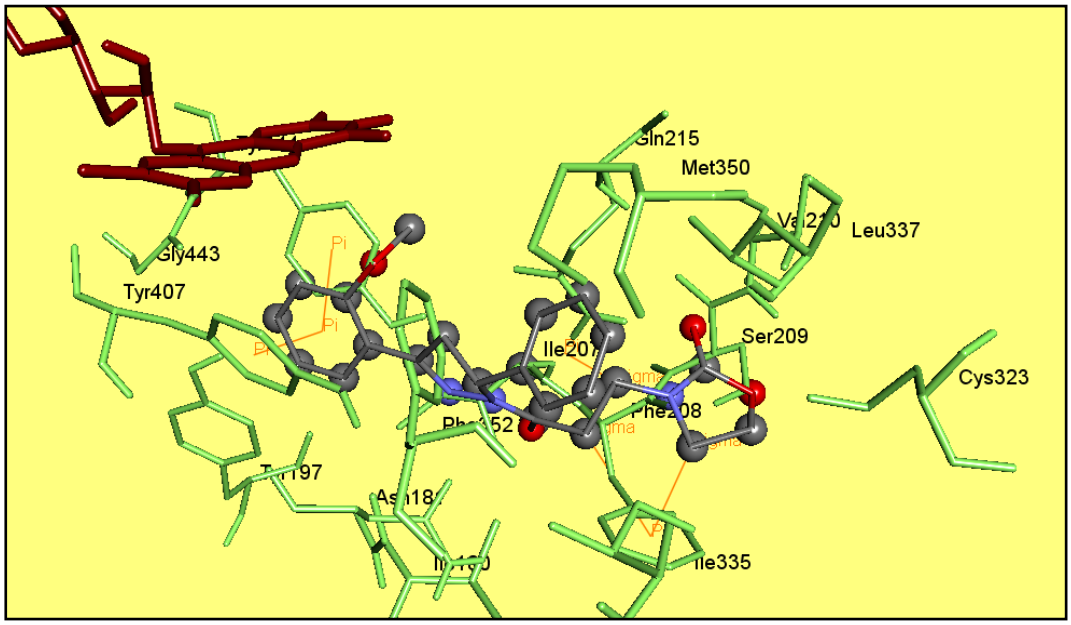

Figure-5.10: Position of 4das ligand in MAO-A enzyme and 3-D representation of its interactions

VdW interactions were formed between the inhibitor and the surrounding Gly443, Tyr197, Tyr407, Phe352, Leu337, Met350, Ile335 amino acids. Polar interactions were formed between the inhibitor and both FAD coenzyme, and Tyr444, Gln215, Val210, Cys323, Ile180, Asn181, Phe208, Ser209, Ile207 amino acids.

For Mao-A AutoDock inhibition constant K_i= 7.81nM, GOLD score= 88.00 and CAESAR score= 107.03. For Mao-B AutoDock inhibition constant K_i= 1.62uM, GOLD score= 81.24 and CAESAR score= 76.25.

The high number of bonding and interactions of this inhibitor with MAO-A, and its positioning right in front of the aromatic cage, show that it is a potentially good MAO-A inhibitor candidate.

When the results of R and S isoforms of the inhibitor are analysed together, strong bonding to the aromatic cage and interactions between coenzyme and the

aromatic cage, make 4dar/4das compounds effective inhibitor candidates for MAO-A. In addition when we compare the docking scores of the inhibitor for both MAO-A and MAO-B, we observe that the scores for MAO-A to be higher and this increases the possibility of the inhibitor to be MAO-A selective.

5.4.1.3 Evaluation of 5bar/5bas Ligands for MAO-A Enzyme

2-D and 3-D images of 5bar inhibitor positioned at the active site cavity of MAO-A enzyme by molecular modelling method are illustrated on Figure-5.11 and 5.12.

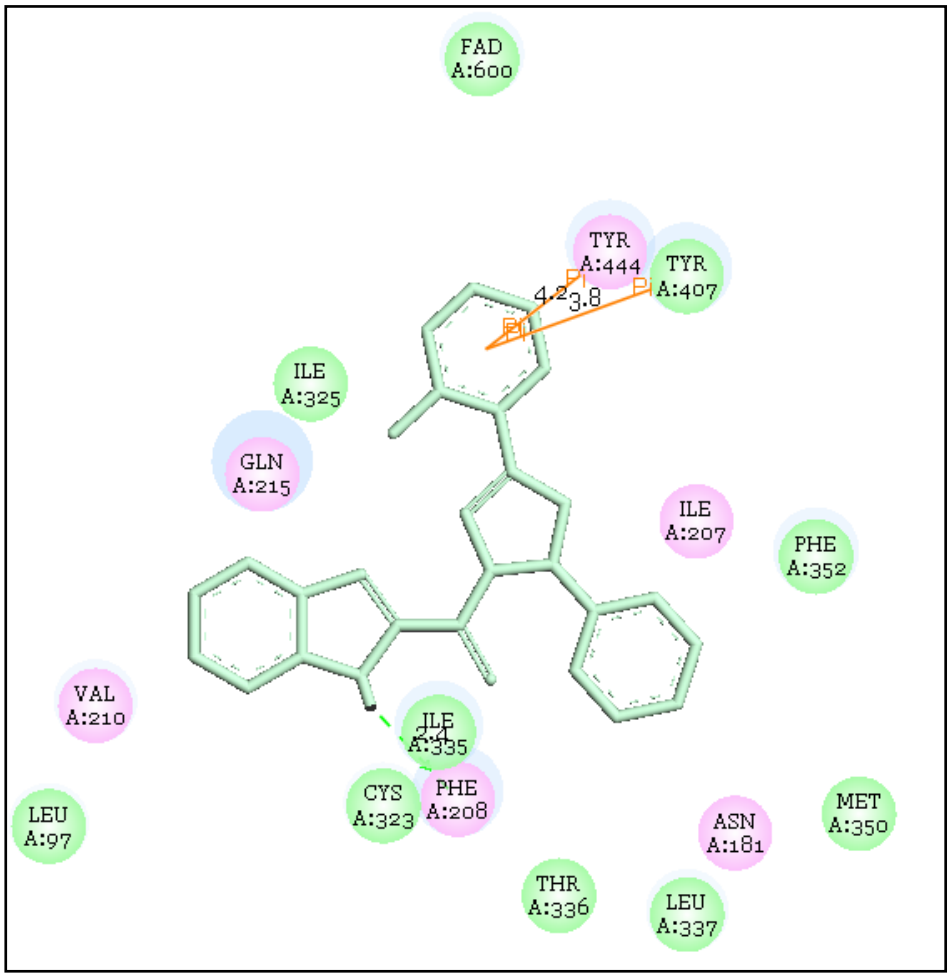

Figure-5.11: Position of 5bar ligand in MAO-A enzyme and 2-D representation of its interactions

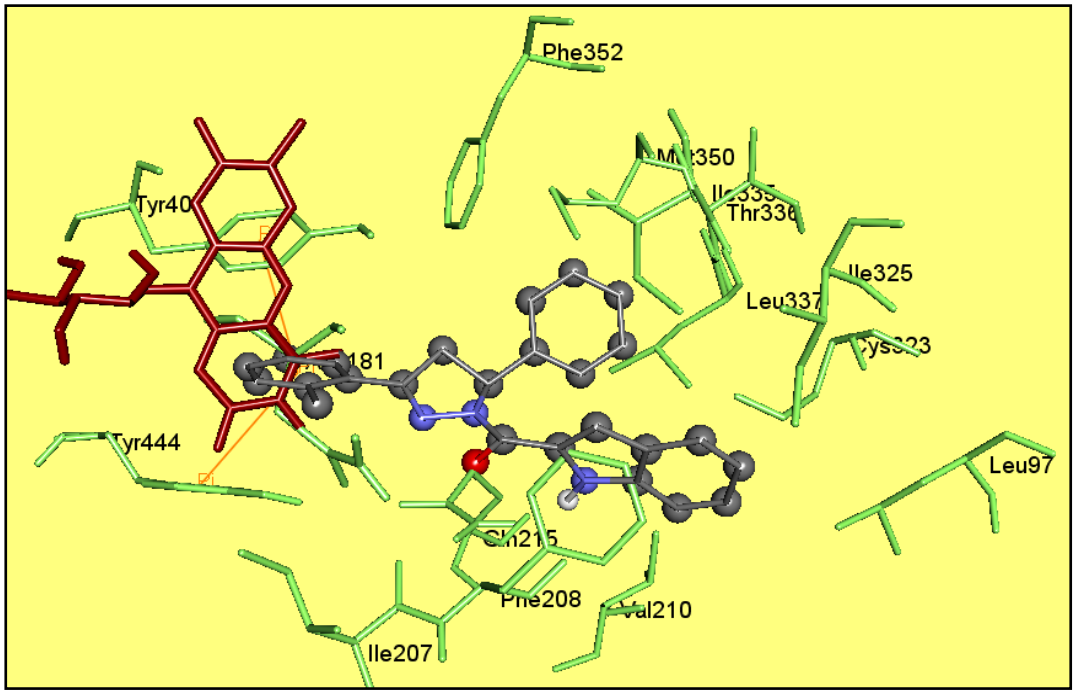

Figure-5.12: Position of 5bar ligand in MAO-A enzyme and 3-D representation of its interactions

Double pi-pi interactions took place between the phenyl ring of the inhibitor and Tyr444 and Tyr407 located in the aromatic cage. Phe208 amino acid formed a hydrogen bond with the group located at the furan ring of the inhibitor.

Polar interactions were formed between the inhibitor and the surrounding Val210, Phe208, Asn181, Ile207, Gln215, Tyr444 amino acids. Polar interactions were formed between the inhibitor and both FAD coenzyme, and Leu97, Cys323, Ile335, Thr336, Leu337, Met350, Phe352, Ile325, Tyr407 amino acids.

For Mao-A AutoDock inhibition constant K_i= 27.13nM, GOLD score= 77.60 and CAESAR score= 115.9. For Mao-B AutoDock inhibition constant K_i= 10.10uM, GOLD score = 77.00 and CAESAR score= 106.11.

The high number of bonding and interactions of this inhibitor with MAO-A, and its positioning right in front of the aromatic cage, show that it is a potentially good MAO-A inhibitor candidate.

2-D and 3-D images of 5bas inhibitor positioned at the active site cavity of MAO-A enzyme by molecular modelling method are illustrated on Figure-5.13 and 5.14.

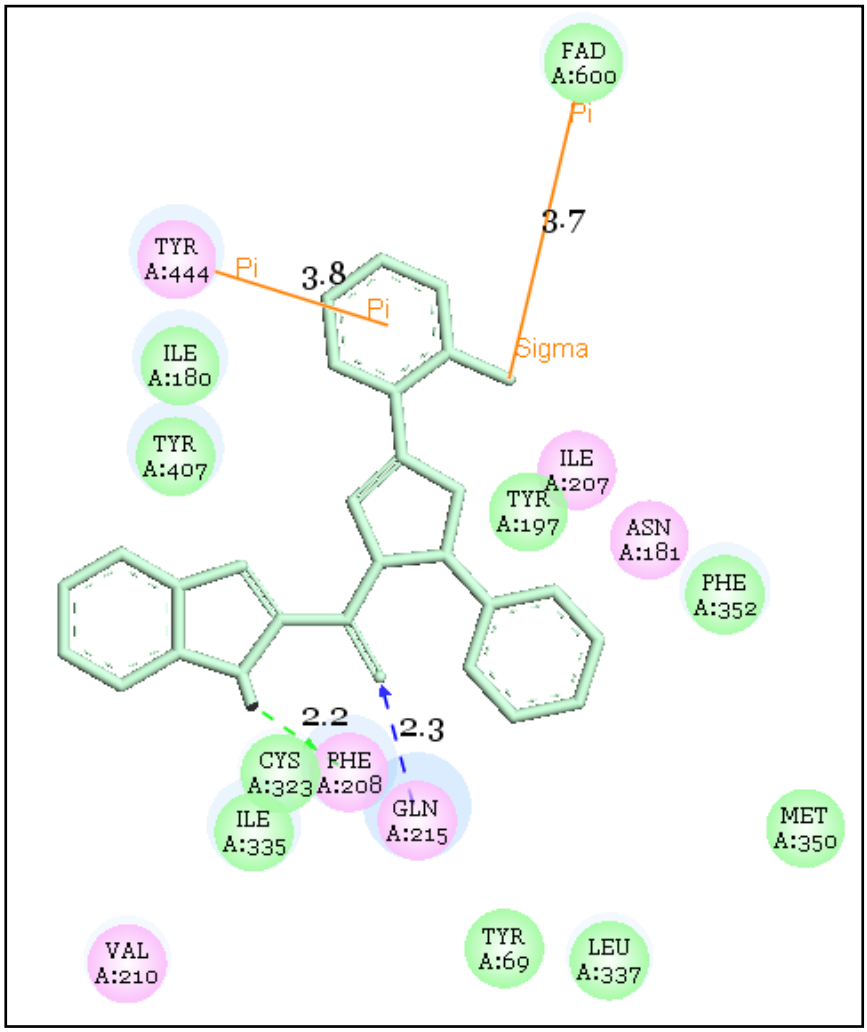

Figure-5.13: Position of 5bas ligand in MAO-A enzyme and 2-D representation of its interactions

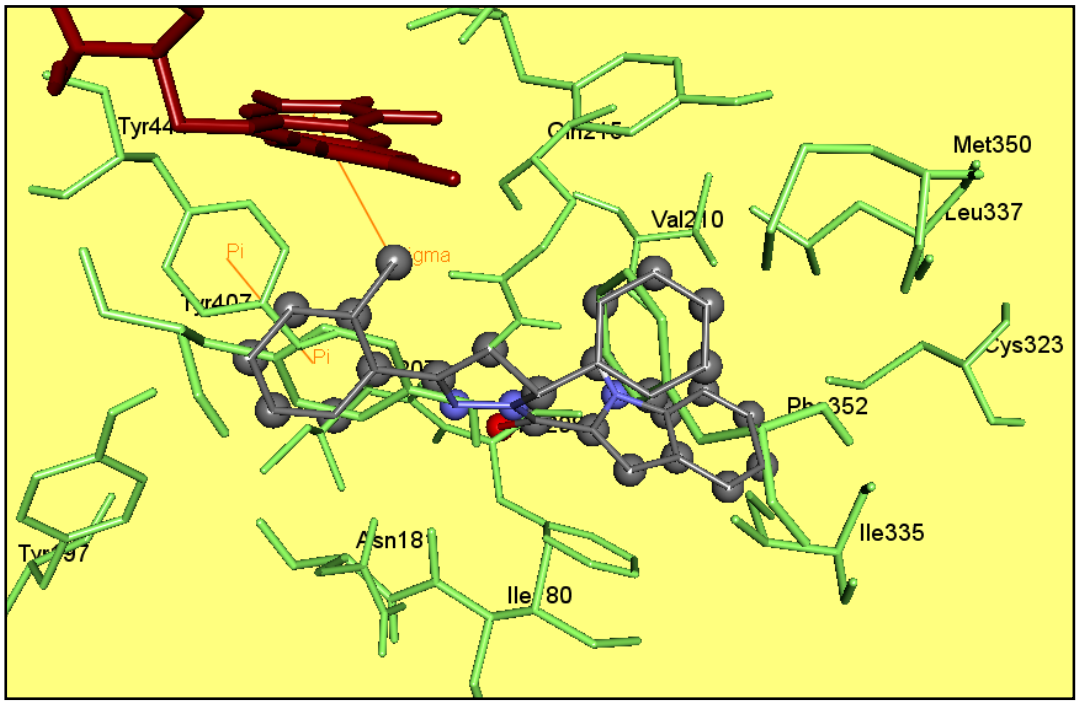

Figure-5.14: Position of 5bas ligand in MAO-A enzyme and 3-D representation of its interactions

A pi-pi interaction took place between the phenyl ring of the inhibitor and Tyr444 located in the aromatic cage. A pi-sigma interaction took between FAD and the inhibitor at 3.7Å. Gln215 and Phe208 formed a hydrogen bond with the ligand.

Polar interactions were formed between the inhibitor and the surrounding Val210, Phe208, Asn181, Gln215, Ile207, Tyr444 amino acids. VdW interactions were formed between the inhibitor and both FAD coenzyme, and Ile180, Tyr407, Ile335, Cys323, Phe352, Leu337, Met350, Tyr69, Tyr197 amino acids.

For Mao-A AutoDock inhibition constant K_i= 41.87nM, GOLD score= 92.28 and CAESAR score= 100.02. For Mao-B AutoDock inhibition constant K_i= 1.31uM, GOLD score= 91.75 and CAESAR score= 81.45.

The high number of bonding and interactions of this inhibitor with MAO-A, and its positioning right in front of the aromatic cage, show that it is a potentially good MAO-A inhibitor candidate.

When the results of R and S isoforms of the inhibitor are analysed together, strong bonding to the aromatic cage and the great number of amino acid residues surrounding the inhibitor, make 5bar/5bas compounds effective inhibitor candidates for MAO-A. In addition when we compare the docking scores of the inhibitor for both MAO-A and MAO-B, we observe that the scores for MAO-A to be higher and this increases the possibility of the inhibitor to be MAO-A selective.

5.4.2 Ligands Selected for MAO-B Enzyme

5.4.2.1 Evaluation of 1der/1des Ligands for MAO-B Enzyme

2-D and 3-D images of 1der inhibitor positioned at the active site cavity of MAO-B enzyme by molecular modelling method are illustrated on Figure-5.15 and 5.16.

A pi-sigma interaction took place between furan ring of the inhibitor and Tyr326. A hydrogen bond was formed between the ligand and Cis172.

VdW interactions were formed between the inhibitor and the surrounding Ile316, Phe168, Tyr188, Tyr398, Tyr326, Phe434, Tyr60 amino acids. Polar interactions were formed between the inhibitor and both FAD coenzyme, and Gln206, Ile198, Ile199, Cys172, Tyr435, Leu171 amino acids.

For Mao-B AutoDock inhibition constant K_i= 214.96nM, GOLD score= 81.16 and CAESAR score= 104.83. For Mao-A AutoDock inhibition constant K_i= 107.95nM, GOLD score= 81.46 and CAESAR score= 86.24.

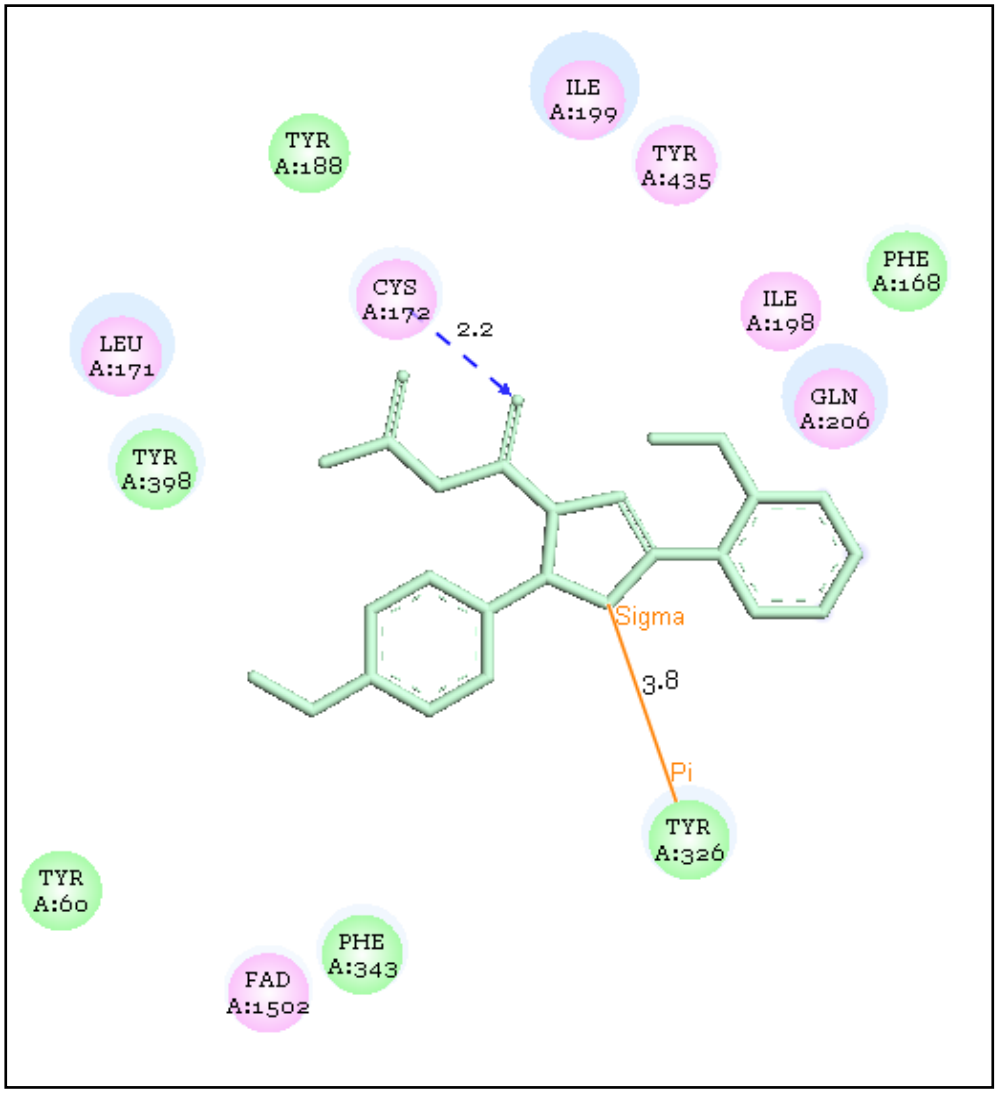

Figure-5.15: Position of 1der ligand in MAO-B enzyme and 2-D representation of its interactions

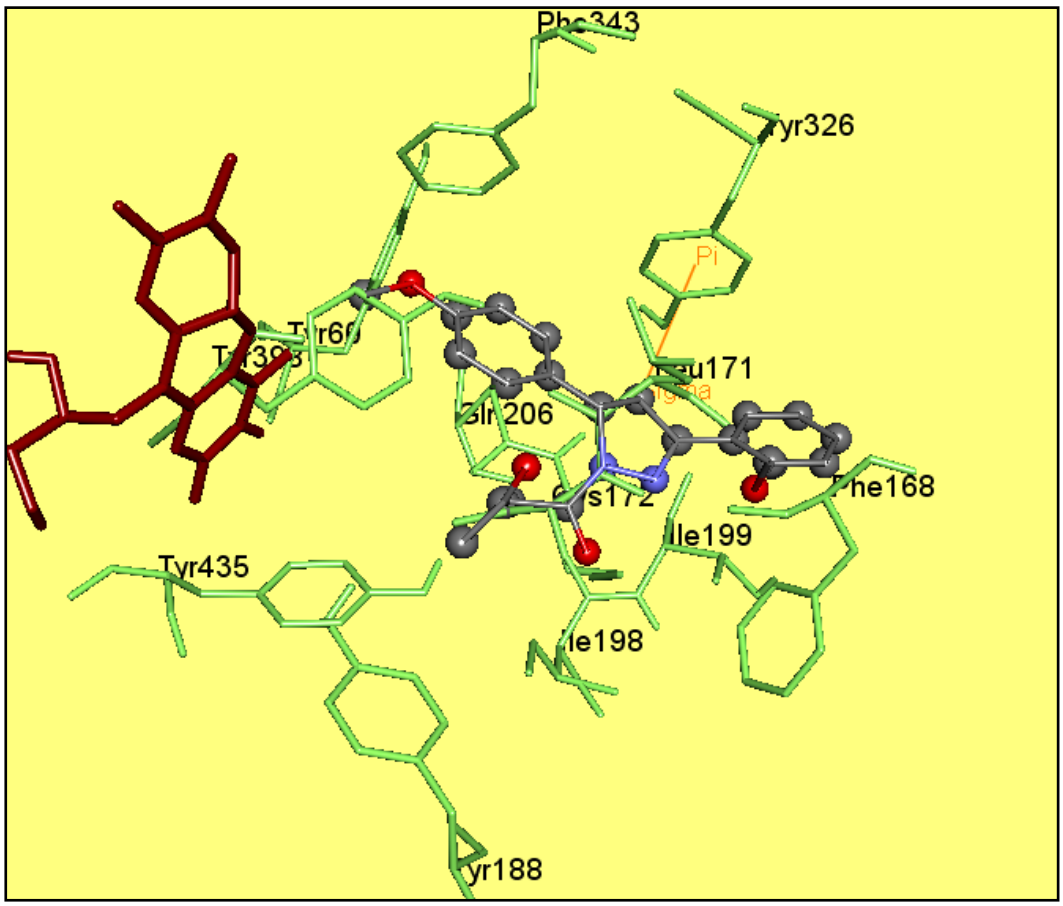

Figure-5.16: Position of 1der ligand in MAO-B enzyme and 3-D representation of its interactions

The high number of bonding and interactions of this inhibitor with MAO-B, and its positioning right in front of the aromatic cage, show that it is a potentially good MAO-B inhibitor candidate.

2-D and 3-D images of 1des inhibitor positioned at the active site cavity of MAO-B enzyme by molecular modelling method are illustrated on Figure-5.17 and 5.18.

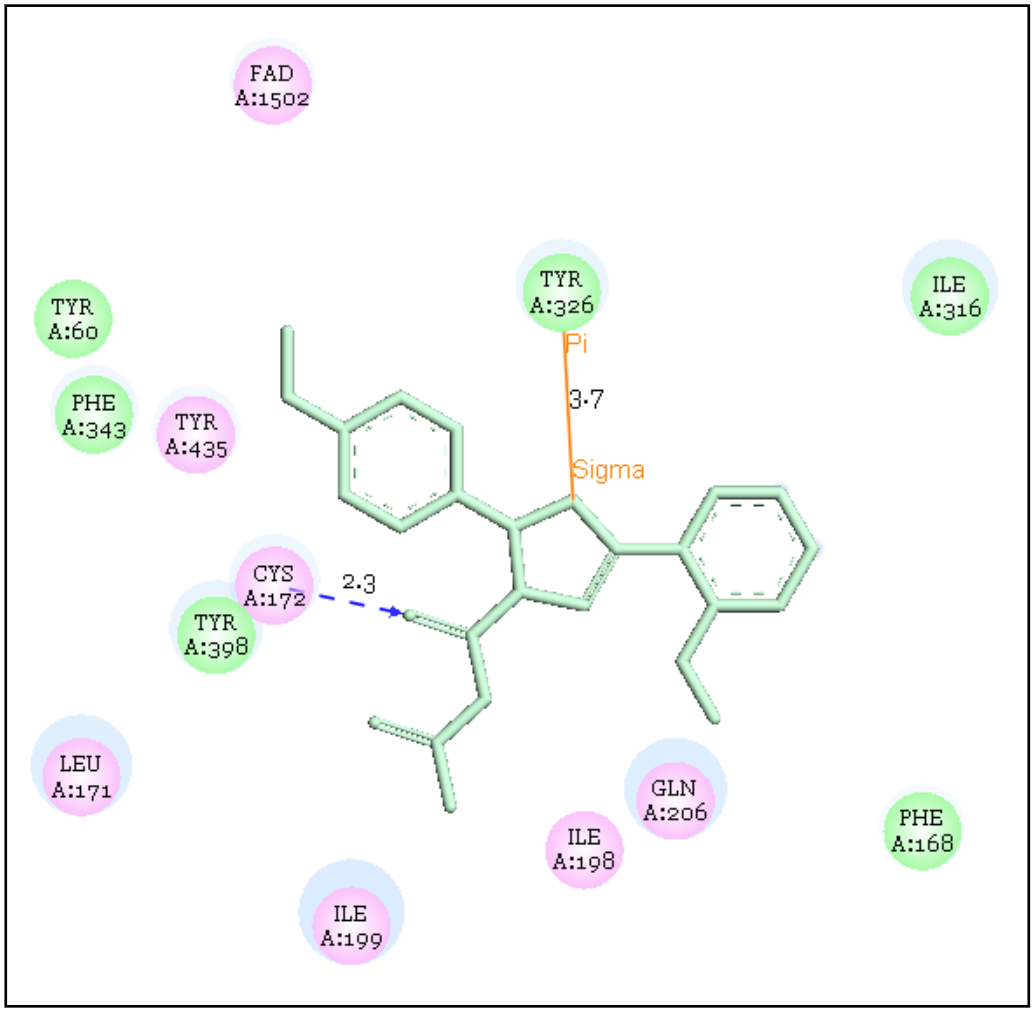

Figure-5.17: Position of 1des ligand in MAO-B enzyme and 2-D representation of its interactions

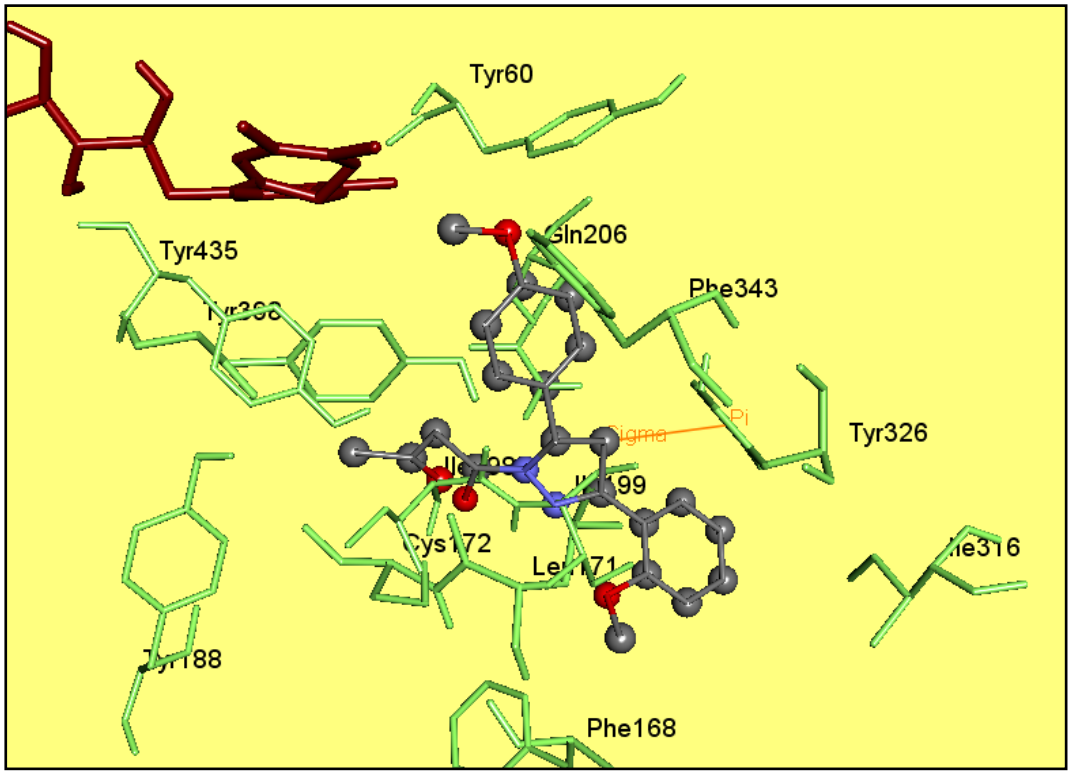

Figure-5.18: Position of 1des ligand in MAO-B enzyme and 3-D representation of its interactions

A pi-sigma interaction took place between furan ring of the inhibitor and Tyr326. A hydrogen bond was formed between the ligand and Cis172.

VdW interactions were formed between the inhibitor and the surrounding Ile316, Phe168, Tyr398, Tyr326, Phe343, Tyr60 amino acids. Polar interactions were formed between the inhibitor and both FAD coenzyme, and Gln206, Ile198, Ile199, Cys172, Tyr435, Leu171 amino acids.

For Mao-B AutoDock inhibition constant K_i= 313.58nM, GOLD score= 81.78 and CAESAR score= 104.65. For Mao-A AutoDock inhibition constant K_i= 135.20nM, GOLD score= 82.87 and CAESAR score= 94.39.

The high number of bonding and interactions of this inhibitor with MAO-B, and its positioning right in front of the aromatic cage, show that it is a potentially good MAO-B inhibitor candidate.

When the results of R and S isoforms of the inhibitor are analysed together, strong bonding to the aromatic cage and the great number of amino acid residues surrounding the inhibitor, make 1der/1des compounds effective inhibitor candidates for MAO-B. In addition when we compare the docking scores of the inhibitor for both MAO-A and MAO-B, we observe that the scores for MAO-B to be higher and this increases the possibility of the inhibitor to be MAO-B selective.

5.4.2.2 Evaluation of 3bar/3bas Ligands for MAO-B Enzyme

2-D and 3-D images of 3bar inhibitor positioned at the active site cavity of MAO-B enzyme by molecular modelling method are illustrated on Figure-5.19 and 5.20.

Pi-sigma interactions took place between the furan rings of the inhibitor and Tyr326 and Tyr435. Hydrogen bonds were formed between the inhibitor and FAD and Cis172.

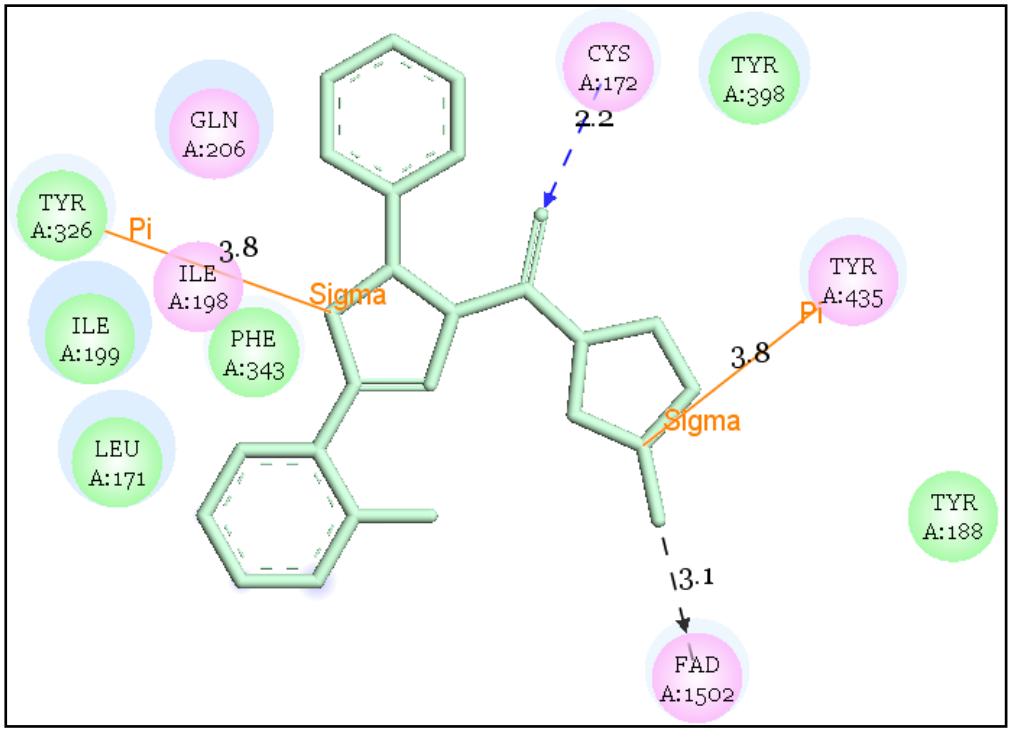

Figure-5.19: Position of 3bar ligand in MAO-B enzyme and 2-D representation of its interactions

VdW interactions were formed between the inhibitor and the surrounding Ile199, Tyr326, Phe343, Leu171, Tyr188, Tyr398 amino acids. Polar interactions were formed between the inhibitor and both FAD coenzyme, and Gln206, Ile198, Cys172, Tyr 435 amino acids.

For Mao-B AutoDock inhibition constant K_i= 30.36nM, GOLD score= 79.14 and CAESAR score=113.856.For Mao-A AutoDock inhibition constant K_i= 118.56nM, GOLD score= 79.35 and CAESAR score= 110.03.

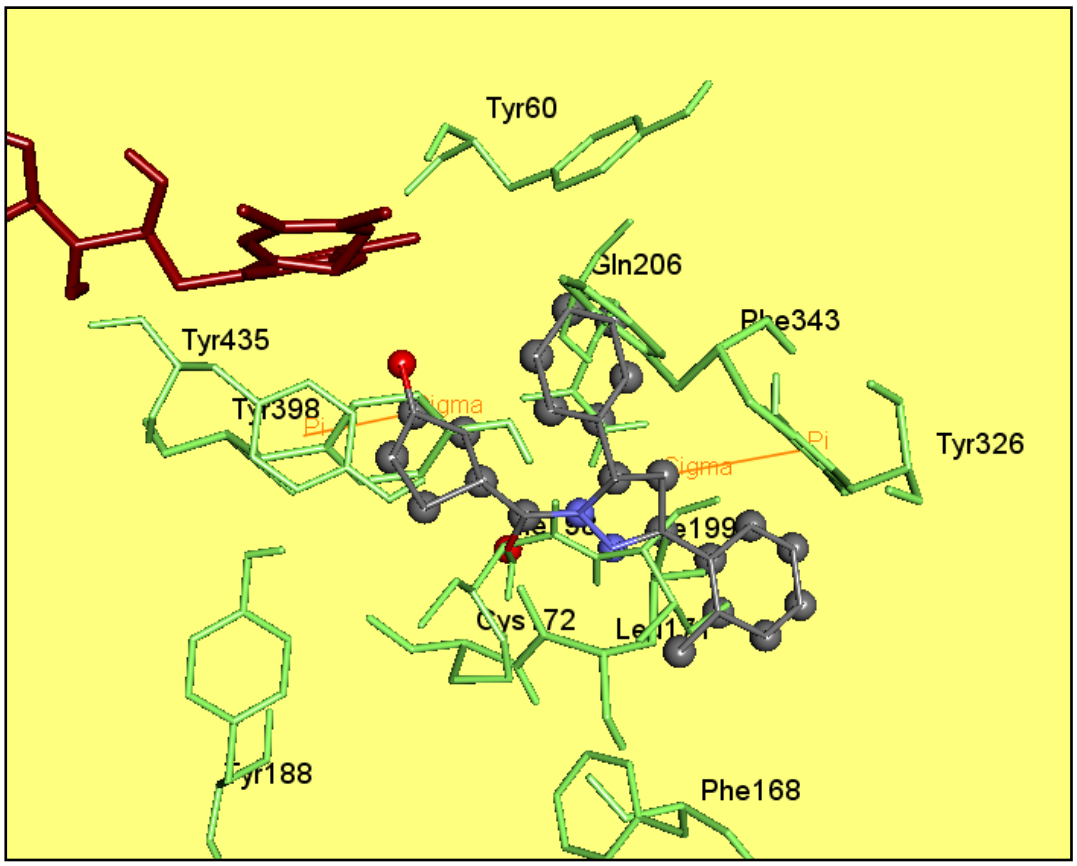

Figure-5.20: Position of 3bar ligand in MAO-B enzyme and 2-D representation of its interactions

The high number of bonding and interactions of this inhibitor with MAO-B, and its positioning right in front of the aromatic cage, show that it is a potentially good MAO-B inhibitor candidate.

2-D and 3-D images of 3bas inhibitor positioned at the active site cavity of MAO-B enzyme by molecular modelling method are illustrated on Figure-5.21 and 5.22.

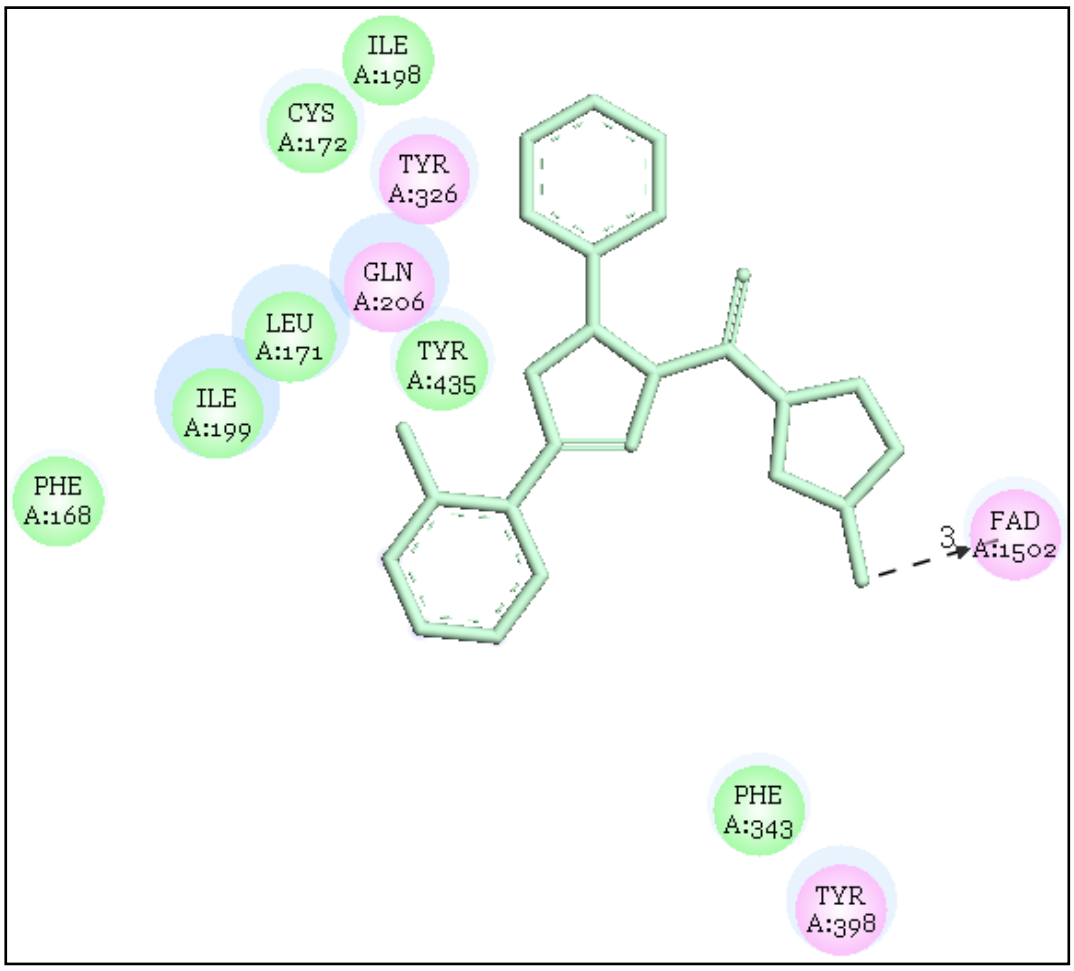

Figure-5.21: Position of 3bas ligand in MAO-B enzyme and 2-D representation of its interactions

VdW interactions were formed between the inhibitor and the surrounding Ile199, Leu171, Phe168, Tyr435, Phe343, Cys172, Ile198 amino acids. Polar interactions were formed between the inhibitor and both FAD coenzyme, and Gln206, Tyr326, Tyr398 amino acids.

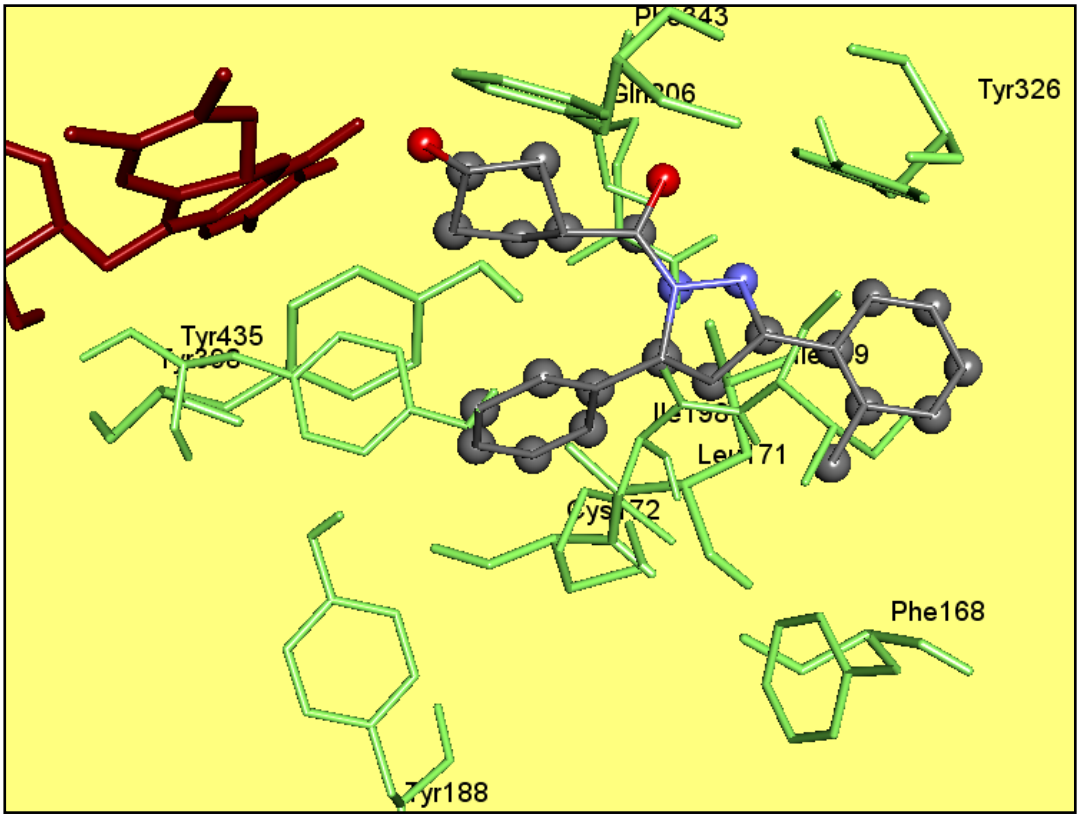

Figure-5.22: Position of 3bas ligand in MAO-B enzyme and 3-D representation of its interactions

For Mao-B AutoDock inhibition constant K_i= 86.11nM, GOLD score= 78.47 and CAESAR score= 85.68. For Mao-A AutoDock inhibition constant K_i= 94.69nM, GOLD score= 79.72 and CAESAR score= 84.02.

The high number of bonding and interactions of this inhibitor with MAO-B, and its positioning right in front of the aromatic cage, show that it is a potentially good MAO-B inhibitor candidate.

When the results of R and S isoforms of the inhibitor are analysed together, strong bonding to the aromatic cage and the great number of amino acid residues surrounding the inhibitor, make 3bar/3bas compounds effective inhibitor candidates for MAO-B. In addition when we compare the docking scores of the inhibitor for both MAO-A and MAO-B, we observe that the scores for MAO-B to be higher and this increases the possibility of the inhibitor to be MAO-B selective.

5.3.2.3 Evaluation of 3car/3cas Ligands for MAO-B Enzyme

2-D and 3-D images of 3car inhibitor positioned at the active site cavity of MAO-B enzyme by molecular modelling method are illustrated on Figure-5.23 and 5.24.

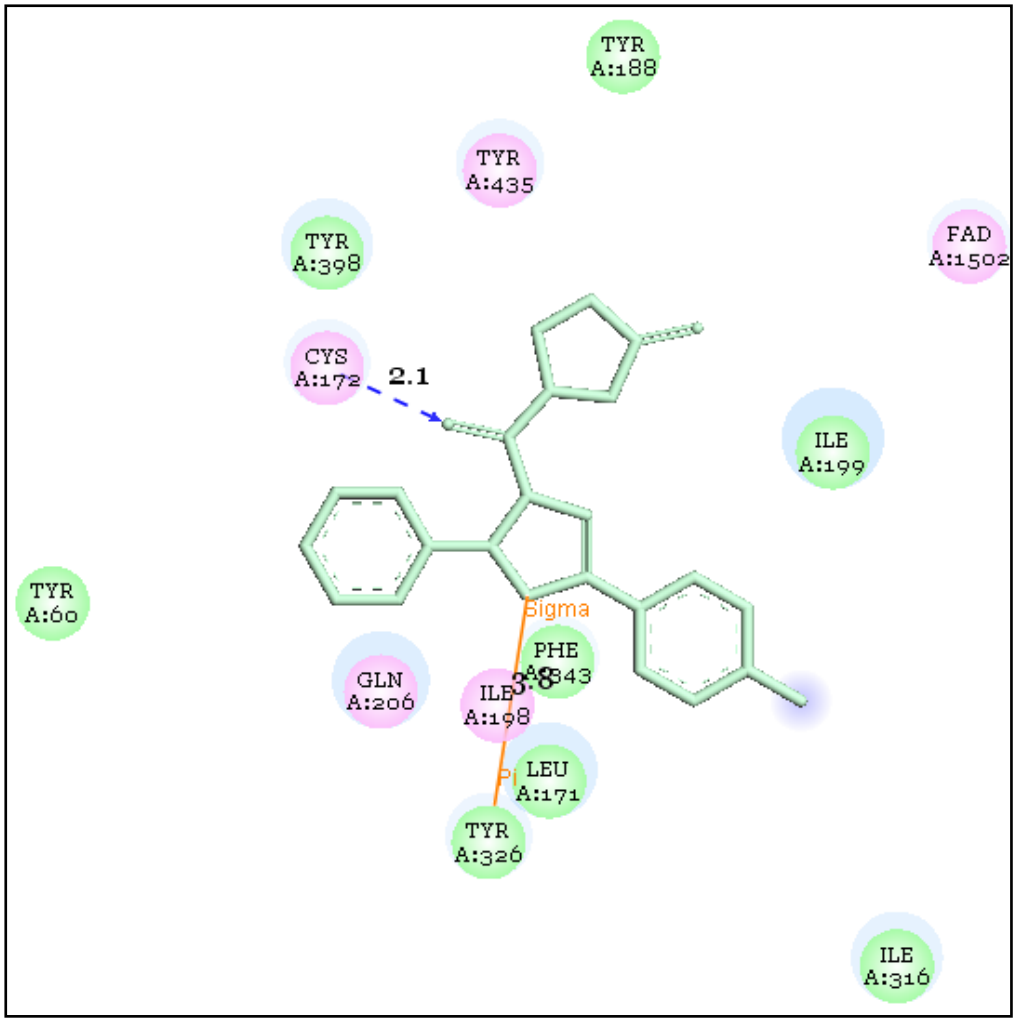

Figure-5.23: Position of 3car ligand in MAO-B enzyme and 2-D representation of its interactions

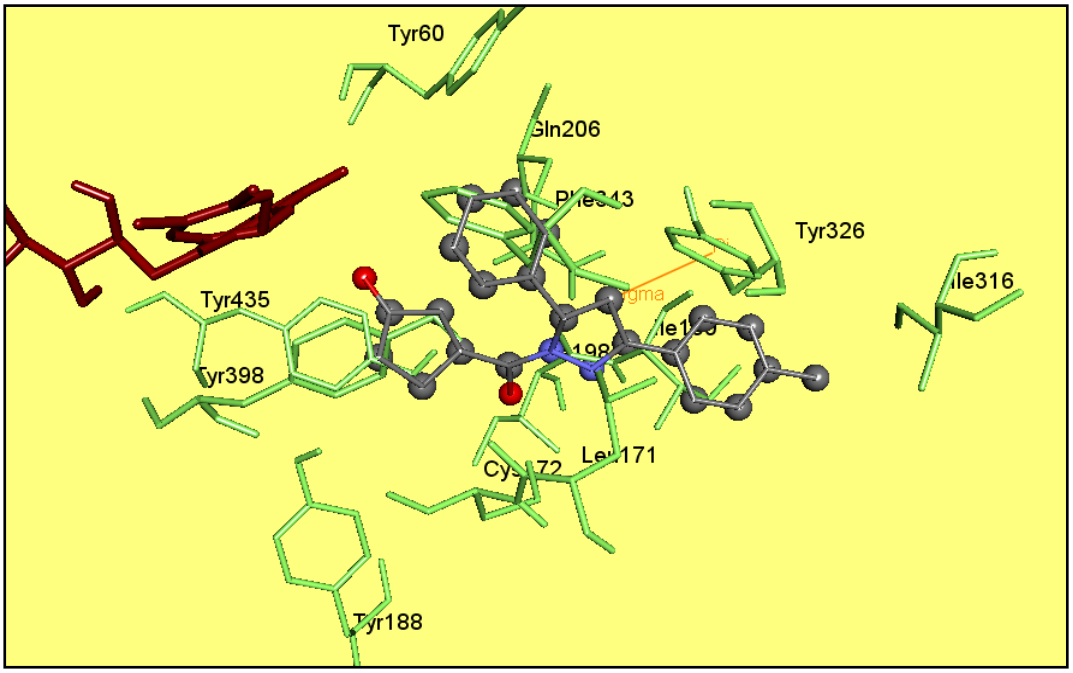

Figure-5.24: Position of 3car ligand in MAO-B enzyme and 3-D representation of its interactions

Pi-sigma interactions took place between the furan rings of the inhibitor and Tyr326 and Tyr435. Hydrogen bonds were formed between the inhibitor and FAD and Cis172.

VdW interactions were formed between the inhibitor and the surrounding Tyr60, Phe343, Leu171, Tyr326, Ile316, Ile199, Tyr398, Tyr188 amino acids. Polar interactions were formed between the inhibitor and both FAD coenzyme, and Gln206, Ile198, Cys172, Tyr435 amino acids.

For Mao-B AutoDock inhibition constant K_i= 17.53nM, GOLD score= 72.68 and CAESAR score= 109.88. For Mao-A AutoDock inhibition constant K_i= 116.42nM, GOLD score= 73.48 and CAESAR score= 105.082.

The high number of bonding and interactions of this inhibitor with MAO-B, and its positioning right in front of the aromatic cage, show that it is a potentially good MAO-B inhibitor candidate.

2-D and 3-D images of 3cas inhibitor positioned at the active site cavity of MAO-B enzyme by molecular modelling method are illustrated on Figure-5.25 and 5.26.

A Hydrogen bond was formed between the inhibitor and FAD. Van der Waals interactions were formed between the inhibitor and the surrounding Ile199, Leu171, Tyr435, Phe343, Cys172, Ile198, Tyr188 amino acids. Polar interactions were formed between the inhibitor and both FAD coenzyme, and Gln206, Tyr326, Tyr398 amino acids.

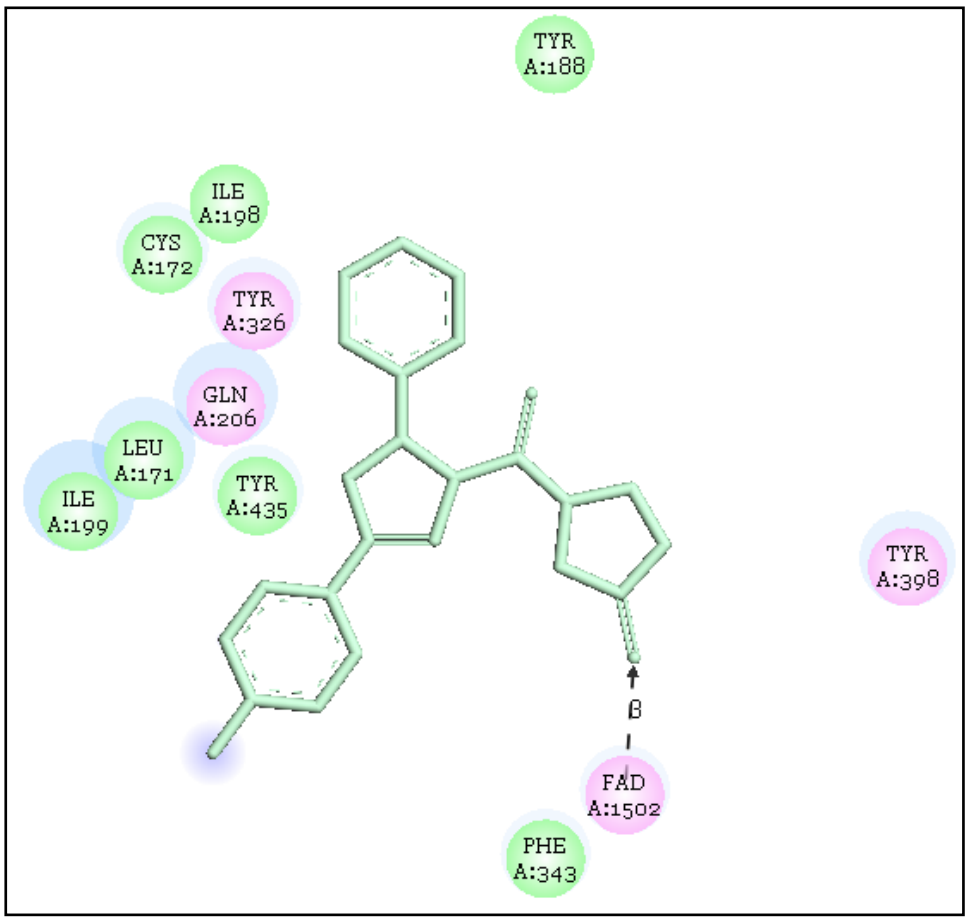

Figure-5.25: Position of 3cas ligand in MAO-B enzyme and 2-D representation of its interactions

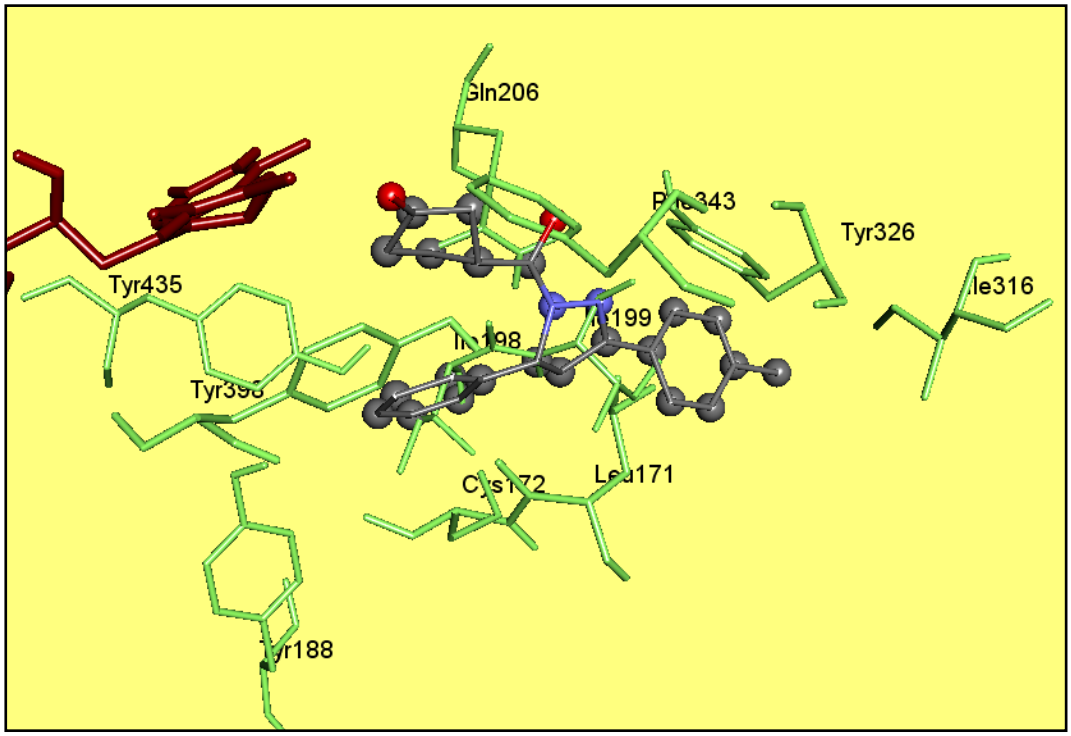

Figure-5.26: Position of 3cas ligand in MAO-B enzyme and 3-D representation of its interactions

For Mao-B AutoDock inhibition constant K_i= 70.07nM, GOLD score= 72.34 and CAESAR score= 111.95. For Mao-A, AutoDock inhibition constant K_i= 1.27uM, GOLD score= 72.29 and CAESAR score= 84.66.

The high number of bonding and interactions of this inhibitor with MAO-B, and its positioning right in front of the aromatic cage, show that it is a potentially good MAO-B inhibitor candidate.

When the results of R and S isoforms of the inhibitor are analysed together, strong bonding to the aromatic cage and the great number of amino acid residues surrounding the inhibitor, make 3car/3cas compounds effective inhibitor candidates for MAO-B. In addition when we compare the docking scores of the inhibitor for both MAO enzymes, we observe that the scores for MAO-B to be higher and this increases the possibility of the inhibitor to be MAO-B selective.

5.5 CONCLUSION

The ligands generated as a result of my molecular modelling studies, interact with MAO isoenzymes marginally. If compared interaction with MAO-A is much greater than MAO-B.

The interaction diagrams and the scores of the ligands in MAO isoenzymes clearly indicate the reason of this. During interaction with MAO-A, all these inhibitors settle right in front of FAD in the active cavities and in aromatic cage, and interact with the amino acids around them. On the other hand, MAO-B interactions take place at the active site, at a longer distance compared to MAO-A. According to the proposed amine oxidation mechanisms of MAO enzyme, the enzymatic reaction takes place at the aromatic cage right in front of the re-face of FAD. For this reason the inhibitors that can settle in this cavity can inhibit the enzyme better.

As a result, I consider the ligands discussed in Chapter 5 as potential selective inhibitor candidates. On the other hand, if main scaffold is taken into account, I believe; significantly better potential inhibitor candidates can be generated by conducting more research based on changing the side groups of the ligands. Thus potentially better MAO-B ligands, that show lower selectivity and binding affinity compared to MAO-A ligands, can be generated, and they can form an important basis for studies about ligands that contain a pyrazoline ring.

Curriculum Vitae

Filiz Varnali was born on 31 July 1981, in Varna/Bulgaria. She received her BS degree in Biology in 2009 from Trakya University, B.S. degree in Pathology Technician in 2005 from Marmara University and blood technician nurse degree in 2000 from Red Cross and Crescent High School. She worked in different areas between 2000-2009 in government and private hospitals. She accepted in Kadir Has University department of computational biology and bioinformatics and starts her works in this area in 2009.

REFERANCES;

1. Yelekçi, K., Uçar, G., Kelekçi, N.G., Erdem, S., Erdem, A., Gökşen, U.S., Türkkan, S.; Monoamin Oksidaz (MAO) İnhibitör Etkili Yeni Pirazolin Türevlerinin Moleküler Modelleme Yöntemiyle Tasarlanması, Sentezi ve İnhibisyon Kinetiklerinin Hesapsal ve Deneysel Olarak Tayini; Tübitak Project, Project number: 108T232; 2010; Istanbul

2. http://icm-institute.org/menu/recherche/pathologies-recherche?lang=en

3. Silverman, R. B.; Organic Chemistry of Drug Design and Drug Action; Second Edition; Elsevier Academic Press; 2003; Chapter1; page 1-3, Chapter 2; page 8, Chapter 4; page 210.

4. http://www.chem.qmul.ac.uk/iubmb/enzyme/EC1/4/3/4.html

5. Ucar, G., Yesilada, A., Ataol, E.; Monoamine Oksidaz Izozimlerinin Substrat ve Inhibitor Özguluklerinin Saptanması; Tübitak Project, Project number: SBAG-AYD-195; (2000-00112); Ankara

6. Edmondson, D.E., Binda, C., Mattevı, A.; Structural Insights into Mechanism of Amine Oxidation by Monoamine Oxidase A and B; Biochem. And Biophy. , 464(2007) 269-276

7. Ebadi, M., Srinivasan, S. K., Baxi, M. D.; Oxidative Stress and Antioxidant Therapy in Parkinson's Disease; Progress in Neurobiology, Volume 48, 1996, Elsevier Science

8. Geha, R. M., Chen, K., Wouters, J., Ooms, F., Shih, J. C.; Analysis of Conserved Active Site Residues in Monoamine Oxidase A and B and Their Three-dimensional Molecular Modeling; The Journal of Biological Chemistry, Vol277, No: 19, 2002

9. http://ekhidna.biocenter.helsinki.fi/dali_server/qz-test

10. http://www.mikeblaber.org/oldwine/BCH4053/Lecture33/Lecture33.htm

11. Wang, J.; Comparative Structural and Functional Properties of Human and Rat Monoamine Oxidase, 2007, PhD. thesis, Emory University

12. http://biology.kenyon.edu/BMB/Chime2/2005/Lara/Images/FADbinding.jpg

13. Edmondson, D.E., Binda, C., Wang, J., Upadhyay, A.K., Mattevi, A.; Molecular and Mechanistic Properties of the Membrane-Bound Mitochondrial Monoamine Oxidases, Biochemistry. 2009 May 26; 48(20): 4220–4230. Doi: 10.1021/bi900413g

14. Youdim, M.B. H., Edmondson, D., Tipton, K.F.; The Therapeutic Potential of Monoamine Oxidase Inhibitors, Nature Rewievs, Neuroscience, vol 7,2006

15. Colibus, L.D.C., Li, M., Binda, C., Lustig, A., Edmondson, D.E., Mattevi, A.; Three-Dimensional Structure of Human Monoamine Oxidase-A: Relation to the Structures of Rat MAO A and Human MAO B

16. Binda, C., Newton-Vinson, P., Hubalek, F., Edmonson, D.E., Mattevi, A.; Structure of Human MAO B, a Drug Target for the Treatment of Neurological Disorders, Nature Structural Biology, vol9, No1, 2002

17. http://opm.phar.umich.edu/

18. http://themedicalbiochemistyrpage.org/nerves.html#catecholamines

19. F., Bolasco, A., Secci, D., Chimenti, P., Granese, A., Carradori, S., Yáñez, M., Orallo, F., Ortuso, F., Alcaro, S; Investigations on the 2-thiazolylhydrazyne scaffold: Synthesis and Molecular Modelling of Selective Human Monoamine Oxidase Inhibitors, Bioorganic & Medicinal Chemistry 18 (2010) 5715–5723

20. http://en.wikipedia.org/wiki/Monoamine_oxidase_inhibitor

21. Hekzahidronazol Türevleri Üzerine Çalismalar, Şimsek, O.; Hacettepe Üniversitesi Farmasötik Kimya Bölumu Doktora Tezi, Ankara, 2009

22. Syrdom, B., Malan, S. F., Castagnoli, N., Bergh, J. J., Petzer, J. P.; Inhibition of Monoamine Oxidase by 8-benzyloxycaffeine Analogues, Bioorganic & Medicinal Chemistry 18 (2010) 1018–1028

23. Reniers, J., Robert, S., Frederick, R., Masereel, M., Vincent, S., Wouters, J.; Synthesis and Evaluation of β-carboline Derivatives as Potential Monoamine Oxidase Inhibitors, Bioorganic & Medicinal Chemistry 19 (2011) 134–144

24. Chimenti, F., Bolasco, A., Secci, A., Chimenti, P., Granese, A., Carradori, S., Yáñez, M., Orallo, F., Ortuso, F., Alcaro, S Investigations on the 2-thiazolylhydrazyne scaffold: Synthesis and Molecular Modelling of Selective Human Monoamine Oxidase Inhibitors, Bioorganic & Medicinal Chemistry 18 (2010) 5715–5723

25. Alcaro, S., Gaspar, A., Ortuso, F., Milhazes, N., Orallo, F., Uriarte, E., Yáñez, M., Borges, F.; Chromone-2- and -3-carboxylic Acids Inhibit Differently Monoamine Oxidases A and B, Bioorganic & Medicinal Chemistry Letters 20 (2010) 2709–2712

26. Chimenti, F., Secci, D., Bolasco, A., Chimenti, P., Carradori, G.S., Maccioni, E., Cardia, M.C., Yáñez, M., Orallo, F., Alcaro, S., Ortuso, F., Cirilli, R., Ferretti, R., Distinto, S., Kirchmair, J., Langer, T.; Synthesis, Semi preparative HPLC separation, Biological Evaluation, and 3-D-QSAR of Hydrazothiazole Derivatives as Human Monoamine Oxidase B inhibitors, Bioorganic & Medicinal Chemistry 18 (2010) 5063–5070

27. Prins, L.H.A., Petzer, J.P., Malan, S.F.; Inhibition of Monoamine Oxidase by Indole and Benzofuran Derivatives, European Journal of Medicinal Chemistry 45 (2010) 4458-4466

28. Gaspar, A., Silva, T., Yáñez, T., Vina, D., Orallo, F., Ortuso, F., Uriarte, E., Alcaro, S., Borges, F.; Chromone, a Privileged Scaffold for the Development of Monoamine Oxidase Inhibitors, J. Med. Chem. 2011, 54, 5165–5173

29. Chimenti, F., Fioravanti, R., Bolasco, A., Chimenti, P., Secci, D., Rossi, F., Yáñez, M., Orallo, F., Ortuso, F., Alcaro, S., Cirilli, R., Ferretti, R., Sanna, M.L.; A new series of flavones, thioflavones, and Flavanones as Selective Monoamine Oxidase-B inhibitors, Bioorganic & Medicinal Chemistry 18 (2010) 1273–1279

30. Kelekçi, N. G., Şimsek, Ö. A., Ercan, A., Yelekçi, K., Şahin, Z. S., Işık, S., Uçar, G., Bilgin, A. A.; Synthesis and Molecular Modelling of Some Novel Hexahydroindazole Derivatives as Potent Monoamine Oxidase Inhibitors, Bioorganic & Medicinal Chemistry 17 (2009) 6761–6772

31. Khalafy, J, Rimaz, M., Panahi, L., Rabiei, H.; A Regiospecific One-Pot, Three Component Synthesis of 4-Aryl-6, 8-dimethylpyrimido [4,5-c] pyridazine-5, 7 (6H, 8H)-diones as New Potential Monoamine Oxidase Inhibitors, Bull. Korean Chem. Soc. 2011, Vol. 32, No. 7, doi 10.5012/bkcs.2011.32.7.2428

32. Lühr, S., Vilches-Herrera, M., Fierro, A., Ramsay, R. R., Edmondson, D.E., Reyes-Parada, M., Cassels, B. K., Iturriaga-Vásquez, P.; 2-Arylthiomorpholine Derivatives as Potent and Selective Monoamine Oxidase B inhibitors, Bioorganic & Medicinal Chemistry 18 (2010) 1388–1395

33. Jiao, Z., Wei, S., Zhu, Q.; Monoamine Oxidase Inhibitors: Benzylidene-prop-2-ynyl-amines Analogues, Biol. Pharm. Bull. 33(4) 725—728 (2010)

34. Vilches-Herrera, M., Miranda-Sepúlveda, J., Rebolledo-Fuentes, M., Fierro, A., Lühr, S., Iturriaga-Vasquez, P., Cassels, B. K., Reyes-Parada, M.; Naphthylisopropylamine and N-benzylamphetamine Derivatives as Monoamine Oxidase Inhibitors, Bioorganic & Medicinal Chemistry 17 (2009) 2452–2460

35. Van der Walt, E.M., Milczek, E.M., Malan, S.F., Edmondson, D. E., Castagnoli, N., Bergh, J.J., Petzer, J.P.; Inhibition of monoamine oxidase by (E)-styrylisatin analogues, Bioorganic & Medicinal Chemistry Letters 19 (2009) 2509–2513

36. http://en.wikipedia.org/wiki/Drug_desig

37. http://www.creative-biostructure.com/drugdesign.htm

38. Funkhouser, T.; Protein-Ligand Docking Methods Princeton University CS597A, Fall 2007

39. Akdoğan, E.D., Erman, B., Yelekçi, K.; In silico Design of Novel and Highly Selective Lysine-specific Histone Demethylase Inhibitors, Turk J Chem, 35 (2011), 523 –542. , Tübitak, doi: 10.3906/kim-1102-985

40. Kitchen, D.B., Decornez, H., Furr, J.R., Bajorath, J.; Docking and Scoring in Virtual Screening for Drug Discovery: Methods and Applications, Nature, doi: 10.1038/nrd1549

41. Morris, G.M., Goodsell, D. S., Huey, R., Olson, A.J.; AutoDock User Guide v.2.4, 1996

42. Huey, R., Morris, G.M.; Using AutoDock 4 with AutoDockTools: A Tutorial, California, USA, 2008

43. http://AutoDock.scripps.edu/faqs-help/manual

44. http://AutoDock.scripps.edu/

45. Ural, G.; Blind Docking Simulations of Benzothiazoles on Triosephosphate Isomerase, Yüksek lisans tezi, Boğaziçi University, 2011

46. Verdonk, M. L., Cole, J. C., Hartshorn, M. J., Murray, C. W., Taylor, R. D.; Improved Protein–Ligand Docking Using GOLD, PROTEINS: Structure, Function, and Genetics 52:609–623 (2003)

47. http://www.ccdc.cam.ac.uk/support/documentation/GOLD/5_1/GOLD_api/index.html#audience_and_intro

48. Schwab, C.H.; Conformations and 3-D Pharmacophore Searching, doi: 10.1016/j.ddtec.2010.10.003

49. Chang, Y., Yang, L., Wang, B.; Pharmacophore Modeling of Tyrosine Kinase Inhibitors: 4-Anilinoquinazoline Derivatives, Journal of the Chinese Chemical Society, 2010, 57, 916-924

50. http://www.ifm.liu.se/compchem/msi/doc/life/catalyst46/help/REFenergy.doc.html

51. http://www.chemicalize.org